Correlative Chemical Imaging of Amyloid Plaque Pathology in Alzheimer's Disease

Junyue Ge

Department of Psychiatry and Neurochemistry

Institute of Neuroscience and Physiology

Sahlgrenska Academy, University of Gothenburg

UNIVERSITY OF GOTHENBURG

Gothenburg 2024

Cover illustration: Junyue Ge

junyue.ge@gu.se

ISBN 978-91-8115-020-9 (PRINT)
ISBN 978-91-8115-021-6 (PDF)

Printed in Borås, Sweden 2024
Printed by Stema Specialtryck AB

世之奇伟、瑰怪，非常之观，常在于险远，

而人之所罕至焉，故非有志者不能至也。

The world's most magnificent sights are often hidden in remote and perilous places, rarely visited by people—accessible only to those with unwavering determination.

Correlative Chemical Imaging of Amyloid Plaque Pathology in Alzheimer's Disease

Junyue Ge

Department of Psychiatry and Neurochemistry, Institute of Neuroscience and Physiology
Sahlgrenska Academy, University of Gothenburg
Gothenburg, Sweden

ABSTRACT

The formation of beta-amyloid (Aβ) plaques and neurofibrillary tangles are key pathological hallmarks of Alzheimer's disease (AD), where amyloid has been identified to precede and even initiate other neurodegenerative processes including Tau. Consequently, studying beta-amyloid pathology has been a central focus in AD research yet the molecular mechanisms underlying plaque formation and its role in initiating AD remain poorly understood. Aβ plaque pathology is characterized by significant heterogeneity in morphology, including variations between cored and diffuse plaques, as well as structural polymorphism in amyloid fibril formation. Moreover, Aβ does not correlate with cognitive performance and is even observed in elderly, cognitively normal individuals. Recent evidence further suggests that neuronal lipids also play a crucial role in amyloid plaque formation and progressing plaque pathology. Together this poses a significant challenge and highlights the need for new, biochemical tools that allow to disentangle the complex molecular interactions associated with AD pathogenesis and plaque formation in particular.

To address this gap, we utilized advanced chemical imaging techniques to probe the molecular events associated with diverse plaque pathologies in AD.

In this thesis, we developed a tetra-modal chemical imaging approach that integrates matrix-assisted laser desorption/ionization mass spectrometry imaging (MALDI-MSI) with fluorescence imaging. This allowed for detailed mapping of lipid and amyloid peptide distributions in brain tissue of genetic AD mouse models. Through the application of novel, multivariate tools for multiblock analysis, we identified distinct lipid profiles linked to different

stages of plaque formation, highlighting the correlation of GM1 ganglioside with both plaque seeding and growth. We further validated the relevance of lipid-amyloid co-aggregation by developing a dynamic imaging approach based on metabolic labeling of lipids and peptides with stable isotopes. This allowed to dissect plaque and lipid coaggregation dynamics and identified the sequence of ganglioside and amyloid deposition in precipitation plaque pathology in AD mouse model.

Furthermore, we examined the co-existence of different Aβ peptides in novel transgenic models harboring the *Uppsala APP* mutation, revealing its significant impact on Aβ aggregation dynamics.

Finally, we applied these advanced imaging techniques to understand heterogenous plaque pathology in the human brain. Here, we successfully identified specific amyloid plaque signatures for distinct plaque types, such as Aβ1-42(ox) and Aβ2-42 in neuritic plaques. Using a novel AI driven plaque segmentation scheme, we identified that Aβ1-40 was found to be associated with plaque maturation into cored deposits in AD patients. Further, Aβ x-40 is present in cored, coarse grain plaques and vascular plaques (CAA) in both sAD and fAD.

Together these findings enhance our understanding of amyloid plaque heterogeneity as well as underscore the importance of lipid-amyloid interactions in AD pathology. This work lays the groundwork for future investigations aimed at elucidating the complex interactions between lipids and amyloid peptides in the context of AD.

Keywords: Alzheimer's disease, amyloid plaque pathology, lipid, correlative chemical imaging, MALDI-MSI, microscopy

ISBN 978-91-8069-020-9 (PRINT)
ISBN 978-91-8069-021-6 (PDF)

SAMMANFATTNING PÅ SVENSKA

Bildandet av beta-amyloid (Aβ)-plack och neurofibrillära nystan är de huvudsakliga patologiska kännetecknen för Alzheimers sjukdom (AD), där amyloid har identifierats som en faktor som föregår och till och med initierar andra neurodegenerativa processer, inklusive Tau-patologi. Följaktligen har studier av beta-amyloidpatologi varit ett centralt fokus inom Alzheimerforskningen. Trots detta är de bakomliggande molekylära mekanismerna som orsakar plackbildning och leder till initiering av AD fortfarande dåligt förstådda.

Aβ-plackpatologi kännetecknas av betydande morfologisk heterogenitet, inklusive variationer mellan kompakta och diffusa plack samt strukturell polymorfism i bildandet av amyloidfibriller. Dessutom korrelerar Aβ inte med kognitiv förmåga; Aβ-avlagringar observeras till och med hos äldre med normal kognitiv funktion. Nya bevis visar att även neuronala lipider spelar en avgörande roll i bildningen av amyloidplack och fortskridandet av plackpatologi. Sammantaget utgör detta en betydande utmaning och belyser behovet av nya biokemiska verktyg för att utreda de komplexa molekylära interaktioner som är förknippade med AD-patogenes och plackbildning.

För att adressera denna kunskapslucka använde vi avancerade kemiska avbildningstekniker för att undersöka de molekylära händelser som är associerade med olika plackpatologier i AD.

I denna avhandling har vi utvecklat en tetramodal kemisk avbildningsmetod som integrerar matrixassisterad laserdesorption/jonisering-masspektrometri (MALDI-MSI) med fluorescensavbildning. Denna unika metod användes för att skapa en detaljerad kartläggning av lipid- och amyloidpeptidfördelningar i hjärnvävnad från genetiska AD-musmodeller. Genom att tillämpa nya multivariata verktyg för multiblockanalys identifierade vi distinkta lipidprofiler associerade med olika stadier av plackbildning, vilket framhävde korrelationer mellan GM1-gangliosid och plackuppkomst samt placktillväxt.

Vidare validerade vi relevansen av lipid-amyloid-samaggregation genom att utveckla en dynamisk avbildningsmetod baserad på metabolisk märkning av lipider och peptider med hjälp av stabila isotoper. Detta möjliggjorde en noggrann granskning av koaggregationsdynamiken mellan plack och lipider och resulterade i identifieringen av den sekvens av gangliosid- och

amyloidavsättning som förekommer i utfällningsplackpatologi i AD-musmodeller.

Utöver detta undersökte vi samexistensen av olika Aβ-peptider i nya transgena modeller med Uppsala APP-mutationen, vilket avslöjade dess betydande inverkan på Aβ-aggregationsdynamiken.

Slutligen tillämpade vi dessa avancerade avbildningstekniker för att förstå heterogen plackpatologi i den mänskliga hjärnan. Här identifierade vi framgångsrikt specifika amyloidplacksignaturer för distinkta placktyper, såsom Aβ1-42(ox) och Aβ2-42 i neuritiska plack. Med hjälp av en ny AI-driven placksegmenteringsmetod identifierade vi associationer mellan Aβ1-40 och plackmognad som resulterade i kompakta Aβ-avlagringar hos AD-patienter. Aβ x-40 återfanns även i kompakta och grovkorniga plack samt vaskulära plack (CAA) i både sAD och fAD.

Sammanfattningsvis förbättrar dessa upptäckter vår förståelse av amyloidplackheterogenitet och understryker vikten av lipid-amyloidinteraktioner i AD-patologi. Detta arbete lägger grunden för framtida undersökningar som syftar till att belysa de komplexa interaktionerna mellan lipider och amyloidpeptider i samband med AD.

中文摘要

β-淀粉样蛋白（Aβ）斑块和神经原纤维缠结的形成是阿尔茨海默病（AD）的主要病理特征，其中淀粉样蛋白被认为在其他神经退行性过程发生之前起到了关键作用，甚至可能是其启动因子，包括 Tau 蛋白的变化。因此，研究 β-淀粉样蛋白病理学一直是 AD 研究的重点。然而斑块形成的分子机制及其在AD病理启动中的作用尚不完全明确。Aβ斑块病理学的一个显著特点是其形态学上的异质性，包括核状淀粉样斑块与弥漫淀粉样斑块之间的差异，以及淀粉样蛋白原纤维形成的结构多样性等。然而，研究显示 Aβ 斑块与认知能力之间没有直接关系。与此同时，有研究显示即使在认知正常的老年人群体中也可观察到淀粉样斑块的存在。近期的研究进一步表明，神经元中的脂质在淀粉样斑块的形成和病理进展中发挥了关键作用。总之，这些发现凸显了 AD 病理研究中的重大挑战，并强调了迫切需要新的分析工具，进一步解开与 AD 发病机制及斑块形成相关的复杂分子相互作用。

为了填补这一研究空白，我们采用了先进的化学成像技术来探测与 AD 相关的斑块病理中的分子机理。本论文中，我们开发了一种四模态化学成像方法，结合了基质辅助激光解吸/电离质谱成像（MALDI-MSI）和荧光成像技术，从而能够详细绘制遗传性 AD 小鼠模型脑组织中的脂质和淀粉样多肽分布。通过应用创新的多变量分析工具，我们在多个组织切片中揭示了与斑块形成不同阶段相关的脂质谱特征，尤其是 GM1 神经节苷脂与斑块初形成和生长之间的密切相关性。我们还开发了一种基于稳定同位素标记的脂质和多肽的动态成像方法，进一步验证了脂质与淀粉样蛋白共聚集的关系。这使得我们能够深入分析斑块和脂质的共聚集动力学，并确定了 AD 小鼠模型中脂质和淀粉样蛋白在斑块沉积中的顺序。

此外，我们还研究了不同 Aβ 多肽在含有 *APPUppsala* 突变的转基因小鼠模型中的共存情况，揭示了不同 Aβ 多肽对其聚集动力学的显著影响。最后，我们将这些先进的成像技术应用于人类大脑中的斑块病理研究，成功地揭示了不同类型斑块的特定化学特征。例如，在神经斑块中，我们识别了 Aβ1-42(ox)和 Aβ2-42 的特征性多肽。通过采用新开发的基于 AI 技术的斑块分类方案，我们发现 Aβ1-40 与 AD 患者斑块成熟

为核心沉积物相关。此外, Aβx-40 同样沉积于散发性和遗传性 AD 病人脑部的核状斑块，粗粒斑块和血管斑块（CAA）中。

这些发现加深了我们对淀粉样斑块异质性的理解，并突显了揭开脂质与淀粉样蛋白相互作用在研究 AD 病理学中的重要性。本研究为未来探讨 AD 背景下脂质和淀粉样多肽之间复杂相互作用的研究奠定了坚实的基础。

LIST OF PAPERS

This thesis is based on the following studies, referred to in the text by their Roman numerals.

I. Wehrli, P. M, **Ge, J**, Michno, W, Koutarapu, S, Dreos, A, Jha, D, Zetterberg, H, Blennow, K, Hanrieder, J. Correlative Chemical Imaging and Spatial Chemometrics Delineate Alzheimer Plaque Heterogeneity at High Spatial Resolution, *JACS Au*, 2023, 3, 762-774.

II. **Ge, J**, Koutarapu, S, Jha, D, Dulewicz, M, Zetterberg, H, Blennow, K, Hanrieder, J. Tetramodal Chemical Imaging Delineates the Lipid-Amyloid Peptide Interplay at Single Plaques in Transgenic Alzheimer's Disease Models, *Anal Chem*, 2023, 95, 4692-4702.

III. **Ge, J***, Dulewicz, M*, Koutarapu, S, Jha, D, Zetterberg, H, Blennow, K, Hanrieder, J. Delineating Aβ Plaque Associated Lipid Co-Aggregation Dynamics Using Pulse-Chase Spatial Multiomics. (Manuscript) (*Contributed equally)

IV. **Ge J***, Pagnon de la Vega M*, Zampar S, Koutarapu, S, Giedraitis V, Lannfelt L, Syvänen S, Hanrieder J[#], Ingelsson M, Sehlin D[#]. The *Uppsala APP* mutation promotes wildtype Aβ aggregation and deposition *in vivo*. (Manuscript) (*Contributed equally)

V. Koutarapu S, **Ge J**, Jha D, Blennow K, Zetterberg H, Lashley T, Michno W, Hanrieder J. Correlative chemical imaging identifies amyloid peptide signatures of neuritic plaques and dystrophy in human sporadic Alzheimer's disease, *Brain Connectivity*, 2022, 13, 297-306.

VI. Koutarapu S*, **Ge J***, Dulewicz, M*, Srikrishna M, Szadziewska A, Wood J, Blennow K, Zetterberg H, Michno W, Natalie S Ryan, Lashley T, Savas J, Schöll M, Hanrieder J. Chemical imaging delineates Aβ plaque polymorphism across the Alzheimer's disease spectrum. (Manuscript) (*Contributed equally)

Additional studies carried out during the PhD period, but not included in the thesis:

1. Rao, N. R., DeGulis, O., Nomura, T., Lee, S., Hark, T. J., Dynes, J. C., Dexter, E. X., Dulewicz, M., **Ge, J.**, Upadhyay, A., Fornasiero, E. F., Vassar, R., Hanrieder, J., Contractor, A., and Savas, J. N. Levetiracetam prevents Aβ42 production through SV2a-dependent modulation of App processing in Alzheimer's disease models, bioRxiv, https://doi.org/10.1101/2024.10.28.620698.
2. Wood, J. I., Dulewicz, M., **Ge, J.**, Stringer, K., Szadziewska, A., Desai, S., Koutarapu, S., Hajar, H. B., Blennow, K., Zetterberg, H., Cummings, D. M., Savas, J. N., Edwards, F. A., and Hanrieder, J. Isotope Encoded chemical Imaging Identifies Amyloid Plaque Age Dependent Structural Maturation, Synaptic Loss, and Increased Toxicity, bioRxiv, https://doi.org/10.1101/2024.10.08.617019.
3. Kasri, A., Camporesi, E., Gkanatsiou, E., Boluda, S., Brinkmalm, G., Stimmer, L., **Ge, J.**, Hanrieder, J., Villain, N., Duyckaerts, C., Vermeiren, Y., Pape, S. E., Nicolas, G., Laquerrière, A., De Deyn, P. P., Wallon, D., Blennow, K., Strydom, A., Zetterberg, H., and Potier, M.-C. Amyloid-β peptide signature associated with cerebral amyloid angiopathy in familial Alzheimer's disease with *APP*dup and Down syndrome,
   Acta Neuropathol. 2024, 148, 8.
4. Klingstedt, T., Lantz, L., Shirani, H., **Ge, J.**, Hanrieder, J., Vidal, R., Ghetti, B., and Nilsson, K. P. R. Thiophene-Based Ligands for Specific Assignment of Distinct Aβ Pathologies in Alzheimer's Disease,
   ACS Chem. Neurosci. 2024, 15, 1581-1595.
5. Michno, W., Bowman, A., Jha, D., Minta, K., **Ge, J.**, Koutarapu, S., Zetterberg, H., Blennow, K., Lashley, T., Heeren, R. M. A., Hanrieder, J. Spatial Neurolipidomics at the Single Amyloid-β Plaque Level in Postmortem Human Alzheimer's Disease Brain,
   ACS Chem. Neurosci. 2024, 15, 877−888.
6. Dreos, A., **Ge, J.**, Najera, F., Tebikachew, B. E., Perez-Inestrosa, E., Moth-Poulsen, K., Blennow, K., Zetterberg, H., Hanrieder, J. Investigating New Applications of a Photoswitchable Fluorescent Norbornadiene as a Multifunctional Probe for Delineation of Amyloid Plaque Polymorphism,
   ACS Sensors, 2023, 8, 1500-1509.

7. Michno, W., Koutarapu, S., Camacho, R., Toomey, C., Stringer, K., Minta, K., **Ge, J.**, Jha, D., Fernandez-Rodriguez, J., Brinkmalm, G., Zetterberg, H., Blennow, K., Ryan, N. S., Lashley, T., Hanrieder, J., et al. Chemical traits of cerebral amyloid angiopathy in familial British-, Danish- and non-Alzheimer's dementias,
   J Neurochem, 2022, 136, 233-246.
8. Michno, W., Wehrli, P. M., Koutarapu, S., Marsching, C., Minta, K., **Ge, J.**, Meyer, S. W., Zetterberg, H., Blennow, K., Henkel, C., Oetjen, J., Hopf, C., Hanrieder, J. Structural amyloid plaque polymorphism is associated with distinct lipid accumulations revealed by trapped ion mobility mass spectrometry imaging,
   J Neurochem, 2021, 160(4):482-498.

CONTENTS

ABBREVIATIONS

AD	Alzheimer's disease
3-APH	3-Aminophthalhydrazide
9-AA	9-Aminoacridine
ABCA7	ATP-binding cassette subfamily A member 7
AICD	APP intracellular domain
APH1	Anterior pharynx defective 1
AP-MALDI	Atmospheric pressure MALDI
APOE	Apolipoprotein E
APP	Amyloid precursor protein
APPArc	The Arctic mutation of the APP
APPSwe	The Swedish mutation of the APP
APPUpp	The Uppsala mutation of the APP
Aβ	Amyloid-beta
Aβwt	Wild-type Aβ
BACE1	β-Site APP-cleaving enzymes 1
BACE2	β-Site APP-cleaving enzymes 2
CAA	Cerebral amyloid angiopathy
Cer	Ceramide
CG	Coarse grain plaques

CHCA	α-Cyano-4-hydroxycinnamic acid
CNS	Central nervous system
CP	Cored plaques
CR	Congo red
CSF	Cerebrospinal fluid
CU-AP	Cognitively unaffected amyloid-positive
CWP	Cotton wool plaque
DAG	Diacylglycerol
1,5-DAN	1,5-Diaminonaphthalene
DESI	Desorption electrospray ionization
DHB	2,5-dihydroxybenzoic acid
DL	Deep learning
DMCA	3,4-Dimethoxycinnamic acid
DN	Dystrophic neurites
DP	Diffuse plaques
EOAD	Early-onset AD
ER	Endoplasmic reticulum
fAD	Familial Alzheimer's disease
FDG	18F-fluorodeoxyglucose
FFPE	Formalin-fixed, paraffin-embedded
FTD	Frontotemporal dementia

FTICR	Fourier transform ion cyclotron resonance
GM	Monosialylgangliosides
GWAS	Genome-wide association studies
HCA	Hierarchical clustering analysis
HDL	High-density lipoproteins
h-FTAA	Heptameric formyl thiophene acetic acid
IHC	Immunohistochemistry
IL-6	Interleukin-6
IT	Ion trap
ITO	Indium tin oxide
KPI	Kunitz protease inhibitor
LacCer	Lactosylceramide
LCO	Luminescent oligothiophenes
LDAM	Lipid-droplet-accumulating microglia
LDL	Low-density lipoproteins
LDs	Lipid droplets
LOAD	Late-onset AD
LPC	Lysophosphatidylcholine
LPI	Lysophosphatidylinositol
LRP1	Lipoprotein receptor-related protein 1

MALDI-MSI	Matrix-assisted laser desorption/ionization mass spectrometry imaging
MCI	Mild cognitive impairment
MRI	Magnetic resonance imaging
NanoSIMS	Nanoscale secondary ion imaging
NCSTN	Nicastrin
NEDC	N-(1-naphthyl)ethylenediamine dihydrochloride
NPs	Neuritic plaques
NTs	Neurotransmitters
OPLS-DA	Orthogonal projections to latent structures Discriminant Analysis
PA	Phosphatidic acids
PC	Phosphatidylcholine
PCA	Principal components analysis
PE	Phosphoethanolamines
PEN2	Presenilin enhancer 2
PET	Positron emission tomography
PHF	Anti-paired helical filament
PI	Phosphatidylinositol
PIB	Pittsburgh compound B
PI3K	Phosphoinositide 3-kinase
PIP2	Phosphoinositide bisphosphate

PLC	Phospholipase C
PP1	Protein phosphatases 1
PP2A	Protein phosphatases 2A
PS	Phosphatidylserine
PSEN	Presenilin
p-tau	Phosphorylated tau
q-FTAA	Tetra formyl thiophene acetic acid
Q-TOF	Quadrupole time-of-flight
ROIs	Regions of interest
ROS	Reactive oxygen species
S1P	Sphingosine-1-phosphate
sAD	Sporadic Alzheimer's disease
sAPPα	Soluble APPα
sAPPβ	Soluble APPβ
SEs	Sterol esters
SILAC	Stable isotope labeling by amino acids in cell culture
SILK	Stable isotope labeling kinetics
SIMS	Secondary ion MS
SM	Sphingomyelin
So	Sphingosine
SPLs	Sphingolipids

ST	Sulfatide
TAGs	Triacylglycerols
TGN	Trans-Golgi network
THAP	2,4,6-Trihydroxyacetophenone
TIC	Total ion count
TOF	Time-of-flight
TREM2	Triggering receptor expressed on myeloid cells 2
WFFM	Wide-field fluorescence microscopy
α-CTF	α-Carboxy-terminal fragment

1 INTRODUCTION

1.1 ALZHEIMER'S DISEASE

1.1.1 HISTORY AND EPIDEMIOLOGY

Alzheimer's disease (AD) is the most common form of dementia, accounting for almost 60% to 80% of all dementia cases[1]. It was first reported by Alois Alzheimer, a German psychiatrist and neuropathologist. His discovery originated from his evaluation of a 51-year-old female patient who exhibited symptoms of presenile dementia. Upon conducting a postmortem examination of her brain, Alzheimer identified two key pathological features—senile plaques and neurofibrillary tangles—which he recognized as distinctive markers of this new disorder, later named Alzheimer's disease[2]. He recognized that dementia is not an inevitable result of aging but a distinct neurocognitive disorder, thus opening a new era for clinical research and treatment of dementia.

Over time, research on AD has expanded significantly, broadening our understanding of its pathology. AD is a chronic neurodegenerative disease marked by a progressive decline in memory and cognitive abilities. Clinically, AD is categorized into two main types: sporadic Alzheimer's disease (sAD) and familial Alzheimer's disease (fAD). Sporadic AD, also known as late-onset AD (LOAD), typically affects individuals over the age of 65 and accounts for the majority of AD cases. In contrast, fAD, or early-onset AD (EOAD), affects individuals younger than 65 and has a strong genetic basis. Early-onset AD comprises only 4-5% of total cases, it is associated with specific genetic mutations that increase disease susceptibility[3].

Today, one in three elderly die from AD and other dementias, as there is currently no cure. It is estimated that 50 million people suffer from dementia, and the prevalence is predicted to triple by 2050[4]. This elevates the risk of disability, increases the burden of illness, and drives up healthcare costs. The current annual cost of AD and other dementias in the United States stands at $305 billion, a figure projected to exceed $1.1 trillion by 2050[1]. This immense economic burden encompasses not only healthcare and hospice expenses for AD patients but also accounts for lost productivity among both patients and caregivers. Moreover, the exact causes of the disease remain unknown, which significantly hampers the development of effective treatment strategies.

1.1.2 CLINICAL SYMPTOMS AND DIAGNOSIS

AD is estimated to begin 20–30 years prior to the onset of clinical symptoms, initiating with a preclinical phase where individuals show no overt symptoms but display measurable changes in brain biology[5]. During preclinical AD, pathological hallmarks such as amyloid-beta (Aβ) and tau protein deposits accumulate, and glucose metabolism in certain brain regions may decrease. Despite these changes, patients maintain normal function, with no visible cognitive decline.

As AD progresses, many patients transition to mild cognitive impairment (MCI), characterized by subtle memory, language, or spatial skill deficits that generally do not disrupt daily activities[6]. Symptoms at this stage usually emerge gradually and become more pronounced over time.
In later stages, AD advances to dementia, where significant cognitive decline is evident. Memory loss, confusion, and impaired reasoning and decision-making interfere considerably with daily life. In the severe stages, patients often experience profound cognitive impairment and ultimately lose the ability to care for themselves, necessitating comprehensive support for basic activities. This continuum from preclinical AD to severe dementia underscores the critical importance of early detection and intervention in managing AD[7, 8].

Over the decades, a range of clinical, imaging, and laboratory techniques has been developed to improve the accuracy of AD diagnosis. For example, biomarkers such as reduced Aβ levels, along with elevated tau and phosphorylated tau (p-tau) in cerebrospinal fluid (CSF) and blood, serve as key indicators for diagnosing AD[9-13].

Additionally, magnetic resonance imaging (MRI) is capable of detecting atrophy in the hippocampus and temporal cortex, which are critical regions associated with memory and cognitive function. Alongside MRI, positron emission tomography (PET) utilizes various tracers, such as Pittsburgh compound B (PIB), to visualize the accumulation of Aβ in the brains of AD patients[14, 15]. PET imaging serves as a valuable tool not only for identifying Aβ accumulation but also for assessing disease-related alterations in cerebral metabolism using ^{18}F-fluorodeoxyglucose (FDG)[16, 17]. This combination of imaging techniques provides comprehensive insights into the structural and functional changes occurring in the brain during the progression of AD.

1.2 AMYLOID PATHOLOGY

1.2.1 AMYLOID PEPTIDE GENERATION

The hallmark of AD is the progressive accumulation of Aβ and hyperphosphorylated-tau protein, into intra- and extracellular deposits (Aβ plaques and Tau tangles) (Figure 1)[18]. Extracellular Aβ plaques are composed of Aβ peptide, originated from sequential cleavage of amyloid precursor protein (APP) by β- and γ-secretase enzymes to a length of 38–43 amino acid residues[19-21].

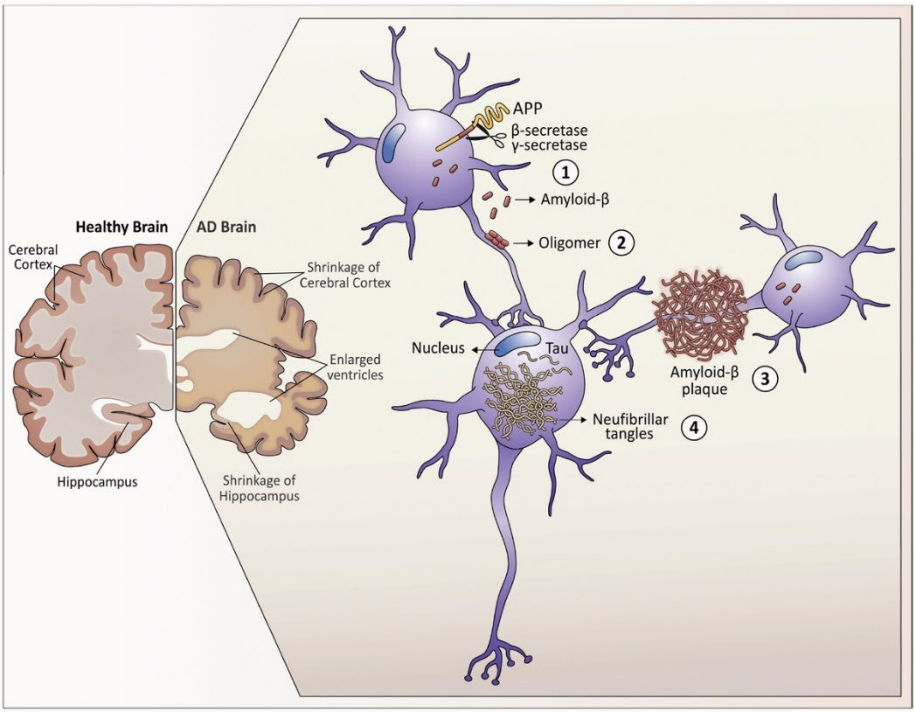

Figure 1. The hallmarks of Alzheimer's disease: progressive accumulation of Aβ and hyperphosphorylated-tau protein, into intra- and extracellular deposits (Aβ plaques and Tau tangles)[22].

1.2.1.1 AMYLOID PRECURSOR PROTEIN

Amyloid precursor protein (APP) is a type I single-pass transmembrane protein encoded by a single gene located on chromosome 21. APP is known to have three primary isoforms—APP695, APP751, and APP770—along with several less common variants, including APP714, APP639, and four leukocyte-

derived forms: APP677, APP696, APP733, and APP752[23]. These isoforms arise from alternative splicing of the *APP* gene[24].

The three main isoforms exhibit differences in protein structure and tissue distribution. Specifically, APP695 lacks the Kunitz protease inhibitor (KPI) domain, making it KPI negative (-), and is predominantly found in the brain. In contrast, APP751 and APP770 contain the KPI domain, categorizing them as KPI positive (+), and are expressed throughout a wider range of tissues[25, 26].

Proteins in the APP family serve a variety of critical functions essential for neuronal development and function. These proteins play a pivotal role in neurogenesis, influencing the proliferation and differentiation of neural stem cells into mature neurons[27, 28]. They also facilitate the growth and guidance of axons, which is vital for establishing proper neuronal connections during brain development[29, 30].

Additionally, APP family proteins are crucial for maintaining the density and dynamics of dendritic spines, which are essential for synaptic plasticity and overall cognitive function. By regulating the formation and stability of these spines, these proteins enhance synaptic transmission and communication between neurons[31-33]. Moreover, APP family proteins are implicated in neuroprotective mechanisms and may help modulate responses to cellular stress, underscoring their significance in maintaining neuronal health. The diverse roles of APP family proteins highlight their importance in both normal brain function and the pathophysiology of neurodegenerative diseases.

1.2.1.2 APP PROCESSING

The Aβ peptide is generated from the cleavage of the APP by the β-secretase and γ-secretase enzymes. There are two major different pathways for the processing of APP, commonly referred to as the non-amyloidogenic and the amyloidogenic pathways[34]. There are typically three different classes of enzymes involved in these two pathways, the α- and β-secretase, and β- and γ-secretase.

In the amyloidogenic pathway of APP processing, APP is initially cleaved by β-secretase (BACE), producing soluble APPβ (sAPPβ) and a membrane-bound fragment, APP-CTF (C99)[35, 36]. The C99 fragment is subsequently cleaved by γ-secretase, resulting in the extracellular release of Aβ and the generation of the APP intracellular domain (AICD), which may translocate to the nucleus[37]. In the non-amyloidogenic pathway, however, APP is first cleaved by α-

secretase, generating soluble APPα (sAPPα) and a different membrane-bound fragment, APP-CTF (C83). When γ-secretase cleaves C83, it produces p3 and AICD, thereby circumventing Aβ production altogether[38].

The α-secretases, which include ADAM9, ADAM10, and ADAM17, are plasma membrane-bound proteases that belong to the family of zinc metalloproteases[39, 40]. These enzymes primarily cleave the APP at the neuronal surface, with some activity occurring in the trans-Golgi network (TGN)[41]. Their cleavage of APP typically leads to the formation of sAPPα and the α-carboxy-terminal fragment (α-CTF) through the non-amyloidogenic pathway. In addition to their role in APP processing, α-secretases also participate in the cleavage of various other substrates, including interleukin-6 (IL-6), cadherins, and Notch receptors[42].

The β-site APP-cleaving enzymes 1 and 2 (BACE1 and BACE2), are transmembrane proteases that are responsible for β-secretase activity. BACE1 is primarily active in the TGN and endosomes, where its enzymatic activity depends on an acidic environment. This enzyme is essential for the production of Aβ[43, 44].

In contrast, BACE2, while structurally similar to BACE1, does not participate in amyloidogenesis and is primarily involved in the processing of other substrates. In brain tissue, the expression of BACE2 is significantly lower than that of BACE1, indicating that BACE1 activity predominantly regulates APP cleavage. Consequently, when BACE1 cleaves APP, it generates Aβ, whereas the lower activity of BACE2 results in cleavage occurring within the Aβ sequence. This differential regulation of BACE1 and BACE2 underscores the complexity of APP processing and highlights the significance of BACE1 in the pathogenesis of AD[45, 46].

The γ-secretase is a multi-subunit protease complex that consists of four individual proteins: presenilin (PSEN) 1 or 2, nicastrin (NCSTN), anterior pharynx defective 1 (APH1) and presenilin enhancer 2 (PEN2)[47, 48]. Presenilin (either PSEN1 or PSEN2) forms the catalytic core of the γ-secretase complex, and mutations in these genes have been linked to early-onset familial Alzheimer's disease. These four components are necessary and sufficient for full γ-secretase activity. When activated, γ-secretase cleaves off the C-terminal fragment of APP to generate Aβ. Cleavage by γ-secretase has traditionally been thought to yield either Aβ 1-40 or Aβ 1-42, along with AICD. However, recent research has revealed that the γ-secretase cleavage is more intricate,

involving additional cleavage sites known as the γ-site, ζ-site, and ε-site[49, 50]. The γ-site defines the final length of Aβ, ending at either Aβ 1-40 or Aβ 1-42, while the ε-site generates AICD, beginning at Aβ 1-49 or Aβ 1-50. The identification of these sites has clarified sequence gaps and led to the discovery of an intermediate ζ-cleavage at Aβ 1-46. Aβ peptides are then further processed through sequential trimming along two main pathways. In the Aβ 1-40 product line, tripeptide trimming occurs along Aβ 1-49 to 46, 43, 40, and finally 37. In the Aβ 1-42 product line, tetrapeptide trimming follows the sequence Aβ1- 48 to 45, 42, and finally 38[51, 52]. Additionally, other Aβ peptides of varying lengths emerge, reflecting multiple interactive cleavage pathways and resulting in the release of tri-, tetra-, penta-, and hexapeptides. These pathways are associated with the main Aβ 1-40 and Aβ 1-42 lines, highlighting the complexity of Aβ generation and its relevance to neurodegenerative diseases.

1.2.2 AMYLOID PEPTIDE AGGREGATION

Aβ peptide sequences contain regions with distinct structural propensities that significantly contribute to their aggregation. Notably, the highly hydrophobic core sequence, residues 17-21 (KLVFFA), is a key aggregation-prone segment that promotes insoluble fibril formation[53, 54]. The tendency for aggregation increases with peptide length, making longer peptides (e.g., Aβ 1-42) more prone to aggregation than shorter forms (e.g., Aβ 1-40)[55, 56]. This variation in aggregation behavior is believed to underlie the differing pathological effects of these peptides in AD.

The aggregation process begins at the monomeric level. Misfolded Aβ monomers often form β-hairpin structures through interactions between their C-terminal and central regions, serving as initial seeds for aggregation. These monomers first associate into lower-order aggregates, such as dimers and trimers, which then self-assemble into higher-order oligomers. Oligomers are considered highly toxic intermediates, potentially exerting neurotoxic effects before forming larger aggregates. As aggregation advances, oligomers transition into protofibrils, which eventually elongate and stabilize into mature amyloid fibrils[57, 58].

The fibrillization of Aβ proceeds through three key steps: primary nucleation, secondary nucleation, and elongation. In primary nucleation, monomers bind together in a manner that enables their addition to occur more rapidly than their dissociation. Secondary nucleation usually produces nuclei from monomers in a reaction catalyzed by already existing aggregates of the same monomer type.

Elongation expands fibrillary aggregates through monomer addition (Figure 2)[59-61]. It is believed that toxic species are predominantly generated during secondary nucleation.

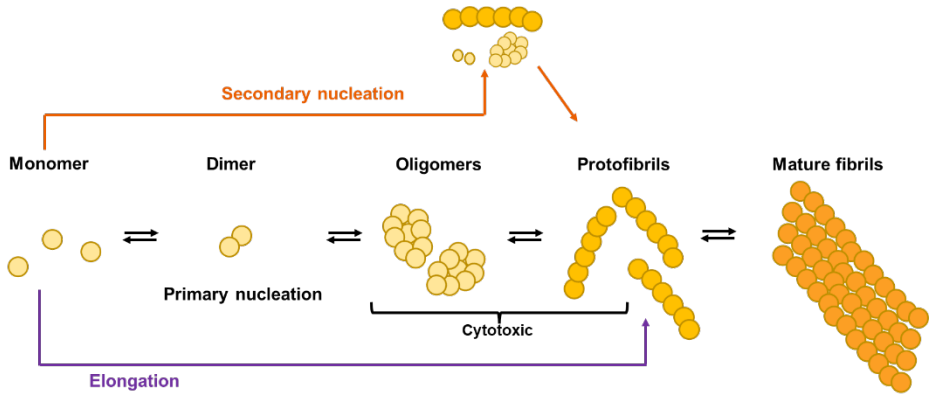

Figure 2. Amyloid-β aggregation. Soluble Aβ monomers aggregate progressively, forming oligomers and protofibrils, which eventually assemble into insoluble fibrils.

The mature amyloid fibrils further adopt a characteristic cross-β-sheet structure—a hallmark of amyloid pathology—and exhibit substantial stability, allowing them to persist in the brain for extended periods. These fibrils cluster into larger plaque structures, where Aβ 1-40 and Aβ 1-42 peptides, along with other cellular components, form thermodynamically stable "sinks" that sequester Aβ into highly insoluble deposits.

1.2.3 THE AMYLOID CASCADE HYPOTHESIS

Numerous theories have been proposed to explain the neurodegenerative processes in AD, with the amyloid cascade hypothesis being the most widely accepted, despite ongoing debate and potential contradictions.

The amyloid cascade hypothesis, now over 30 years old, states that the accumulation of Aβ is the primary trigger for a cascade of molecular events leading to neurodegeneration[62]. According to this hypothesis, Aβ buildup initiates processes that promote the formation of hyperphosphorylated tau aggregates, activation of neuronal death pathways, and, ultimately, the progression to dementia.

Over time, as AD research has progressed, the amyloid cascade hypothesis has faced significant challenges. For example, multiple studies have shown that

the accumulation of senile plaques does not consistently correlate with cognitive decline[63-65]. Furthermore, Aβ pathology has been observed in cognitively healthy older individuals[66, 67]. Increased Aβ production is not a characteristic associated with many fAD mutations. In fact, several fAD mutations have been linked to a reduction in Aβ production.

Consequently, research has shifted focus to other forms of Aβ that may play a more central role in disease progression. In particular, soluble Aβ oligomers are now considered more cytotoxic than the fibrillar Aβ found in plaques[68-70]. The selective toxicity of these oligomers in cellular models has provided additional support for their potential role in AD pathogenesis.

Senile plaques, which consist of post-translationally modified, oxidized, and truncated Aβ in fibrillar β-sheet conformations, likely represent a later stage of aggregation that may occur over many years. These plaques accumulate well before clinical symptoms appear and may be less directly involved in AD pathogenesis than their precursor oligomers[71, 72]. This distinction emphasizes the importance of early aggregation intermediates, which are now thought to play a more active role in neuronal damage than the mature plaques themselves.

In addition to the primary criticism regarding the lack of correlation between cognitive function and amyloid deposition, further evidence from clinical trials and epidemiological studies reveals that while many interventions have successfully reduced amyloid levels as measured by PET imaging, this reduction has not resulted in clinical benefits[73, 74]. Moreover, anti-Aβ interventions have demonstrated ineffectiveness in patients with fAD[75]. These findings highlight the need for a deeper understanding of amyloid pathology and the molecular mechanisms underlying complex disorders, particularly in relation to genetic mutations.

1.3 Aβ NEUROPATHOLOGY

Amyloid plaques deposited in the extracellular space of the brain parenchyma exhibit diverse morphologies, including cored and diffuse plaques.

Cored plaques, formed by insoluble Aβ aggregates, are also known as congophilic plaques. Their characteristic β-sheet structure allows them to be stained with Congo red (CR)[76] and thioflavin-S[77]. These plaques are associated with dystrophic neurites, inflammation, activated microglia and astrocytes, and

a general loss of synapses and neurons[78, 79]. In contrast, diffuse plaques are not detectable with these staining methods and require anti-Aβ antibodies for visualization. Both cored plaques (CP) and diffuse plaques (DP) are present in sAD. However, diffuse plaques are more common in cognitively unaffected amyloid-positive (CU-AP) individuals, also referred to as pathological aging[80]. Unlike cored plaques, diffuse plaques typically lack abnormal neurites. Specific Aβ isoforms are associated with distinct plaque types. Aβx-40 is found in the cores of amyloid plaques, while Aβx-42 is primarily localized in diffuse aggregates[81-84].

In addition to cored and diffuse plaques, other plaque subtypes have also been identified: cotton wool plaques (CWP) and coarse grain plaques (CG). Cotton wool plaques are large, lack amyloid cores, and are frequently observed in certain presenilin-1 mutant cases of autosomal dominant AD and some non-familial cases[85-87]. A recently identified subtype is coarse grain plaque, which contains multiple small cores and is rich in Aβ1-40. They are associated with advanced AD, *APOE4* homozygosity, and cerebral amyloid angiopathy (CAA) (Figure 3)[88].

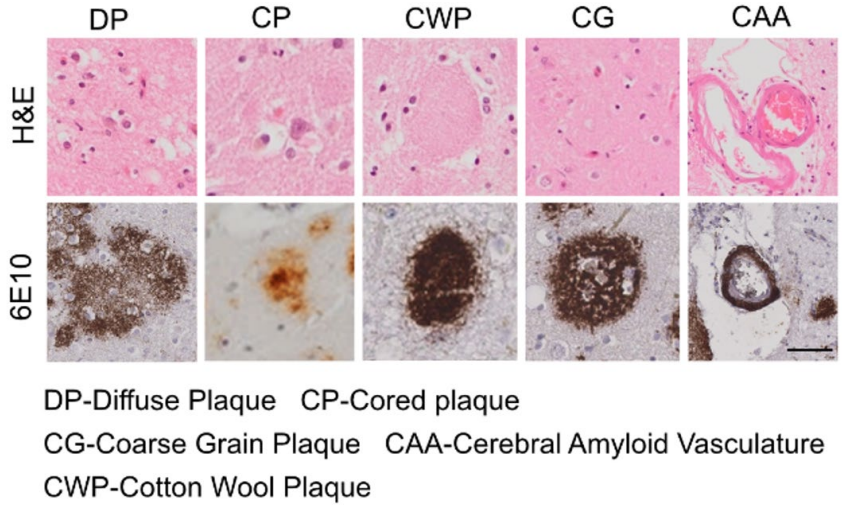

Figure 3. Different types of amyloid plaques, including cored, diffuse, coarse grain and cotton wool plaques, and CAA in AD brains. (Image from Paper VI)

Based on analysis of human brains with different degrees of plaque accumulation, Aβ deposition and spread in AD are well characterized and divided into five phases, which is known as Thal stages. In the first phase, plaques first appear in the neo(iso)cortex. In phase II, the allocortex,

hippocampus, and amygdala are affected. By phase III, plaques develop in the basal ganglia and diencephalon. In phase IV, the plaques spread to the midbrain and medulla oblongata, and in the final phase, they extend to the cerebellar cortex (Figure 4)[89]. However, the progression of the disease is not directly linked to the spread or size of Aβ plaques.

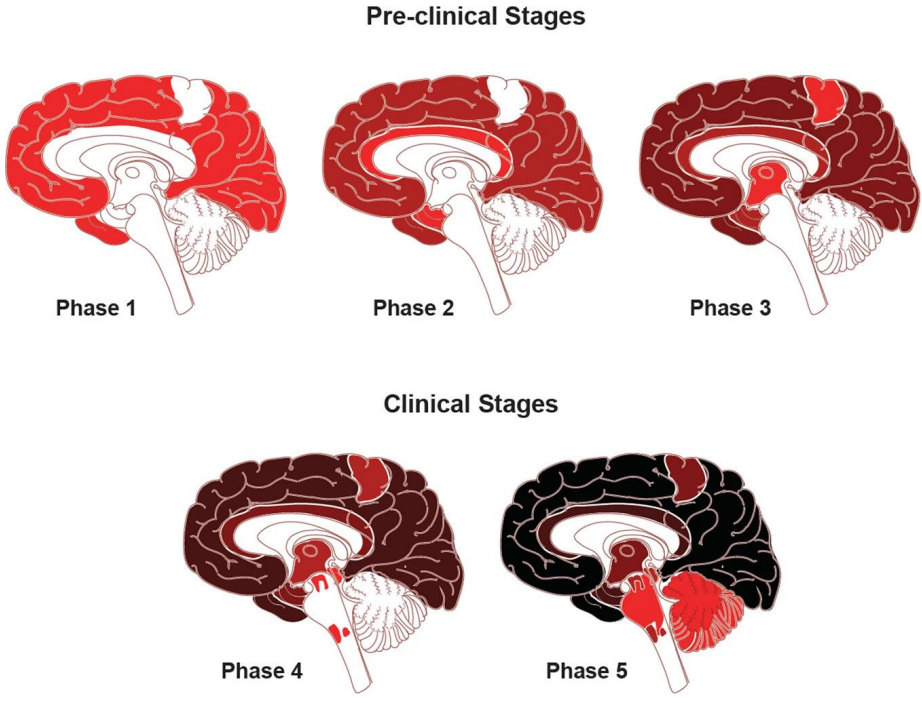

Figure 4. The phases of Aβ plaque distribution in the brain[90].

Apart from the parenchyma plaques, Aβ also deposits in the walls of arteries, arterioles, and sometimes in capillaries and veins within the central nervous system, which is identified as CAA. Recent studies revealed that almost 50% of individuals diagnosed with AD exhibit moderate-to-severe CAA pathology. Large-vessel CAA is considered severe, with arterioles more frequently affected than veins in approximately 25% of end-stage AD patients. Capillary CAA is less common, being severe in approximately 10% of cases. In advanced large-vessel CAA, amyloid deposits often extend through the tunica adventitia into the surrounding parenchyma, which contains tau-immunoreactive abnormal neurites. The amyloid peptides in these CAAs also exhibit heterogeneity. Early-stage large-vessel CAA is characterized by a predominance of Aβ42, whereas Aβ40 becomes more dominant in later stages.

In contrast, capillary CAA is more often associated with Aβ42 than Aβ40. This distinction suggests that the deposition of Aβ in capillaries occurs through a mechanism different from that in large vessels or Aβ plaques (reviewed in [91]).

The characterization of amyloid plaques and CAAs highlights the complexity of amyloid pathology in AD and raises important questions about the underlying molecular mechanisms that drive plaque and CAA formation and their subsequent development. Although significant progress has been made in identifying the different types of plaques and CAAs, the precise molecular events involved in their formation, the extent of their heterogeneity, and their potential neurotoxic effects remain poorly understood. Further research is essential to elucidate these aspects, as it may lead to a better understanding of the relationship between amyloid pathology diversity and the clinical manifestations of AD.

1.4 ALZHEIMER'S DISEASE RISK FACTORS

The primary risk factors for AD include advanced age, particularly in individuals over 65 years old, although this age threshold is not universally defined[92]. Another significant risk factor is the presence of at least one apolipoprotein E (*APOE*) ε4 allele, which is associated with a higher likelihood of developing the disease[93, 94]. Interestingly, sex differences also play a role in the risk of AD, as women are more prone to develop the condition than men, especially after the age of 80[95].

Research indicates that women with Alzheimer's disease tend to exhibit a higher tau burden, even when their levels of amyloid β are similar to those of men[96, 97]. This suggests that gender may influence the underlying pathophysiology of the disease and its progression.

Additionally, several modifiable risk factors contribute to an increased risk of dementia. These include cardiovascular diseases, diabetes, and obesity, all of which have been linked to cognitive decline. Furthermore, lifestyle factors such as poor diet, physical inactivity, and smoking are also associated with a heightened risk of developing AD[98]. Addressing these risk factors through lifestyle modifications and early intervention may be crucial in mitigating the incidence of AD and improving overall cognitive health. Understanding these multifaceted risk factors is essential for developing targeted prevention strategies and enhancing public health initiatives aimed at reducing the burden of Alzheimer's disease in the aging population.

1.4.1 GENETICS FACTORS IN AD

1.4.1.1 AUTOSOMAL DOMINANT GENES IN FAMILLIAL AD

Mutations in the *APP* and *PSEN* genes account for fewer than 2% of all AD cases[99, 100]. However, the majority of genetically resolved cases of early-onset fAD (EOFAD) are attributed to mutations in the *PSEN* genes, which are responsible for up to 70% of EOFAD instances. These mutations alter the enzymatic cleavage of γ-secretase in the C-terminal region of Aβ, resulting in an increased ratio of Aβ1-42 to Aβ1-40, a change that is critical in the pathology of AD[101, 102].

In contrast, *APP* mutations are less common in EOFAD, accounting for only 10% to 15% of cases[99]. These mutations can occur both within and outside the Aβ sequence, and they have been linked to abnormal synaptogenesis and synaptic dysfunction[103, 104]. To date, over 65 *APP* mutations have been documented (Figure 5); however, the pathogenicity of 36 of these mutations remains uncertain. Understanding the mechanisms by which these genetic alterations contribute to the onset and progression of AD is essential for developing targeted therapeutic strategies.

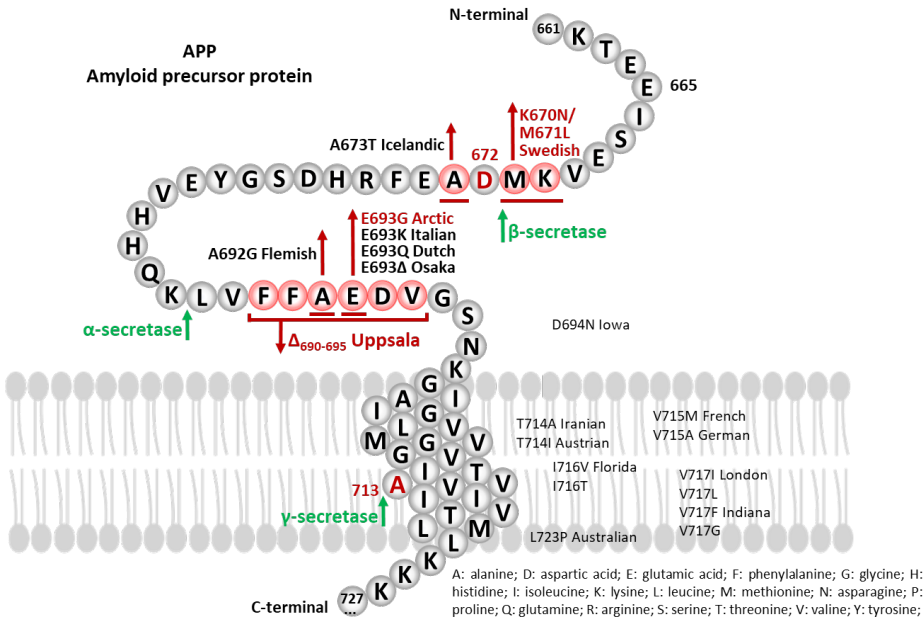

Figure 5. Schematic overview of the APP sequence with some of the mutations. The cleavage sites are marked with green arrows.

Of note, three distinct mutations of the *APP*, the *Swedish* (*APPSwe*), *Arctic* (*APPArc*), and *Uppsala* (*APPUpp*) mutations, have been identified and characterized by our collaborators at Uppsala University.

The *APPSwe* mutation is characterized as a double mutation occurring at codons 670 and 671 of the *APP* gene[105]. This mutation has been shown to enhance β-secretase cleavage, resulting in an increased overall production of Aβ peptides[106].

The *APPArc* mutation is a single point mutation located at codon 693, which has been associated with early-onset AD. Peptides containing this mutation tend to form protofibrils more rapidly and in greater quantities than wild-type Aβ, although the rate of fibrilization remains unchanged[107].

The *APPUpp* mutation is a newly identified alteration characterized by a six-amino-acid deletion within the mid-region of Aβ. This mutation appears to significantly reduce non-amyloidogenic α-secretase processing of APP, leading to the generation of rapidly aggregating Aβ peptides that lack amino acids 19 to 24[108]. Understanding these mutations enhances our knowledge of the mechanisms underlying AD pathology and could inform future therapeutic approaches.

1.4.1.2 GENETICS RISKFACTORS FOR SPORADIC AD

Sporadic AD is characterized by the absence of a documented family history, unlike familial AD[100]. This form of AD is thought to be primarily caused by a failure of the mechanisms responsible for clearing Aβ from the brain, leading to its accumulation and subsequent neurotoxic effects. Studies have shown that sporadic AD is influenced by multiple genetic factors, many of which have been identified through genome-wide association studies (GWAS)[109].

These studies have highlighted several key genomic variants that play an important role in the pathogenesis of sporadic AD. Of these, the *APOE* gene is the best known and is considered the strongest genetic risk factor for late-onset AD[110]. The presence of the *APOE* ε4 allele significantly increases the risk of disease and is associated with an earlier onset and more severe pathology[111].

Within the central nervous system (CNS), the *APOE* gene is expressed by multiple cell types, each responding differently to various physiological and pathological conditions. These investigations of APOE4 at a single-cell resolution have demonstrated that APOE4 is generally produced by diverse

CNS cell types, such as astrocytes, neurons, microglia, oligodendrocytes, and vascular cells, and it plays multifaceted roles in AD pathology[112]. For instance, in astrocytes, APOE4 has been shown to influence lipid metabolism and neuroinflammation[113], while in microglia, it affects phagocytic activity and the immune response to amyloid-beta plaques[114, 115]. In neurons, APOE4 may alter synaptic function and resilience to neurodegenerative processes[116, 117]. The identification of these cell type-specific effects of APOE4 underscores the complexity of its contributions to AD and highlights the need for targeted therapeutic strategies that consider the diverse roles of APOE in the CNS.

Other notable genetic variants discovered through GWAS include *TREM2* (triggering receptor expressed on myeloid cells 2)[118] and *ABCA7* (ATP-binding cassette subfamily A member 7)[119]. Variants in the *TREM2* gene are associated with increased risk of AD, likely due to their role in immune responses and inflammation in the central nervous system. TREM2 is a transmembrane glycoprotein receptor located on the cell surface, and it plays a crucial role in various biological processes, including phagocytosis, inflammatory signaling, as well as myeloid cell proliferation, migration, and survival[120, 121]. The activation of TREM2 can be triggered by a diverse array of ligands, including lipids and proteins such as phospholipids, high-density lipoproteins (HDL), low-density lipoproteins (LDL), as well as APOE and Aβ[122]. Notably, the variants R47H and R62H in the *TREM2* gene have been associated with an increased risk of AD[123]. These mutations are known to reduce the binding affinity between TREM2 and APOE, which may impair the receptor's function and contribute to the pathogenesis of the disease. Moreover, TREM2 deficiency has been shown to significantly impair the ability of microglia to migrate toward apoptotic neurons, which is a critical aspect of the neuroinflammatory response.

ABCA7 is identified to be involved in lipid metabolism and production and clearance of Aβ[124, 125], further supporting the link between genetic factors and amyloid clearance mechanisms.

The interplay between these genetic variants and environmental factors contributes to the complex etiology of sporadic AD, highlighting the need for a comprehensive understanding of how these factors interact to influence disease development and progression. Future studies should focus on elucidating the molecular pathways affected by these genomic variants and exploring potential therapeutic strategies aimed at enhancing Aβ clearance and

mitigating the impact of genetic risk factors on the development of Alzheimer's disease.

1.4.2 ROLES OF LIPIDS IN AD PATHOLOGY

In 1907, the presence of 'adipose inclusions' or 'lipoid granules' in the brains of patients with AD has been described as the third hallmark of AD by Alois Alzheimer[126]. Over the decades, there is mounting evidence suggesting that changes in the neuronal lipid biochemistry are essentially associated with protein misfolding and amyloidogenic aggregation into mature, neurotoxic plaques. It has been found that neuronal lipids are implicated in controlling trafficking and activity of membrane-bound proteins in Aβ production and processing, modulating the aggregation propensity of the peptide[127]. *APOE4* has been identified as the most significant risk factor for developing AD[111]. APOE is a lipid-binding protein that plays a crucial role in maintaining cholesterol homeostasis[128], suggesting a critical role of lipid in AD pathology. This is further supported by the fact that TREM2 is implicated in neuronal and synaptic damage induced by microgliosis[129]. Also, several potential loss-of-function *ABCA7* mutations and deletions have been identified to be linked to AD[130]. This emphasizes the need for advanced research tools that feature the necessary sensitivity and specificity to delineate molecular events on a subcellular level.

1.4.2.1 CHOLESTEROL INVOLVED IN PATHOGENESIS OF AD

Cholesterol is a major component of cellular membranes. It is essential for maintaining membrane fluidity, preventing fatty acid crystallization, and reducing permeability to water-soluble molecules[131, 132]. Cholesterol is abundant in lipid rafts, which supports the anchoring of functional molecules, including membrane receptors[133-135]. In neurons, cholesterol is particularly abundant in myelin sheaths, facilitating saltatory nerve impulse propagation[136-138].

Neurons acquire cholesterol either by synthesizing it or by recapturing it from the extracellular environment. Once synthesized, free cholesterol binds to APOE and is transported across the cell membrane via the ABCA1 transporter. It then binds to low-density lipoprotein receptor-related protein 1 (LRP1) on the neuronal membrane, allowing internalization into the endolysosomal compartment[139]. Here, APOE is degraded, and free cholesterol is released and reintegrated into cholesterol-enriched membrane domains.

Key proteins implicated in AD pathology, including APP, BACE1, and the γ-secretase complex, localize within lipid rafts, underscoring cholesterol's potential role in their processing activities.

1.4.2.2 SPHINGOLIPIDS INVOLVED IN PATHOGENESIS OF AD

Sphingolipids (SPLs) constitute a structurally intricate and diverse class of lipids that include key compounds such as sphingosine (So), ceramide (Cer), sphingomyelin (SM), sphingosine-1-phosphate (S1P), glucosylceramide, and acidic glycosphingolipids, especially gangliosides and sulfatides[140]. Enriched in the CNS, these SPL metabolites are essential for maintaining the structural and functional integrity of neuronal cells[141]. Emerging evidence suggests that SPLs play a pivotal role in the progression of neurodegenerative diseases, including AD, where their dysregulation may contribute to pathological processes.

The monosialylgangliosides (GM), a glycosphingolipid predominantly located in CNS membrane fractions, have gained particular interest for their potential role in AD. Analyses of human brain ganglioside content across individuals aged 20 to 100 have shown that ganglioside patterns change with normal aging and are further altered in neurodegenerative conditions such as AD[142].

Specifically, levels and expression patterns of GM1 are believed to modulate AD pathology through interactions with Aβ peptides[143]. Research indicates that GM1 may facilitate the aggregation of neurotoxic Aβ fibrils on cell surfaces, contributing to the pathological formation of amyloid plaques[144]. Clustering of GM1 within membrane microdomains, or "lipid rafts", appears essential for this interaction. Within these domains, GM1 may drive the initial deposition and nucleation of Aβ fibrils by stabilizing conformational changes in Aβ that promote aggregation[145]. This pro-aggregative role of GM1 underscores the intricate relationship between lipid metabolism and protein misfolding in AD, positioning SPLs as mediators in these processes.

Since SPLs like GM1 are known to impact membrane fluidity, receptor activity, and signal transduction, alterations in ganglioside composition may disrupt neuronal signaling pathways, contributing to the synaptic dysfunction observed in AD.

Besides GMs, ceramides are involved in AD pathology as well. Ceramide activation of protein phosphatases 1 (PP1) and protein phosphatases 2A (PP2A) has been reported to be involved in apoptosis induction[146]. Moreover,

it was previously reported that both CerP and PE-Cer were suggested to prevent ceramide-induced apoptosis and might indicate the mechanism of cellular defense during Aβ seeding[147]. Further, sphingomyelin, as a major component of cell membranes and myelin, can interact with TREM2[148-150] and/or TAM receptors[151] after their exposure on the cell surface for marking the cells out for clearance.

Sulfatides (STs) are lipids found in the myelin sheath surrounding axons, primarily synthesized by oligodendrocytes[152, 153]. These lipids play crucial roles in oligodendrocyte differentiation and survival, myelin maintenance, glia-axon interactions, and the proper localization of axonal proteins[154-159]. Alterations in sulfatide levels in human brain tissue have been linked to neurodegenerative diseases, including AD, multiple sclerosis, and Parkinson's disease[160-162]. Notably, it has been reported that sulfatides are significantly depleted in the earliest clinically recognizable stages of AD, as well as in preclinical stages[163-165]. In addition, APOE is involved in the regulation of sulfatide transport and turnover in the brain, and adult-onset sulfatide deficiency has been shown to induce neuroinflammation and cognitive impairment, resembling AD pathology[166-168]. Furthermore, our previous studies have demonstrated that sulfatide deficiency is associated with plaque pathology in transgenic AD mouse models[169, 170].

In recent years, growing evidence has highlighted the crucial role of lactosylceramide (LacCer) in the progression of neurodegeneration[171]. LacCer is an important intermediate in sphingolipid synthesis. As a biologically active sphingolipid, it participates directly in cell signaling and can be broken down in ganglia, exerting significant effects in the body through the involvement of active enzymes, glycosides, and lipid rafts[172, 173]. LacCer has been shown to contribute to neurodegeneration by activating astrocytes, leading to neuroinflammation. Induction by pro-inflammatory factors and toxic substances promotes LacCer accumulation in cells, which activates the Ras-MEK-ERK1/2 and IκB/NF-κB pathways, driving astrocyte proliferation and neuronal apoptosis[174].

Furthermore, recent studies have linked plasma LacCer concentrations to cognitive performance, and showed that genetically modified LacCer levels being associated with AD risk[175]. LacCer is a central intermediate in the synthesis of complex sphingolipids and serves as the precursor for all gangliosides[176]. Gangliosides have been reported to be associated with amyloid

pathology. Therefore, as alterations in LacCer levels are implicated in changes to gangliosides, this highlights its potential role in AD pathology.

Therefore, elucidating the roles of SPLs, particularly gangliosides like GM1, ceramides and LacCer could yield critical insights into lipid-related mechanisms underlying AD pathology and inspire new therapeutic approaches aimed at modulating SPL metabolism and function in the brain.

1.4.2.3 PHOSPHOLIPIDS INVOLVED IN PATHOGENESIS OF AD

Phospholipids also play a crucial role in the progression of AD, and alterations in their metabolism can significantly impact disease pathology. Lysophosphatidylinositol (LPI) and phosphatidylinositol (PI) are frequently associated with phosphoinositide bisphosphate (PIP2) species, which are involved in signaling pathways relevant to AD. Acting as a second messenger, PIP2 can participate in phospholipase C (PLC) signaling to generate diacylglycerol (DAG) or engage in phosphoinositide 3-kinase (PI3K) signaling to recruit protein complexes to the cell membrane[177]. Additionally, LPI serves as an endogenous ligand for GPR55, a receptor increasingly linked to neurodegenerative diseases[178]. This evidence suggests that both LPI and PI may contribute to Aβ plaque pathology and AD progression.

Research using MALDI-MSI has shown altered lipid profiles in transgenic AD models, such as the 5xFAD mouse model with increased lysophosphatidylcholine (LPC) and decreased phosphatidylcholine (PC) levels[179]. Elevated LPC levels are associated with enhanced Aβ oligomer formation, contributing to AD pathology through mechanisms like focal demyelination and disruption of myelin lipid integrity. LPC accumulation in amyloid plaques may also amplify Aβ oligomerization and fibrillation, potentially accelerating plaque formation and driving neuronal damage[180, 181].

The effect of LPC on myelin integrity may further exacerbate neurodegeneration in AD. By altering myelin lipid composition, LPC may induce focal demyelination, impair neuronal function, and contribute to cognitive decline[182]. These findings underscore the potential roles of LPI, PI, LPC, and PC in AD-related neurodegenerative processes and highlight the importance of lipid metabolism in AD pathology. This area of research offers promising insights into therapeutic strategies that target phospholipid signaling and metabolism for AD prevention and treatment.

1.4.2.4 OTHER LIPIDS INVOLVED IN AD PATHOGENESIS

Recent research has focused on the biology of lipid droplets (LDs) in the brain, revealing their significant roles in cellular lipid turnover and stress response[183]. LDs are dynamic organelles within the cell cytoplasm that contribute substrates for energy metabolism, provide building blocks for biological membranes, and produce signaling molecule precursors[184]. Additionally, they act as a buffer against lipotoxicity. LDs are thought to originate *de novo* in the endoplasmic reticulum (ER) [185].Structurally, LDs consist of a hydrophobic core filled with neutral lipids—such as triacylglycerols (TAGs), sterol esters (SEs), and acylceramides—encased in a phospholipid monolayer, which contains various proteins on its surface and embedded within.

Under normal physiological conditions, LD levels in the brain are low; however, their accumulation increases during development, aging, and various pathological states, including neurodegenerative diseases, cancer, and stroke[186]. This accumulation is particularly prominent in neuroglia, such as astrocytes and microglia, and is seldom observed in neurons.

In the aging brain, a novel state of microglia has been identified in which these cells accumulate lipid droplets, termed 'lipid-droplet-accumulating microglia' (LDAM). LDAM displays a distinct transcriptional profile, exhibits impaired phagocytic function, generates elevated levels of reactive oxygen species (ROS), and releases increased amounts of proinflammatory cytokines. Specific genes—including *SLC33A1*, *SNX17*, *VPS35*, *CLN3*, *NPC2*, and *GRN*—have been identified as genetic regulators of lipid-droplet formation in microglia, with mutations in these genes associated with autosomal-dominant neurodegenerative disorders. Furthermore, studies have validated the presence of LDAM in $Grn^{-/-}$ mice, which model frontotemporal dementia (FTD), supporting the link between lipid-droplet accumulation and neurodegeneration[187, 188].

1.5 MOUSE MODELS OF AD PATHOLOGY

Animal models that closely replicate disease pathology are crucial for studying molecular mechanisms and disease progression, as well as for preclinical testing of novel therapeutic approaches. In AD research, mouse models are widely employed. Since the Aβ and tau pathologies are morphologically similar in both sporadic and familial AD cases, genetically engineered mouse models carrying fAD mutations have been developed to mimic the disease.

However, it is important to recognize that these models do not fully capture the complexity of AD pathology seen in humans.

1.5.1 TRANSGENIC MODELS

The first transgenic mouse model for AD research, PDAPP, introduced in 1995, carries the *Indiana APP* mutation[189]. These mice exhibit hallmark AD pathologies, including extracellular Aβ deposition, dystrophic neurites, gliosis, and reduced synaptic and dendritic density in the hippocampus. Subsequently, the Tg2576 model, which overexpresses the *APP* gene with the *Swedish* mutation, was developed by Karen Hsiao Ashe[190]. Both PDAPP and Tg2576 have become foundational tools in AD research.

Over the past decades, numerous mouse models based on *APP* mutations have been created to study AD pathology, including APP23[191], 3xTg[192], and J20 (PDGF-APPSw,Ind)[193]. Beyond *APP* mutations, many models have been developed based on *PSEN1* mutations, which are associated with familial AD. Some models, such as APPswe/PS1A246E, APPswe/PSEN1dE9, and 5×FAD mice, combine *APP* and *PSEN1* mutations to mimic more complex aspects of the disease[194-196].

Over the course of this thesis, two main transgenic models studied were tgSwe and tgArcSwe, along with tgUppSwe and its cross with tgSwe (tgUppSwe/Swe).

The transgenic mouse model with the *Swedish APP* mutation (tgSwe) is derived from a C57BL/6-CBA-F1 genetic background. These mice were created by inserting *APP* cDNA clones containing the *Swedish APP* mutation under the control of the Thy-1323-promoter. TgSwe mice exhibit a late-onset pathology, with senile plaques typically beginning to accumulate around twelve months of age. CAA may start to manifest as early as seven months. Amyloid plaques predominantly consist of Aβ1-40 and are typically round in morphology, with a central core of variable size. Microgliosis and astrogliosis are most pronounced in the hippocampus but are also observed around deposits in the cerebral cortex and thalamus, particularly by approximately 11-12 months of age[197].

The transgenic mice carrying both *Arctic* and *Swedish APP* mutations is based on a C57BL/6-CBA-F1 genetic background and exhibits early-onset pathology. Intracellular Aβ deposition is evident as early as two months of age. Aβarc peptides are highly aggregation-prone and demonstrate increased

resistance to proteolysis. Senile plaques, forming between five and six months of age, are characterized by compact, patchy patterns with minimal diffuse fibril regions surrounding multiple cores. These plaques predominantly consist of Aβarc1-40 and are primarily localized in the cerebral cortex, hippocampus, and thalamus. Their deposition increases progressively with age[197].

Finally, upon the discovery of the *APPUpp* mutation[108], a tgSwe-based mouse model carrying the *APPUpp* deletion was developed, referred to as tgUppSwe. Here, the *APPUpp* deletion results in earlier deposition than in tgSwe showing prominent deposition at 8months (as compared to 11-12months in tgSwe). Plaques predominantly consist of Aβupp1-42$_{\Delta 19\text{-}24}$. When crossed with tgSwe (tgUppSwe/Swe), plaque deposition also starts at 8months, though showing co-deposition with Aβwt1-40.

Together, transgenic mouse models provide a convenient model system to study basic features of amyloid plaque pathology. However, while these transgenic models successfully replicate certain AD features, they also have notable limitations. Most exhibit minimal neuronal death, lack tau pathology, and develop Aβ deposition in ectopic brain regions not typically affected in human AD brains.

1.5.2 APP KNOCK-IN MODELS

Transgenic AD mouse models are widely used even though there are some concerns. The main issue is that overexpression of the transgene may lead to additional phenotypes unrelated to AD pathology. To address this issue, second generation mouse models employing *APP* knock-in strategies have been developed to produce the Aβ which more closely resembles that found in human AD. The APP^{NLF} and $APP^{NL\text{-}G\text{-}F}$ mouse models are the most commonly used. Recently, the App^{SAA} knock-in mouse model was introduced, characterized by amyloid deposition beginning at four months of age and the presence of AT8-positive dystrophic neurites from eight months onward.

The APP^{NLF} knock-in mouse models effectively replicate several AD-associated pathologies[198]. These include the formation of amyloid plaques in the cortex and hippocampus, as well as synaptic loss, microgliosis, and astrocytosis, particularly around the plaques. Amyloid plaque development begins at six months of age, with cognitive impairment becoming evident by 18 months. The amyloid plaques are around 40-80 μm, and mainly consist of Aβ1-42.

In *APP*$^{NL\text{-}G\text{-}F}$ model, potential artifacts introduced by APP overexpression are avoided by using a knock-in approach to express APP at wild-type levels and with appropriate cell-type and temporal specificity. However, the presence of three mutations linked to fAD results in elevated levels of pathogenic Aβ. In homozygous mice, amyloid plaques begin to develop at two months of age, reaching near saturation by seven months. The predominant peptide in these plaques is Aβ1-42[199].

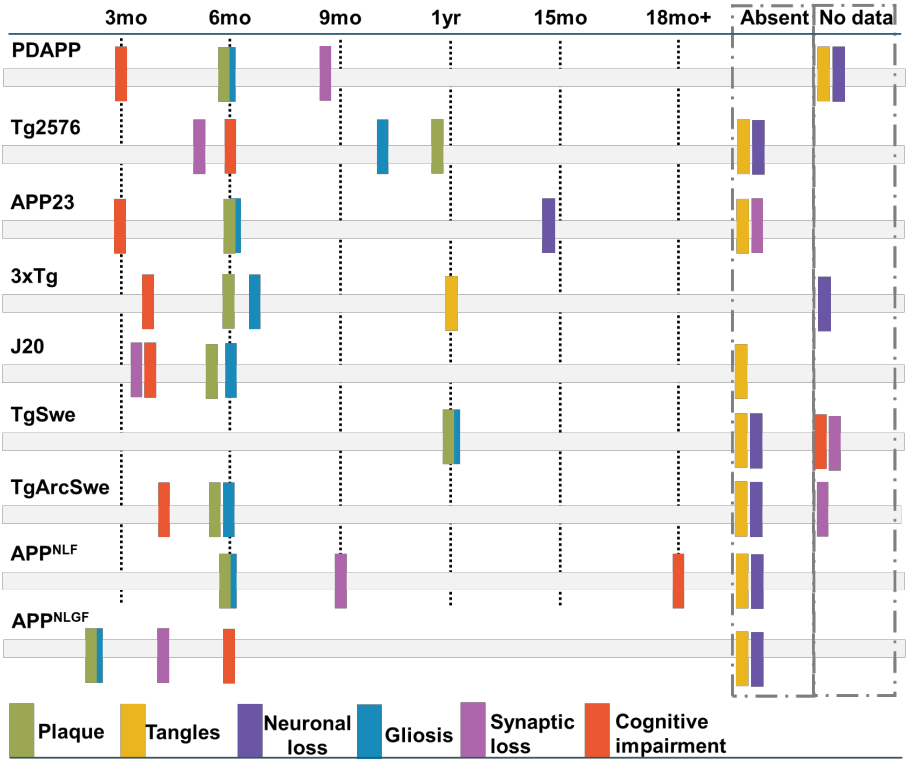

Figure 6. Schematic overview of the neuropathology observed in the transgenic and knock-in mouse models mentioned above. Various pathologies, including plaques, cognitive impairment, and gliosis, emerge at different time points in these models.

2 AIMS

2.1 GENERAL AIMS

The primary objective of this research is to investigate the molecular events at the subcellular level within amyloid plaques in Alzheimer's disease (AD). The mechanisms underlying AD pathogenesis remain poorly understood, particularly regarding the relationship between amyloid and lipids. Thus, we focused on the interactions between lipids and amyloid peptides that contribute to amyloid aggregation and deposition in both AD mouse models and post-mortem human brain tissue. Additionally, we aimed to examine the biochemical factors that may underlie amyloid plaque polymorphism.

Current chemical imaging techniques lack the specificity and sensitivity necessary to fully capture the dynamics of proteinopathy in AD. To overcome these challenges, the study aims to explore the molecular architecture of the complex pathology associated with AD using a range of advanced correlative chemical imaging tools including MALDI-MSI and microscopy.

2.2 SPECIFIC AIMS

Paper I

To develop a spatial chemometrics strategy for comprehensive analysis of multimodal MSI, including lipid and peptide imaging and microscopy data to interrogate molecular histopathology in complex biological tissues.

Paper II

To delineate lipid/amyloid patterns at the single plaque level using advanced multimodal chemical imaging, including tri-modal MALDI-MSI and fluorescence amyloid imaging.

Paper III

To investigate the dynamic interactions between lipid and Aβ in amyloid plaque pathology over time, utilizing stable isotope labeling in conjunction with advanced correlative chemical imaging techniques.

Paper IV

To study the potential co-deposition of Aβwt and AβUpp by *in vitro* co-aggregation studies with synthetic peptides and to examine the aggregation process and the evolution of plaque pathology *in vivo* by IHC and MALDI-MSI analysis.

Paper V

To characterize chemical traits of neuritic and cored plaques in post-mortem human brain tissue of sporadic AD using correlative MSI and immunohistochemistry.

Paper VI

To investigate the amyloid peptide signatures present in morphologically diverse plaque populations in brain tissue from sporadic and familial Alzheimer's disease.

3 MATERIALS AND METHODS

3.1 ETHICAL STATEMENTS

Animal procedures were approved by an ethical committee and performed in compliance with national and local animal care and use guidelines (DNr #C17⁄14 at Uppsala University) in Paper I and II. Animal experiments in Paper III on *APP* knock-in mice are performed at UCL together with Prof Frances Edwards in agreement with the Animals (Scientific Procedures) Act 1986, with local ethical approval at UCL (06/05/2016). All experimental procedures and protocols were performed in accordance with the relevant guidelines and regulations and the study protocol was approved by the Uppsala Animal Experimental Ethical Committee (#5.8.18-13350/2017) in Paper IV.

All human cases in Paper V and VI were obtained through the brain donation program of the Queen Square Brain Bank for Neurological Disorders (QSBB), Department of Clinical and Movement Neurosciences, UCL Queen Square Institute of Neurology. The standard diagnostic criteria were used for the neuropathological diagnosis of AD. Ethical approval for the study was obtained from the Local Research Ethics Committee of the National Hospital for Neurology and Neurosurgery, as well as the Ethics Review Board at the University of Gothenburg (Gothenburg, 04/16/2015; DNr 012-15). All studies abide by the principles of the Declaration of Helsinki.

3.2 SAMPLE COLLECTION

The animals were anesthetized with isoflurane and sacrificed by decapitation. Brains were rapidly dissected within a 3-minute post-mortem interval and immediately frozen using dry ice/liquid nitrogen.

Fresh brain tissue samples were collected from the temporal cortex of clinically and pathologically confirmed sAD cases, and fAD cases.

All brain tissues were stored at -80°C until analysis.

3.3 METHODS

3.3.1 MALDI MASS SPECTROMETRY IMAGING

Mass spectrometry imaging (MSI), well-known for its label-free, *in situ*, untargeted and imaging properties, has become a unique and robust tool to obtain and characterize the spatial distribution of individual molecules from tissues in the past decades. MSI adds critical spatial-chemical dimension which is usually lost in homogenization-based analysis. In the field of MSI, matrix-assisted laser desorption/ionization (MALDI), secondary ion MS (SIMS), and desorption electrospray ionization (DESI) are the most commonly used techniques.

Of these, MALDI-MSI is currently the most widely used technology. In MALDI-MSI, a UV laser is typically used to desorb and ionize molecules from tissue sections pre-coated with a UV-absorbing matrix (Figure 7)[200]. In 1988, Karas et al. and Tanaka et al. successfully demonstrated the laser ionization of macromolecular compounds with molecular weights of up to 10 kDa and 34 kDa, respectively, marking the birth of MALDI technology[201, 202]. This breakthrough enabled the mass spectrometric detection of biomacromolecules, opening a new frontier in analytical detection for life sciences. With the continued advancement of MALDI technology, it has been successfully applied to molecular imaging, allowing for the visualization of multiple molecular components on tissue surfaces. MALDI-MSI was first introduced by Spengler et al. and Caprioli et al. in the 1990s[203, 204]. With a wide variety of available matrices, MALDI-MSI can probe diverse molecular species. This technology has since gained significant attention in research areas such as disease marker discovery, tumor tissue pathology, and the tissue distribution of drugs and their metabolites.

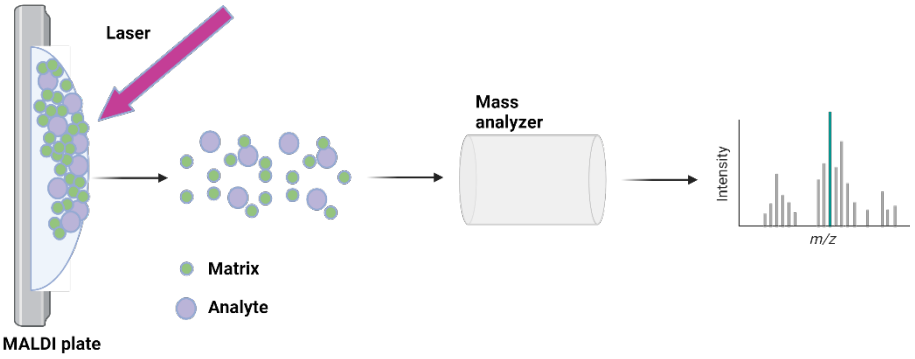

Figure 7. Principle of MALDI technique. (Created in BioRender)

However, this technology has certain limitations. For instance, commonly used small molecule matrices often produce interference peaks in the low molecular weight region and can cause significant ion suppression. Additionally, the acquisition speed of MALDI mass spectrometry data is influenced by factors such as laser frequency and mass spectrometer resolution. When analyzing a large number of samples at high spatial and mass resolution, the process can be time-consuming. Furthermore, the cost of MALDI-MSI remains relatively high.

3.3.1.1 SAMPLE COLLECTION FOR MALDI MSI

Biological samples commonly analyzed by MALDI-MSI typically consist of tissues from laboratory animals or humans, as well as plants, microorganisms, and cells, etc. These samples can be formalin-fixed, paraffin-embedded (FFPE) and fresh frozen tissues. FFPE tissue samples can be conveniently and cost-effectively stored at room temperature for extended periods due to their high stability and limited degradation processes, making them routinely used in both clinical diagnostics and research. However, MALDI-MSI analysis on FFPE tissues poses some obstacles that are challenging to overcome. These include modification of biomolecules of interest caused by chemical fixation of the tissue, and lipid and small metabolite depletion due to paraffin wax and organic solvent use during the process of deparaffinization.

To date, fresh frozen tissue remains the most widely utilized sample type in MALDI-MSI. The process involves rapidly cooling freshly dissected tissue by immersing it in liquid nitrogen or dry ice, commonly known as "snap-freezing" or "flash-freezing." This procedure must be completed within three minutes of

tissue isolation to effectively reduce degradation of proteins and peptides caused by proteolytic enzymes. After snap-freezing, the tissues are stored at -80°C.

For MALDI-MSI, 5-20 μm tissue sections are usually cut using cryostat. Thinner sections are prone to tearing, while thicker sections, although easier to handle, may lack electrical conductivity and take longer to dry, leading to potential cracking and warping. As a result, tissues are typically sliced to a thickness of 10−20 μm, roughly the diameter of a mammalian cell, to ensure that most cells are cut open, exposing intracellular contents for analysis.

After preparing the frozen sections, they need to be melt-mounted onto a target plate that is compatible with the ion source. The most commonly used target plate is indium tin oxide (ITO) conductive glass, which effectively prevents the accumulation of surface charges on the sample. It is important to note that for atmospheric pressure MALDI (AP-MALDI) mass spectrometry, the choice of target plate material is more flexible. Melt-mounting is the most common method for transferring tissue sections. This technique directly adheres the frozen tissue sections to the target plate, offering simplicity and reduced contamination risk. However, an improper melting and mounting process can cause analyte displacement due to the condensation of excess water from the sample and surrounding air.

Prior to matrix application, tissue sections may be washed depending on the goals of the MALDI-MSI analysis and the analytes of interest. Excess lipids and salts can interfere with matrix crystallization and suppress peptide and protein ionization. To address this, tissue washing with solutions such as 70% ethanol, ammonium formate, or ammonium acetate can be used to remove salts, while organic solvents like chloroform or xylene are typically employed to eliminate excess lipids[205]. Optimizing the washing process is crucial for various MALDI-MSI applications.

3.3.1.2 MATRIX APPLICATION

In MALDI-MSI, selecting a suitable matrix and deposition method is a crucial step in sample preparation. Currently, commonly used organic small molecule matrices include 2,5-dihydroxybenzoic acid (DHB), α-cyano-4-hydroxycinnamic acid (CHCA), 9-aminoacridine (9-AA), N-(1-naphthyl)ethylenediamine dihydrochloride (NEDC), and 1,5-diaminonaphthalene (1,5-DAN), among others[206]. DHB and CHCA are suitable for detecting lipids, peptides, and other small metabolites in positive

mode in tissues. 9-AA, NEDC, and 1,5-DAN are commonly used in negative ion mode for analyzing lipids, organic acids and related compounds. However, matrices like DHB and CHCA tend to produce significant interference peaks in the low molecular weight region ($m/z < 500$), leading to peak overlap and ion suppression for analytes within this range. As a result, the search for organic matrices that offer less background interference, higher desorption/ionization efficiency, and stronger specificity is an active area of MALDI-MSI research.

Additionally, several new organic small molecule matrices have been reported, including 2,4,6-trihydroxyacetophenone (THAP), 3,4-dimethoxycinnamic acid (DMCA), and 3-aminophthalhydrazide (3-APH)[207]. Ayorinde et al. also developed the porphyrin compound meso-tetrakis(pentafluorophenyl)porphyrin as a high molecular weight matrix, which reduces matrix peaks in the low molecular weight region, making it well-suited for detecting small metabolites such as organic acids[208].

Table 1. Common organic matrices and their applications.

Matrix	Structure	Work mode	Applications
2,5-Dihydroxybenzoic acid (DHB)	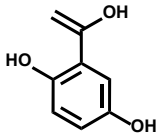	Positive	Lipids and small peptides
α-Cyano-4-hydroxycinnamic acid (CHCA)	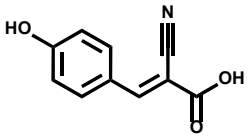	Positive	Peptides
9-Aminoacridine (9-AA)	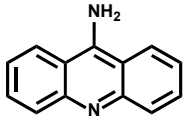	Negative	Organic acids, lipids and other small metabolites
N-(1-naphthyl)ethylenediamine dihydrochloride (NEDC)	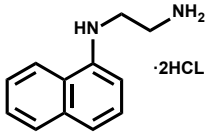	Negative	Organic acids, lipids and other small metabolites
1,5-Diaminonaphthalene (1,5-DAN)	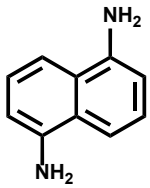	Positive and negative	Lipids
2,4,6-Trihydroxyacetophenone (THAP)	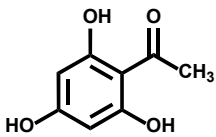	Positive and negative	Lipids
3,4-Dimethoxycinnamic acid (DMCA)	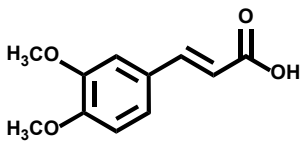	Positive	Lipids, oligopeptides, and metabolites

Nanomaterials have also shown promise as new MALDI matrices. These include nanomaterials such as gold and silver, metal oxides like iron oxide and titanium dioxide, and composite materials modified with organic small molecules. Nano matrices typically produce low background noise and exhibit stable chemical properties, offering a highly sensitive MALDI-MSI method for analyzing small molecule compounds. Most recent developments in matrix technology also focus on analyzing endogenous substances in animal tissues.

Matrix coating methods also play a significant role in MALDI-MSI analysis. The size of the matrix crystals affects spatial resolution, while the application method can influence molecular extraction and delocalization within tissues. Therefore, optimizing the matrix application method is essential to maximize analyte extraction while minimizing molecular delocalization within tissues.

The two primary coating methods are gas-assisted spraying and sublimation (Figure 8). Automated sprayers, such as M3+ sprayer (HTX Technologies, NC, USA) and SunCollect MALDI sprayer (SunChrom, Friedrischsdorf, Germany) are commonly used, and they provide uniform atomization of the matrix solution, producing smaller, more uniform droplets. By optimizing the parameters of the spraying method, such as matrix concentration, solvent, flow rate, velocity, and nozzle temperature, matrix deposition uniformity and adsorption are improved, ultimately enhancing the repeatability and reproducibility of imaging results.

In contrast, the sublimation method is a fast and uniform "dry" matrix coating technique that does not involve solvents, eliminating the risk of analyte displacement. However, without a solvent, the interaction between the matrix and analyte is reduced, potentially leading to a weaker mass spectrometric response for some analytes. This issue can be addressed by "hydration-recrystallization," where solvent vapors are used to recrystallize the sublimated matrix on the sample surface, significantly enhancing the mass spectrometric response.

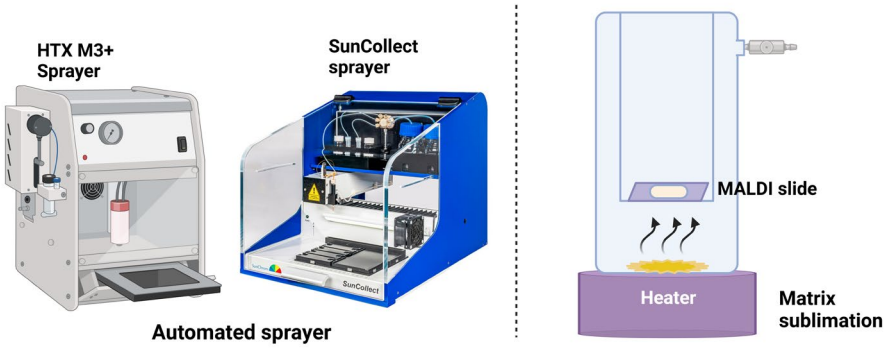

Figure 8. Automated sprayers (left), HTX M3+ Sprayer and SunCollect MALDI sprayer and matrix sublimation setup (right). (Created in BioRender)

3.3.1.3. MASS SPECTROMETRY IMAGING DATA ACQUISITION

In MALDI-MSI, the ion source can be paired with various mass analyzers, including time-of-flight (TOF), quadrupole time-of-flight (Q-TOF), ion trap (IT), and Fourier transform ion cyclotron resonance (FTICR) analyzers. MALDI combined with TOF offers fast data acquisition and high throughput, but its mass resolution is relatively low, making it insufficient for precise molecule identification. In contrast, MALDI FTICR provides excellent resolution and accuracy for clear molecular identification, but its slow scanning speed is a drawback. Orbitrap, however, has become increasingly popular due to its distinct advantages over FTICR, such as lower instrument and maintenance costs, comparable mass resolution, acceptable isotope ratios, better mass distribution at the lower mass range, and faster signal acquisition. Among the above analyzers, the MALDI-TOF combination is the most commonly used.

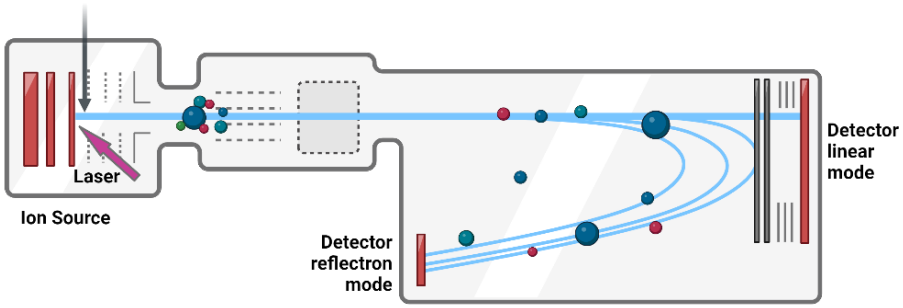

Figure 9. Schematic of TOF analyzer showing reflectron and linear mode. (Created in BioRender)

In MALDI-TOF-MS, two primary modes of operation are available: linear and reflectron (Figure 9). Initially, linear mode is often preferred for peptide and protein analysis, as it provides straightforward data acquisition and higher intensity. However, if enhanced resolution and mass accuracy are required, reflectron mode can be employed. Reflectron mode uses an ion mirror to correct the flight paths of ions, leading to improved accuracy and resolution. Although reflectron mode is less sensitive than linear mode and requires higher laser power to obtain quality spectra, it ultimately delivers more precise measurements, which is especially beneficial for lipid analysis. Standard parameters can be applied initially in both modes and adjusted as needed to achieve the best spectrum quality.

Therefore, we conducted lipid analysis in reflectron mode to achieve better mass resolution, while peptide analysis was performed in linear mode to obtain higher signal intensity.

3.3.1.4 MSI DATA PROCESSING AND ANALYSIS

There are currently many commercial and open-source software tools available for processing MSI data. These tools enhance MSI image quality by removing noise, correcting m/z peak deviations, and applying normalization. The primary goal of normalization is to minimize signal variations between pixels, which may result from uneven matrix coating, surface ion suppression, and other factors. Total ion count (TIC) normalization is the most commonly used method for improving image quality in MSI. However, for compounds that are highly concentrated in small areas, TIC normalization can lead to data distortion, necessitating the use of alternative normalization methods. Additionally, in targeted MSI analysis, normalization can be achieved by

applying an appropriate internal standard, enabling semi-quantitative and quantitative MALDI-MSI analysis.

Given the large volume of data generated by MALDI-MSI, processing and analyzing the data can be challenging. To address this, we have developed the following workflow for data processing and analysis. All lipid MS imaging data were externally calibrated using batch-processing function in Flex Analysis (v 4.0 Bruker Daltonics). Image analysis of MSI data was first performed in SCiLS (v 2021c, Bruker Daltonics, Bremen, Germany). For the image segmentation, the lipid and peptide imaging data were evaluated in SCiLS using corresponding pipeline. Regions of interest (ROIs) were identified by bisecting k-mean clustering-based image segmentation. Total ion current normalized average spectra of the annotated ROIs were exported as csv file in SCiLS. This was followed by binning analysis for data reduction. Here, all ROI data were imported into Origin (v 8.1 OriginLab, Northampton, MA, USA) and peak widths were detected on average spectra of each ROI using the implemented peak analyzer function. The determined bin borders for peak integration were exported as tab delimited text file. The bin borders were used for area under curve peak integration within each bin (peak-bin) of all individual ROI average spectra using an in-house developed R script. The bin data generated by R script was used for further analysis to extract relevant information from these large datasets.

Univariate statistics were performed in GraphPad Prism (v.9, GraphPad, San Diego, CA, USA).

Multivariate analyses of MSI data were performed in MetaboAnalyst 5.0 (https://www.metaboanalyst.ca/) and comprised Pearson correlation analysis, principal components analysis (PCA), and orthogonal projections to latent structures Discriminant Analysis (OPLS-DA).

3.3.2 APPLICATIONS OF MALDI-MSI IN NEURODEGENERATIVE DISEASE

MALDI-MSI enables the detection and characterization of a broad spectrum of molecules, including proteins, peptides, lipids, and small metabolites, within tissue samples. In neurodegenerative diseases, lipids dysregulation and protein/peptide misfolding play a crucial role in disease pathogenesis. MALDI-MSI's capability to detect intact lipids, peptides, and proteins directly *in situ* makes it particularly valuable for analyzing these molecular changes in

the context of neurodegenerative diseases. For different categories of biomolecules, MALDI-MSI analysis typically requires various sample preparation procedures.

3.3.2.1 PROTEINS AND PEPTIDES

Proteins and peptides are of great importance in biology, and considerable effort has been dedicated to their study. Professor Caprioli pioneered the exploration of protein distribution in biological tissues using MALDI-MSI[209]. Detecting proteins and peptides in brain tissues, however, requires optimized sample preparation due to the high presence of lipids and other small molecules that often interfere with protein and peptide signals. Techniques such as serial washing, acid treatment, on-tissue digestion and nanosecond photochemical reactions can enhance these signals, allowing for more accurate analysis of protein and peptide distribution *in situ*. To date, MALDI-MSI has been successfully utilized for robust *in situ* neuroproteomics and neuropeptidomics in single nerve cells[210], as well as in invertebrate tissues and both rodent and human CNS tissues in the context of neurological diseases[81, 170].

3.3.2.2 LIPIDS

Lipids are essential components of biological membranes and widely distributed in various tissues. Dysregulated lipid metabolism has been linked to neurodegenerative diseases, including Alzheimer's disease, Parkinson's disease, and amyotrophic lateral sclerosis.

By carefully selecting an appropriate matrix to minimize interference in the low mass range, researchers can achieve robust detection of lipid signals in tissue samples. Additionally, washing tissue sections with solvents such as ammonium formate has been shown to enhance lipid signals, particularly for lipids with a polar head group like gangliosides. Furthermore, various derivatization methods have been employed to facilitate the analysis of non-polar lipids, such as cholesterol, improving the sensitivity and specificity of lipid detection in complex biological matrices. These strategies collectively contribute to a more accurate characterization of lipid profiles in tissue, providing valuable insights into their roles in neurodegenerative disease.

3.3.2.3 OTHER METABOLITES

Neurotransmitters (NTs) are small molecule signaling messengers that facilitate or modulate synaptic transmission between neurons in the brain. Dysregulation of the NT system is characteristic of various neurological and psychiatric disorders. Understanding the abundance and spatial distribution of

these messengers in the brain is crucial for elucidating the mechanisms underlying neurological processes and diseases. Therefore, quantifying and imaging imbalances in different classes of NTs is essential for enhancing our understanding of these disorders. Recent advancements in derivatization methods (i.e. on-tissue chemoselective derivatization)[211] and novel matrices (i.e. fluoromethylpyridinium-based reactive matrices)[212] have enhanced the detection of NTs through MALDI-MSI analysis. By utilizing these innovative methods, researchers can achieve more precise imaging and quantification of neurotransmitters, further advancing our understanding of their dynamics in various neurological contexts.

In this thesis, amyloid peptide imaging was performed across all studies. Building on methods previously established by our group, sample preparation, including tissue section washing, hydrolysis, and matrix application for mouse and human samples was further optimized. MALDI-MSI analysis of lipids was performed in Paper I, II and III. 1,5-DAN was employed as the matrix in all three studies. Details are provided in the respective papers.

3.3.3 STABLE ISOTOPE LABELING IN MALDI-MSI

Stable isotope labeling by amino acids in cell culture (SILAC) is a widely used technique in MS-based quantitative proteomics. It involves incorporating non-radioactive, stable isotope-containing amino acids into proteins during normal metabolic processes. Cells grown in media containing "heavy" SILAC amino acids replace natural "light" amino acids, and after multiple rounds of cell division, proteins are labeled. SILAC allows for accurate protein quantification by comparing MS signal intensities of heavy and light amino acids, without requiring chemical modification. It also enables functional assays in proteomics[213].

In addition to SILAC, stable isotope labeling kinetics (SILK) studies use isotopes that are fractionally heavier but chemically identical to natural elements. These isotopes participate in normal reactions and are incorporated into proteins and other organic molecules. Mass spectrometry can distinguish isotope-labeled compounds by their mass difference, allowing researchers to measure dynamic processes like protein synthesis, release, and clearance[214]. Therefore, SILK is widely combined with mass spectrometry to study protein kinetics *in vivo*. This approach provides real-time insights into protein dynamics in clinical trials, delivering immediate evidence of target engagement and supporting therapeutic development.

Furthermore, chemical imaging technologies such as mass spectrometry imaging can make it possible to delineate the spatial changes of isotope incorporation in proteins. The combination of protein isotope labeling with nanoscale secondary ion imaging (NanoSIMS), called multi-isotope imaging, enables measurement of spatial protein turnover kinetics in cells and tissues. Notably, this technique, also known as SILK-SIMS, has demonstrated isotope incorporation in plaques in a hospice study of AD patients and in transgenic *APP* mice[215, 216].

Although NanoSIMS imaging provides high-resolution data on isotopic enrichment at the nanoscale, it remains limited in its ability to retrieve detailed molecular information, thereby restricting analysis of intact peptides and proteins. MALDI-MSI overcomes this limitation and has been effectively used to monitor spatial enrichment and metabolism of stable isotope-labeled drug candidates administered intraperitoneally, as well as phospholipids delivered intranasally or intraperitoneally. Notably, MALDI-MSI enables comprehensive and chemically specific imaging of Aβ peptides, supporting detailed studies of Aβ pathology in AD mouse models and postmortem human AD brain tissue.

In this thesis, metabolic SILs were applied to a recently developed knock-in mouse model of AD with familial *APP* mutations. ^{15}N was supplemented to the diet of 6–10-week-old APP^{NLGF} mice, coinciding with the time frame prior to plaque deposition (which begins at 8 weeks). Tissue sections were analyzed by MALDI-MSI to analyze spatial lipid and peptide patterns and to quantify lipid turnover kinetics encoded in the isotope pattern of distinct lipid species related to amyloid plaque pathology (Figure 10).

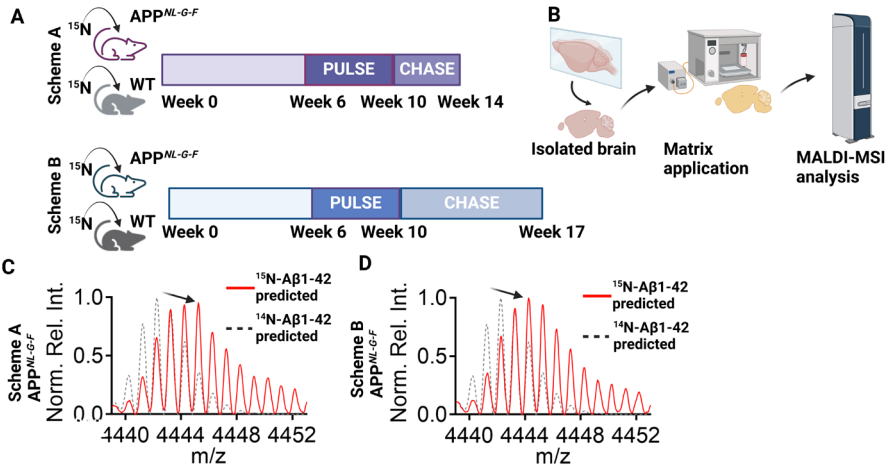

Figure 10. Schematic of imaging stable isotope labeling kinetics workflow. (A) Isotope labeling schemes. (B) MALDI-MSI analysis of labeled samples and (C) Isotope incorporation into amyloid peptide in two groups revealed by MS. (Created in BioRender)

3.3.4 LCO-BASED AMYLOID STANING

Conformation sensitive, fluorescent amyloid probes (luminescent oligothiophenes, LCO) could be employed to validate and characterize the identity of amyloid plaques. These molecules exhibit differential binding properties towards varying degrees of amyloid maturity. Moreover, different thiophene oligomers have different electrooptic properties, i.e., absorption/emission. This in turn allows for double staining strategies with differently binding LCO probes that can be delineated upon hyperspectral fluorescent microscopy. In detail, we used tetra (q) and heptameric formyl thiophene acetic acid (h-FTAA) for LCO double staining. Here, h-FTAA binds to immature pre-fibrilla amyloid aggregates. In contrast, q-FTAA binds solely to mature amyloid fibrils. Further, both probes have distinct emission profiles (Figure 11) that enable delineation of mature and immature/pre-fibrillar structures within single plaque[217-219].

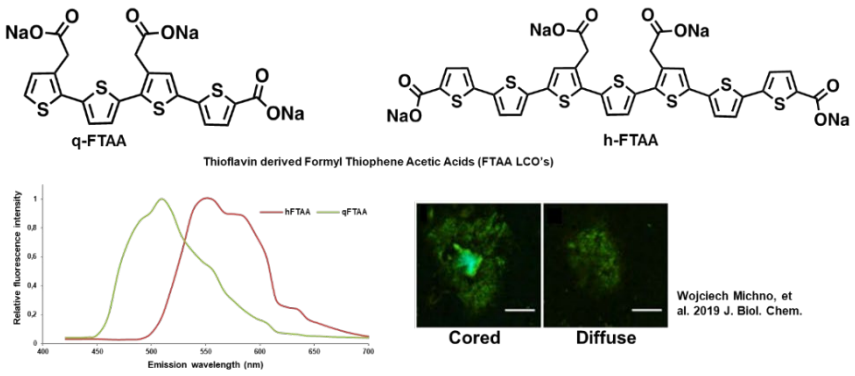

Figure 11. Structural amyloid staining using conformation-sensitive LCO probes (q/h-FTAA) with different emission properties that can be delineated with microscopy.

3.3.5 FLUORESCENCE MICROSCOPY

Fluorescence microscopy, developed in the early 20th century, has become an essential tool in biological and medical research for visualizing cellular structures and processes. It works by transmitting light through microscope components to produce high-resolution images. Wide-field fluorescence microscopy (WFFM), also known as epi-fluorescence microscopy, is a basic form of this technique. It uses a light source, excitation and emission filters, and a microscope to elicit and capture fluorescent light from samples. The emitted light, at a longer wavelength, is collected through the objective lens and viewed either through the eyepiece or digitized by a camera.

A key advancement in fluorescence microscopy has been the incorporation of Light Amplification by Stimulated Emission of Radiation (laser), which provides an efficient source of excitation energy. The advent of pulsed lasers has further enhanced fluorescence microscopy capabilities, particularly in techniques such as two-photon excitation microscopy. This method allows for deeper tissue penetration and reduced photodamage, making it invaluable for studying live cells and tissues in real-time.

Furthermore, the ability to measure fluorescent lifetimes in two- and three-dimensional contexts has opened new avenues for understanding dynamic biological processes. The fluorescence microscope functions similarly to a filter fluorometer, necessitating the development of various wavelength selection devices that can precisely select excitation and emission wavelengths.

Fluorescence microscopy detectors have also diversified, ranging from photomultiplier tubes that facilitate quantitative measurements to advanced imaging detectors that enable the acquisition of two-dimensional fluorescence images. As a result, fluorescence microscopy continues to be an essential technique for elucidating complex biological systems, providing insights into molecular interactions, cellular dynamics, and disease mechanisms.

3.3.6 IMMUNOHISTOCHEMISTRY

Immunohistochemistry (IHC) is a widely used method for detecting and visualizing specific proteins within tissue samples by leveraging the specificity of antigen-antibody binding interactions. The technique relies on the binding of antibodies tagged with detectable labels to their corresponding antigens in tissues, allowing researchers to visualize both the localization and distribution of specific antigens. Antibodies used in IHC can be monoclonal or polyclonal, binding to distinct epitopes on the target antigen. Common detection labels include fluorescent compounds, enzymes, and metals (Figure 12). This technique can be applied to FFPE or fresh frozen tissue samples, making it highly adaptable across sample types. Additionally, IHC can be multiplexed or applied sequentially to detect multiple targets within the same tissue section, offering flexibility to study complex protein interactions and expression patterns within intricate tissue structures.

Due to its precision and adaptability, IHC is indispensable in diagnostic pathology, supporting not only diagnostic accuracy but also patient staging, treatment planning, and prognostic assessment. IHC is particularly effective for visualizing tissue morphology, facilitating assessment of cellularity and tissue architecture alongside specific protein expression.

Despite its widespread utility, IHC does have certain limitations. Challenges include difficulties in studying multiple targets simultaneously, subjectivity in visual assessments leading to intra- and inter-observer variability, the risk of false-negative results, and issues with protocol standardization and quality control. Additionally, cross-reactivity and reproducibility concerns remain. To address these limitations, combining IHC with other robust imaging technologies presents a promising approach for enhancing pathological studies and achieving more comprehensive tissue analysis.

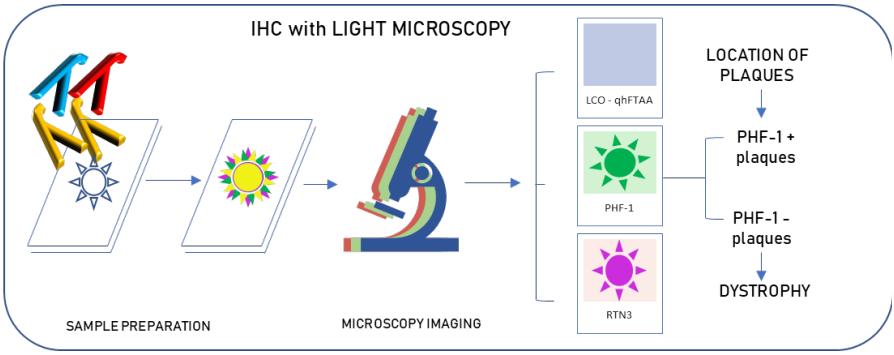

Figure 12. Schematic overview of IHC using light microscopy for plaque visualization in tissue sections. Antibodies tagged with detectable labels bind to specific epitopes on the target antigen in the tissue, enabling imaging through light microscopy. (Image from Paper V)

4 RESULTS AND DISCUSSION

4.1 PAPER I

Correlative Chemical Imaging and Spatial Chemometrics Delineate Alzheimer Plaque Heterogeneity at High Spatial Resolution

Amyloid plaque formation is a key feature of AD, with the prevailing hypothesis suggesting that Aβ aggregation initiates a cascade of neurotoxic events[220]. While the precise mechanisms remain unclear, recent phase 3 results for the amyloid-targeting antibody lecanemab provide strong support for this hypothesis[221]. Various Aβ aggregation intermediates (monomers, oligomers, protofibrils, fibrils) are implicated in AD pathogenesis to differing degrees. Both intrinsic factors (e.g., Aβ truncation) and extrinsic factors, such as neuronal lipids, influence Aβ pathology. Notably, the *APOE* ε4 allele, a lipid transporter gene, significantly raises the risk of sporadic AD, while genome-wide studies link AD risk to lipid-related genes like *ABCA7* and *TREM2*[111, 129, 130]. These insights underscore the need for analytical tools with high chemical specificity and sensitivity to map plaque-associated biochemical species and explore Aβ aggregation dynamics *in situ*.

MALDI-MSI has proven to be a powerful technique for examining amyloid plaque pathology in AD brain tissue. Our group has developed robust MSI methods for analyzing lipids and intact amyloid peptides alongside (immuno-) fluorescence imaging, allowing us to investigate biochemical changes associated with amyloid plaques in AD patients and mouse models[81, 169, 222]. However, challenges related to matrix application, formic acid treatment, and laser ablation have prevented the simultaneous use of lipid and peptide MSI with fluorescence analysis on a single tissue section.

To address these challenges, we have developed a novel correlative chemical imaging system that, for the first time, combines trimodal MALDI-MSI with fluorescence microscopy. This innovative approach allows us to probe amyloid plaque-associated lipid patterns on a single brain section from a transgenic AD mouse, enabling a comprehensive analysis of biochemical changes within a unified workflow.

Cryo-sections from a transgenic mouse model carrying the *APPSwe* mutation (tgSwe) were prepared. To integrate trimodal MALDI-MSI with fluorescence imaging on a single section, we implemented the following workflow: (1) lipid-negative MSI, (2) lipid-positive MSI, (3) fluorescence imaging, and (4) amyloid peptide MSI. Based on prior research, we found that lipid analysis in negative mode requires minimal laser shots and power, thus preserving tissue morphology. Therefore, lipid-negative MSI was conducted first, followed by lipid-positive MSI. For lipid analysis, we used 1,5-DAN as the matrix, which is suitable for dual-polarity lipid imaging.

Plaque morphology was then visualized using q- and h-FTAA LCO probes. Moreover, a coverslip was used during hyperspectral fluorescence microscopy to enhance signal detection. To ensure that the coverslip and mounting medium did not interfere with peptide MSI, we also optimized the coverslip removal procedure. Since formic acid is commonly used in peptide MSI to enhance peptide signals but can alter tissue histology, we performed fluorescence imaging before peptide MSI to preserve tissue integrity. This workflow enables comprehensive, high-resolution analysis of AD-associated biochemical changes within a single tissue section.

Following multimodal imaging data acquisition, several challenges arise. Registering MSI images can be particularly difficult due to image noise and low contrast. Additionally, a major bottleneck lies in the comprehensive statistical analysis required to evaluate multimodal imaging data effectively.

Hence, we introduced an innovative computational workflow that facilitates efficient data processing and automated image alignment, allowing for the incorporation of multivariate statistical analysis of chemical data across diverse imaging modalities while minimizing human bias.

PCA was employed to capture the variance in the MSI datasets while isolating noise, following a previously presented approach where magnetic resonance imaging (MRI) and MSI data were aligned[223]. We chose reference images that highlighted key anatomical or pathological features and were also the best match across the modalities. Next, we applied an intensity-based, automated image registration technique to determine the geometric transformation needed to align the corresponding pixels between the two reference images and the MSI modalities. Further, we implemented 1+1-evolutionary image registration for precise geometric alignment of multimodal imaging data. Spatial chemometrics using OnPLS modeling reveals covariation of multi-modal

chemical signatures in pathological features. Analytes that were increased or decreased within plaque structures compared to non-plaque regions were identified. The strongest global joint correlations were observed for LPE (18:0) (m/z 480.3, negative ion mode lipids), LPC (16:0) (m/z 496.3, positive ion mode lipids), and Aβ1−40 (m/z 4331, average mass, peptides), all of which have been previously noted to localize within Aβ plaques[170, 224]. In contrast, several lipid species showed a general depletion pattern specific to plaques, including sulfatides ST(d18:1_24:1) (m/z 888.6) and ST(d18:1_24:0(2OH)) (m/z 906.6) in negative ion mode, as well as PC (38:2) (m/z 852.6) in positive ion mode. Also, the core and peripheral localizing analytes are identified. Increased core localization levels were identified for PE-Cer (38:1) (m/z 715.6) and CerP(d36:1) (m/z 644.5) in negative ion mode, and PE(P-34:3) (m/z 720.5) in positive ion mode. In contrast, depletion at the plaque core was observed for LPI 18:0 (m/z 599.3), ST(d18:1_22:0) (m/z 862.6), and ST(d18:1_22:0(2OH)) (m/z 878.6). Additionally, multiblock component analysis indicated peripheral localization patterns for PI 38:4 (m/z 885.5) and PI 36:4 (m/z 857.5) surrounding plaque structures (Figure 13).

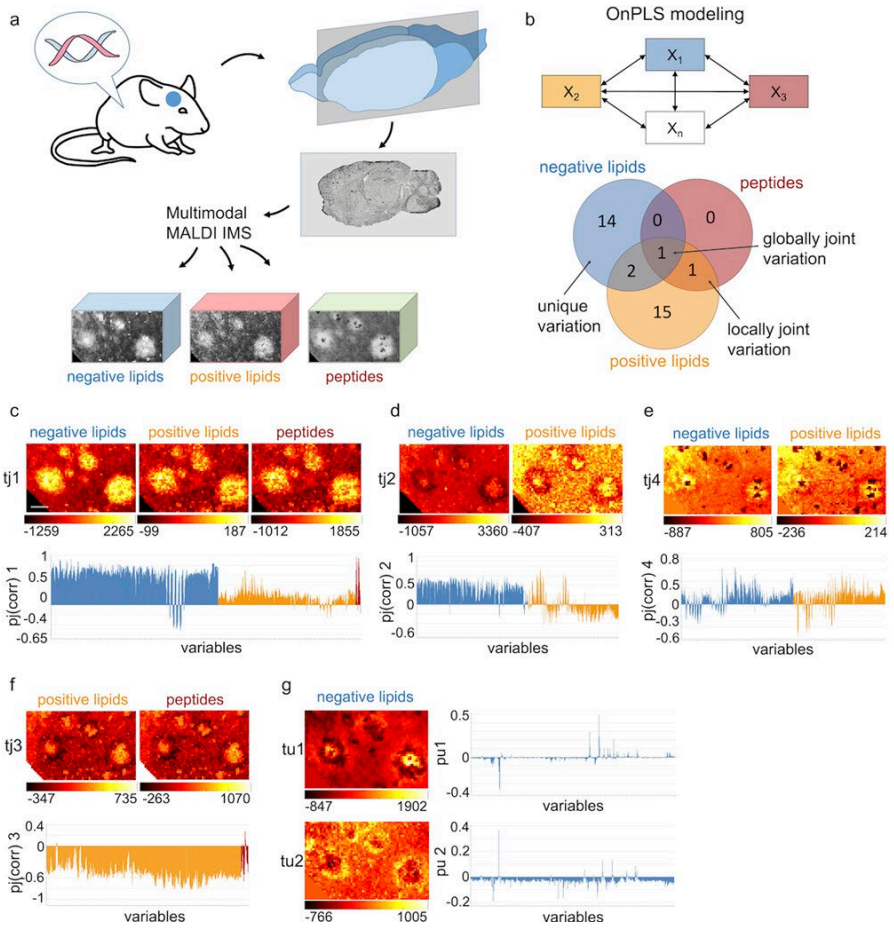

Figure 13. Spatial chemometrics analysis of multimodal MALDI MSI data of AD pathology. (a) Brain sections from tgSwe mouse were analyzed by MALDI MSI. Negative ion mode lipid-, positive ion mode lipid-, and peptide imaging data were acquired on the same brain section. (b) Unsupervised modeling using OnPLS was performed for the analysis of relationships across all modalities. The Venn diagram illustrates the partition of variation within the three datasets, with numbers indicating OnPLS components of globally joint, locally joint, and unique variation. (c) Globally joint component score image and loadings describing the covariance among all three modalities. (d, e) Locally joint component of negative- and positive ion mode lipid data. (f) Locally joint component of positive ion mode lipid- and peptide data. (g) Unique variation in the negative ion mode lipid modality. Normalization: root mean square; scale bar = 100 µm. (Image from Paper I)

This workflow also incorporated image data fusion to predict MSI ion distributions at microscopy image resolution (300 nm) from MSI data with a spatial resolution of 10 µm. This enabled high-resolution prediction of correlative, multimodal MSI signatures associated with distinct amyloid

structures within individual plaque features, which are crucially involved in Aβ pathogenicity. Microscopy-resolution predictions from individual MSI ion images and their fusion, supported by hyperspectral LCO microscopy, provided detailed insights into lipids and peptides associated with amyloid polymorphisms. Notably, the phosphoinositide species PI (18:0_20:4) (m/z 885.5) and PI (16:0_20:4) (m/z 857.5) achieved high reconstruction scores, accurately predicting their localization at the periphery of diffuse plaques. In contrast, Aβ1-38 and Aβ1-40 showed strong prediction scores throughout the entire plaque region (Figure 14b). Consistent with the OnPLS model described above, a plaque-specific depletion of the sulfatide ST(d18:1_24:1) (m/z 888.6) and its oxidized form, ST(d18:1_24:1(2OH)) (m/z 904.6), was observed.

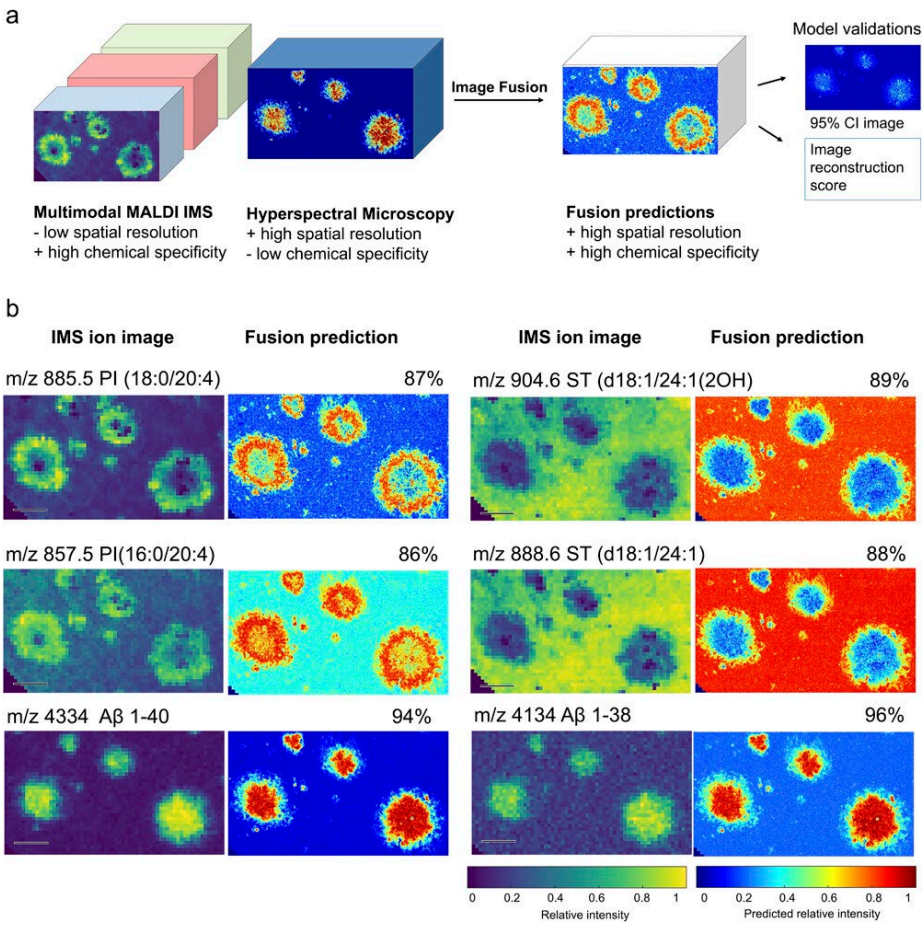

Figure 14. The workflow of data-driven image fusion to predict molecular distribution at microscopy resolution. (a) Image fusion utilizing multimodal MALDI

MSI and hyperspectral fluorescence imaging, integrating the high chemical specificity of MSI with the fine spatial resolution of microscopy. (b) Single ion images and their predicted fusion at microscopy resolution. Reconstruction score in %. Scale bar: 100 µm. (Image from Paper I)

In this study, a newly established imaging technique for transgenic AD mouse brains, combined with an enhanced data registration and image fusion approach for correlative MSI and functional fluorescence microscopy, enabled us to precisely map the co-localization of lipids and Aβ peptides associated with Aβ plaques. The specific distribution of lipids such as LPI and sulfatides in plaques aligns with previous findings[169, 170, 225]. Additionally, our analysis revealed distinct patterns of lysophospholipids, including LPE and LPC, as well as ceramides. Together, the multimodal imaging and spatial chemometrics strategy presented here provides a powerful framework for integrating molecular information from diverse imaging modalities, paving the way for deeper biological insights and maximizing the potential of multimodal imaging studies.

4.2 PAPER II

Tetramodal Chemical Imaging Delineates the Lipid-Amyloid Peptide Interplay at Single Plaques in Transgenic Alzheimer's Disease Models

In Paper I, we developed a tetramodal correlative chemical imaging approach combining trimodal MALDI-MSI with hyperspectral fluorescence amyloid microscopy. In this work, we applied this method to two AD mouse models, tgSwe and tgArcSwe, to investigate the molecular architecture of single plaques at microscale resolution. The *Arctic* mutation in tgArcSwe mice modifies the chemical properties of Aβ, leading to accelerated aggregation. We hypothesize that comparing these models will provide insight into how lipid–amyloid interactions influence plaque formation, growth, and fibrillation rates.

Our tetramodal correlative imaging workflow includes (1) lipid-negative MSI, (2) lipid-positive MSI, (3) fluorescence imaging, and (4) amyloid peptide MSI. Based on samples from the two AD models, we optimized and validated sample preparation (e.g., matrix application) and imaging parameters, including laser shot adjustments in MSI and wide-field fluorescence microscopy. To analyze the tetramodal data without bias, we developed new methods for examining multimodal imaging signatures from single plaques using multivariate statistical approaches.

First, hierarchical clustering analysis (HCA, bisecting k-means) on MSI data enabled segmentation, identifying plaque-like features in tgArcSwe and tgSwe brain tissue. Fluorescence imaging validated these segmented regions, as the clustering maps showed strong colocalization with amyloid plaques detected using LCO probes. These ROIs allowed us to conduct further targeted analyses (Figure 15A-D).

Both tgArcSwe and tgSwe plaques showed ST depletion, consistent with previous findings[170, 222], while numerous lipid species were enriched at plaques in both models. To further delineate lipid and peptide accumulation patterns, we performed multivariate statistical analyses, including PCA and OPLS-DA, on MSI data at the single-plaque level.

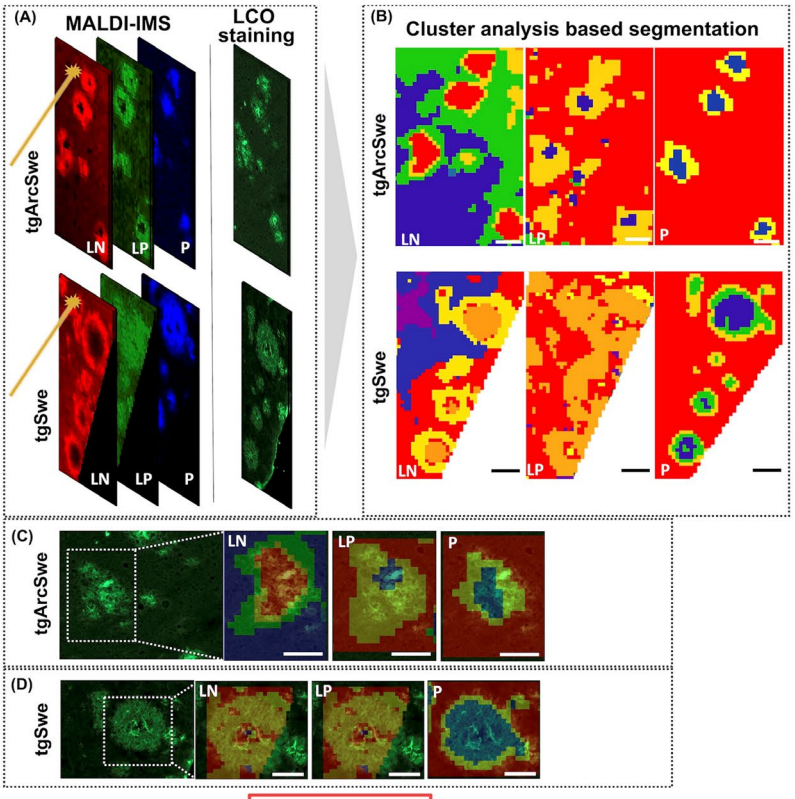
(A)
MALDI-IMS
LCO staining
tgArcSwe
tgSwe
LN
LP
P
(B)
Cluster analysis based segmentation
tgArcSwe
tgSwe
LN
LP
P
(C)
tgArcSwe
LN
LP
P
(D)
tgSwe
LN
LP
P

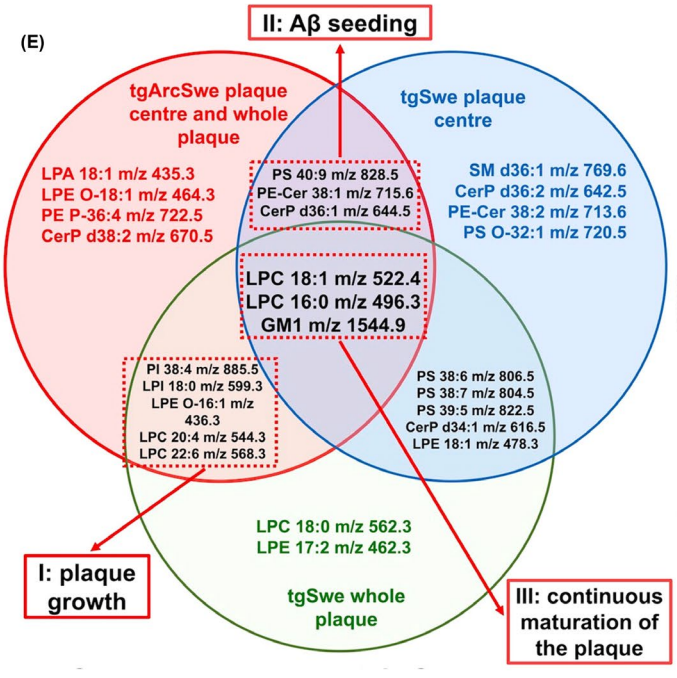
(E)
II: Aβ seeding
tgArcSwe plaque centre and whole plaque
tgSwe plaque centre
LPA 18:1 m/z 435.3
LPE O-18:1 m/z 464.3
PE P-36:4 m/z 722.5
CerP d38:2 m/z 670.5
PS 40:9 m/z 828.5
PE-Cer 38:1 m/z 715.6
CerP d36:1 m/z 644.5
SM d36:1 m/z 769.6
CerP d36:2 m/z 642.5
PE-Cer 38:2 m/z 713.6
PS O-32:1 m/z 720.5
LPC 18:1 m/z 522.4
LPC 16:0 m/z 496.3
GM1 m/z 1544.9
PI 38:4 m/z 885.5
LPI 18:0 m/z 599.3
LPE O-16:1 m/z 436.3
LPC 20:4 m/z 544.3
LPC 22:6 m/z 568.3
PS 38:6 m/z 806.5
PS 38:7 m/z 804.5
PS 39:5 m/z 822.5
CerP d34:1 m/z 616.5
LPE 18:1 m/z 478.3
LPC 18:0 m/z 562.3
LPE 17:2 m/z 462.3
tgSwe whole plaque
I: plaque growth
III: continuous maturation of the plaque

Figure 15. Multivariate image analysis was conducted on trimodal MSI data, aligned with LCO-stained fluorescence data, yielding the following results: A) Tetramodal images derived from tgArcSwe and tgSwe mice. (B) Segmentation images, generated through hierarchical clustering analysis (HCA), showing plaque features in both lipid and peptide data in tgArcSwe and tgSwe AD mouse models. Scale bar: 80 µm. (C, D) Overlay of LCO-based microscopy images and MSI segmentation images in tgArcSwe (C) and tgSwe (D) mice. (E) The Venn diagram reveals the top 15 lipids that correlate with Aβ1–40 within the whole plaque, core and periphery of the plaque in these two mouse models. Scale bars: 60 µm and 80 µm, respectively. (Image adapted from Paper II)

These analyses revealed distinct enrichment levels of specific lipid and peptide species in plaques across the two genotypes. Aβ1-42 and Aβ1-39 showed higher enrichment across plaques in tgSwe mice, whereas certain phospholipids, including phosphoethanolamines (PE) and phosphatidic acids (PA), were more enriched in tgArcSwe mice, potentially accounting for the more prolonged plaque deposition in tgArcSwe.

The *APPArc* mutation drives the morphological differences in plaque structure between the two models. Plaques in tgArcSwe mice begin to deposit earlier and exhibit a more compact, homogeneous structure, while tgSwe plaques display a heterogeneous morphology, with dense cores and diffuse peripheral fibrils. Additionally, we observed distinct lipid distribution patterns at plaque centers in both models, underscoring the variability in lipid and amyloid deposition between tgArcSwe and tgSwe mice. These results also highlight the significance of lipid and amyloid deposition polymorphisms.

We also conducted a correlation analysis of lipid and amyloid peptide data to investigate lipid–amyloid interactions in these two mouse models. Aβ1-40 is the predominant peptide in both models, so our analysis primarily focused on its correlation with lipid species. Specifically, we examined the top 15 lipid species correlated with Aβ1-40 at three levels: whole plaque, plaque center, and plaque periphery.

Interestingly, in tgArcSwe mice, the top 15 lipid species correlated with Aβ 1-40 were identical across the whole plaque, center, and periphery. In contrast, tgSwe mice showed variations in the lipid species associated with Aβ 1-40 across these regions, suggesting distinct lipid involvement in different stages of amyloid fibril deposition. Our analysis revealed that ceramides, sphingomyelin, and phosphatidylserine (PS) were linked to Aβ seeding, while LPI and PI were specifically correlated with plaque growth. Ganglioside GM1 and LPC showed continuous association with plaque maturation, indicating co-deposition through later stages (Figure 15E).

Numerous studies have implicated GM1 and LPC in amyloid pathology[226, 227], and this study further corroborates those findings. Additionally, through correlative chemical imaging of two transgenic mouse models with distinct amyloid plaque pathologies, our results highlight the diverse roles of various lipid species in amyloid aggregation.

It has been shown that Aβ can recognize a GM1 "cluster" in membranes, which promotes the seeding of Aβ fibrils. Additionally, the formation of this cluster is facilitated by cholesterol. Increases in intramembrane cholesterol content, which are likely to occur with aging, may act as a risk factor for the formation of amyloid fibril[228]. Our results in this study further support the fact that GM1 is implicated in Aβ fibrillation and plaque formation. Further, TREM2 is involved in detecting anionic and zwitterionic lipids, which associate with fibrillar Aβ in lipid membranes and are exposed on damaged neurons, playing a key role in microglia activation and plaque clearance[148]. The specific distribution of LPI and PI further supports the idea that anionic lipids, as TREM2 ligands, are associated with amyloid plaque pathology. In addition, lipid-droplet-accumulating microglia has been reported to represent a dysfunctional and proinflammatory state in the aging brain and further contribute to neurodegeneration[229, 230]. Taken together, this supports the multifaceted roles of lipids in plaque pathology, including their contributions to Aβ plaque growth, formation, fibrillation, and ongoing plaque maturation.

Notably, our tetramodal correlative chemical imaging puts these lipid–amyloid interactions into a spatial context. This delivers valuable insights into the molecular mechanisms underlying amyloid plaque pathology and the regio-specific molecular and cellular response that would otherwise be truncated in whole-tissue analysis.

4.3 PAPER III

Delineating Aβ Plaque Associated Lipid Co-Aggregation Dynamics Using Pulse-Chase Spatial Multiomics

In Paper II, we identified various lipid species associated with distinct plaque pathologies. Ceramides, sphingomyelin, and PS were linked to Aβ seeding, while LPI and PI showed specific correlations with plaque growth. Additionally, ganglioside GM1 and LPC demonstrated a continuous association with plaque maturation, indicating co-deposition throughout the later stages[231]. Understanding the dynamics of lipid-amyloid interactions is crucial for further elucidating amyloid plaque pathology. One effective method for investigating biomolecule dynamics is stable isotope labeling, which involves incorporating non-radioactive isotopes, such as ^{15}N and ^{13}C, into specific biomolecules. In AD research, feeding experimental cells and animals a diet enriched with ^{15}N- or ^{13}C-labeled precursors allows for the metabolic incorporation of these isotopes into newly synthesized lipids and peptides, including Aβ, providing a means to track these molecules within brain tissue.

To explore lipid-amyloid co-aggregation dynamics further, we utilized stable isotope labeling combined with advanced multimodal correlative chemical imaging. Our group has demonstrated the robustness of stable isotope labeling and chemical imaging for revealing Aβ peptide-specific aggregation dynamics in an AD mouse model[216].

For this study, we designed two pulse-chase labeling schemes in *APP* knock-in mice ($APP^{NL\text{-}G\text{-}F}$). These mice were fed a ^{15}N-labeled diet starting at 6 weeks of age, prior to plaque deposition, until 10 weeks. This was followed by a washout (CHASE) period of 4 weeks in Scheme A and 7 weeks in Scheme B.

Cryo-sections were collected from both groups, and lipid and peptide MSI analyses were performed on the same brain tissue section. Additionally, LCO staining was conducted to validate the presence of amyloid plaques (Figure 16A-D).

With the ^{15}N-labeled diet, MALDI-MSI data revealed distinct isotopic patterns for lipids, particularly gangliosides GM1 (d36:1), GM2 (d36:1), and GM3 (d36:1) in both schemes, indicating successful incorporation of ^{15}N into these lipid molecules. Furthermore, MALDI-MSI peptide analysis showed a mass

shift in Aβ 1-42 peptide within the plaques, confirming ^{15}N incorporation into the Aβ peptide (Figure 16E-F).

The MALDI-MSI data indicated that GM2 (d36:1) and GM3 (d36:1) were exclusively present in the plaques, while GM1 (d36:1) was enriched in the plaques in both Scheme A and Scheme B. To investigate lipid-amyloid co-aggregation dynamics, we calculated the enrichment of ^{15}N incorporation in both GM species and Aβ (primarily Aβ1-42). Between Schemes A and B, GM1 (d36:1), GM2 (d36:1) and GM3 (d36:1) exhibited a higher level of ^{15}N enrichment in Scheme A, which had a shorter washout period. This suggests that more unlabeled gangliosides accumulated in the plaques during the longer washout period in Scheme B (Figure 16G).

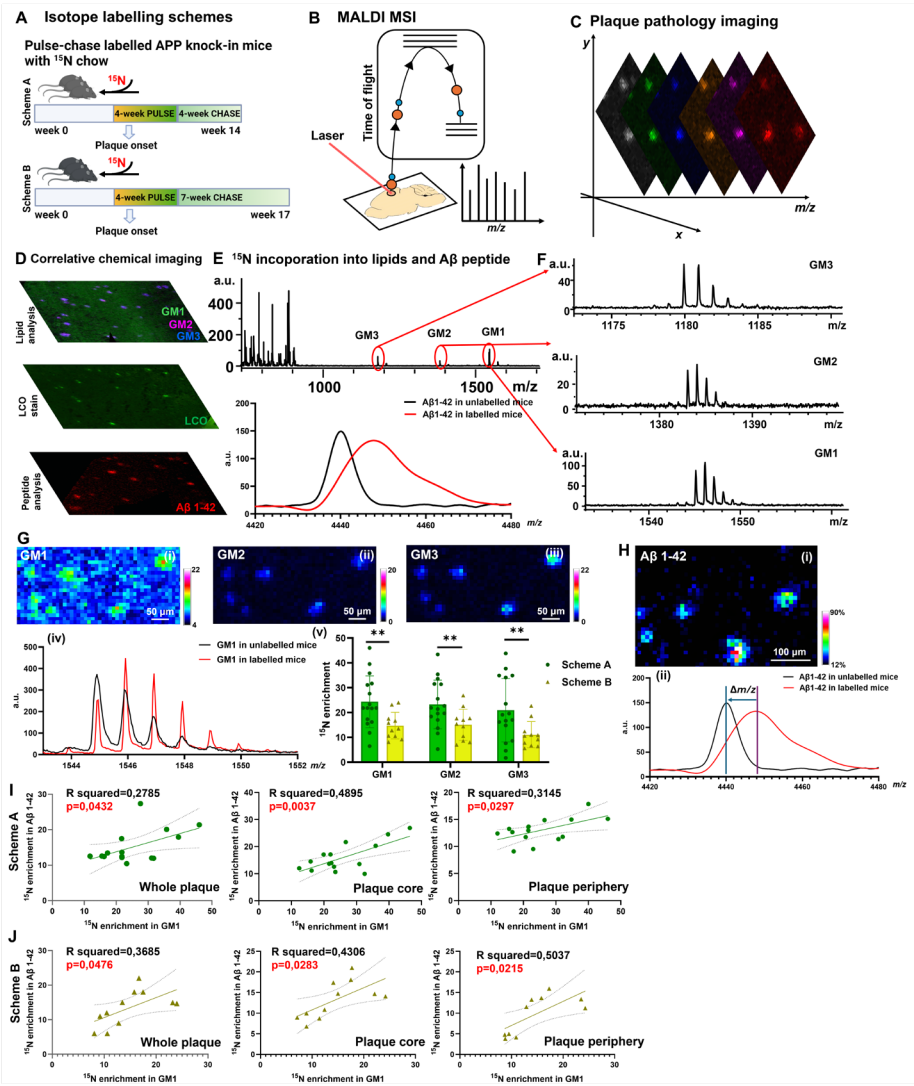

Figure 16. (A-C) Isotope labeling schemes in APP^{NL-G-F} mice, along with MALDI-MSI analysis of lipids and peptides in brain sections, were used to depict amyloid plaque pathology. (D-F) Gangliosides and amyloid peptides with ^{15}N incorporation were detected by MALDI-MSI. (G) Isotopic patterns of GM1(d36:1) and group comparison of ^{15}N enrichment in GM1 (d36:1), GM2 (d36:1), and GM3 (d36:1) within the whole plaque between Scheme A and Scheme B. (H) MALDI-MSI image of Aβ 1-42 reveals its aggregation in the plaque, while the mass shift of Aβ 1-42 indicates the ^{15}N enrichment. (I) The ^{15}N enrichment in GM1 (d36:1) positively correlates with ^{15}N enrichment in Aβ 1-42 within the whole plaque and core, periphery of the plaque in Scheme A and Scheme B. (Image from paper III)

To investigate lipid–Aβ interactions during plaque deposition, we conducted a correlation analysis of ^{15}N enrichment in gangliosides and Aβ1-42. Notably, the ^{15}N enrichment of GM1 (d36:1) showed a positive correlation with the ^{15}N enrichment of Aβ1-42 across the core, periphery, and whole plaque in both Scheme A and Scheme B. These findings suggest that GM1 (d36:1) exclusively interacts with Aβ1-42 throughout the entire plaque deposition process (Figure 16H-I).

In summary, we established a novel correlative chemical imaging method combined with stable isotope labeling, allowing us to elucidate the dynamic interactions between lipids and Aβ peptides at the subcellular level. The constant interactions between GM1 (d36:1) and Aβ1-42 during the plaque deposition process were revealed. This finding further supports the notion that GM1 plays a role in plaque formation, growth, and ongoing maturation as proposed in Paper II and indicated by other previous interaction studies[232-234]. Additionally, this study demonstrated the potential of correlative imaging techniques to deepen our understanding of the inter- and intracellular molecular events involved in the pathology of AD.

4.4 PAPER IV

The *Uppsala APP* mutation promotes wildtype Aβ aggregation and deposition *in vivo*

The *Uppsala APP* (*APPUpp*) mutation (690-695Δ), identified and characterized by our collaborators at Uppsala University, results in a six-amino acid deletion within the Aβ sequence. This mutation increases Aβ production by enhancing β-secretase activity and altering anti-amyloidogenic α-secretase activity, while also making Aβ highly prone to rapid fibril formation. In patients with the *Uppsala APP* mutation, AβUpp1-42$_{\Delta 19\text{-}24}$ is the predominant species, although wild-type Aβ (Aβwt) peptides are also found in deposits.

Transgenic mouse models with *APP* mutations have been crucial in advancing our understanding of AD mechanisms and assessing potential treatments. To examine Aβ plaque pathology specific to the *Uppsala APP* mutation, the tg-UppSwe model was developed. This model combines the *Uppsala* and *Swedish APP* mutations, leading to human AβUpp$_{\Delta 19\text{-}24}$ production, though it does not fully replicate the amyloid pathology seen in human *APPUpp* mutation carriers.

To explore the co-deposition potential of Aβwt and AβUpp, we performed *in vitro* co-aggregation studies with synthetic peptides in varying proportions to simulate the brain environment of an *APPUpp* mutation carrier. To further investigate aggregation dynamics and plaque evolution *in vivo*, we crossed the tg-UppSwe line with the tg-Swe line, creating a tg-UppSwe/Swe model. This combined approach allowed us to study Aβ aggregation and pathology in a controlled, translatable model.

Using a ThT assay, we found that AβUpp peptides promote Aβwt aggregation *in vitro*. Immunostaining results revealed plaque formation starting at 8 months in both tg-UppSwe and tg-UppSwe/Swe, while no plaques were observed in tgSwe at this age. All plaques in tg-UppSwe resembled the diffuse plaques typical of tgSwe mice, whereas tg-UppSwe/Swe mice developed cored plaques similar to those in tg-Swe. Notably, CAA, stained primarily by the Aβ40 antibody, was prevalent in both tg-Swe and tg-UppSwe/Swe mice at 18 months but was absent in tg-UppSwe at all ages (Figure 17).

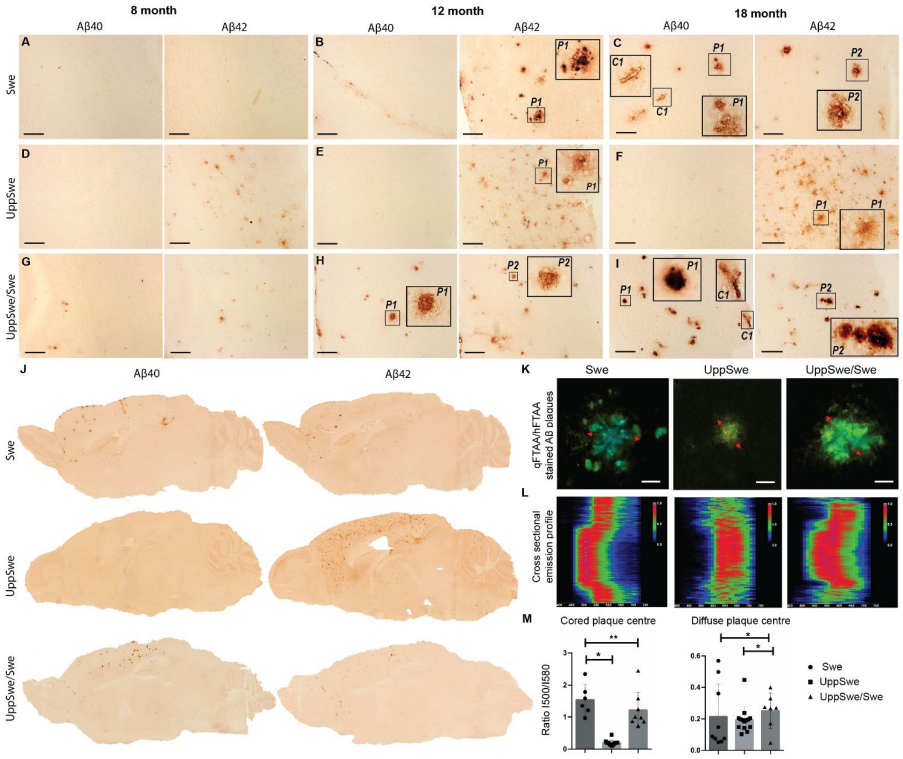

Figure 17. Immunostaining images of Aβ40 and Aβ42 in tg-Swe(A-C), tg-UppSwe (D-F) and tg-UppSwe/Swe mice (G-I) at 8, 12 and 18 months of age. (J) Whole brain section immunostaining images of Aβ40 and Aβ42 from tg-Swe, tg-UppSwe and tg-UppSwe/Swe mice at 18-month-old. (K) Aβ plaques stained by q-/h-FTAA from tg-UppSwe, tg-Swe and tg-UppSwe/Swe mice. (L) Cross-sectional emission profiles of the plaques obtained through line scan analysis across Aβ plaques, as marked by the red double-headed arrows. (M) LCO spectral statistics of the emission profiles from different mouse lines, comparing core and diffuse plaques. The data points in the graph are individual plaques (N=2-4) sampled across n=3 animals per mouse model. (Image from Paper IV)

To analyze the Aβ species in these models, we conducted ELISA, which confirmed the presence of both Aβ1-40 and Aβ1-42 across the models but could not differentiate between AβUpp$_{\Delta 19\text{-}24}$ and Aβwt. For more detailed insights into Aβ composition and pathology progression, we applied correlative chemical imaging on 8-, 12-, and 18-month-old samples from each model.

In tg-Swe mice, amyloid plaques and CAA consisting solely of Aβwt peptides were detected from 12 months of age. Aβwt1-40 is the predominant species in

CAA, while both Aβwt1-40 and Aβwt1-42 show similar levels of enrichment in plaques at 12 months. In 18-month-old mice, Aβwt1-40 is the primary peptide in large, round plaques.

In tg-UppSwe mice, only AβUpp peptides were observed, with AβUpp1-$42_{\Delta 19\text{-}24}$ as the main peptide; age-related increases in N-terminally truncated peptides were also noted.

In tg-UppSwe/Swe mice, both Aβwt and AβUpp peptides coexisted. At 8 and 12 months, plaques were small and compact, primarily composed of AβUpp1-$42_{\Delta 19\text{-}24}$, while at 18 months, larger round plaques developed with Aβwt1-40 as the main component. Another type of plaque was identified in the HCA segmentation map of 18-month-old tg-UppSwe/Swe mice. This type of plaque is generally small and primarily composed of AβUpp1-$42_{\Delta 19\text{-}24}$. Furthermore, CAA began to appear at 8 months, primarily consisting of Aβwt1-40 and Aβwt1-42 in tg-UppSwe/Swe mice (Figure 18).

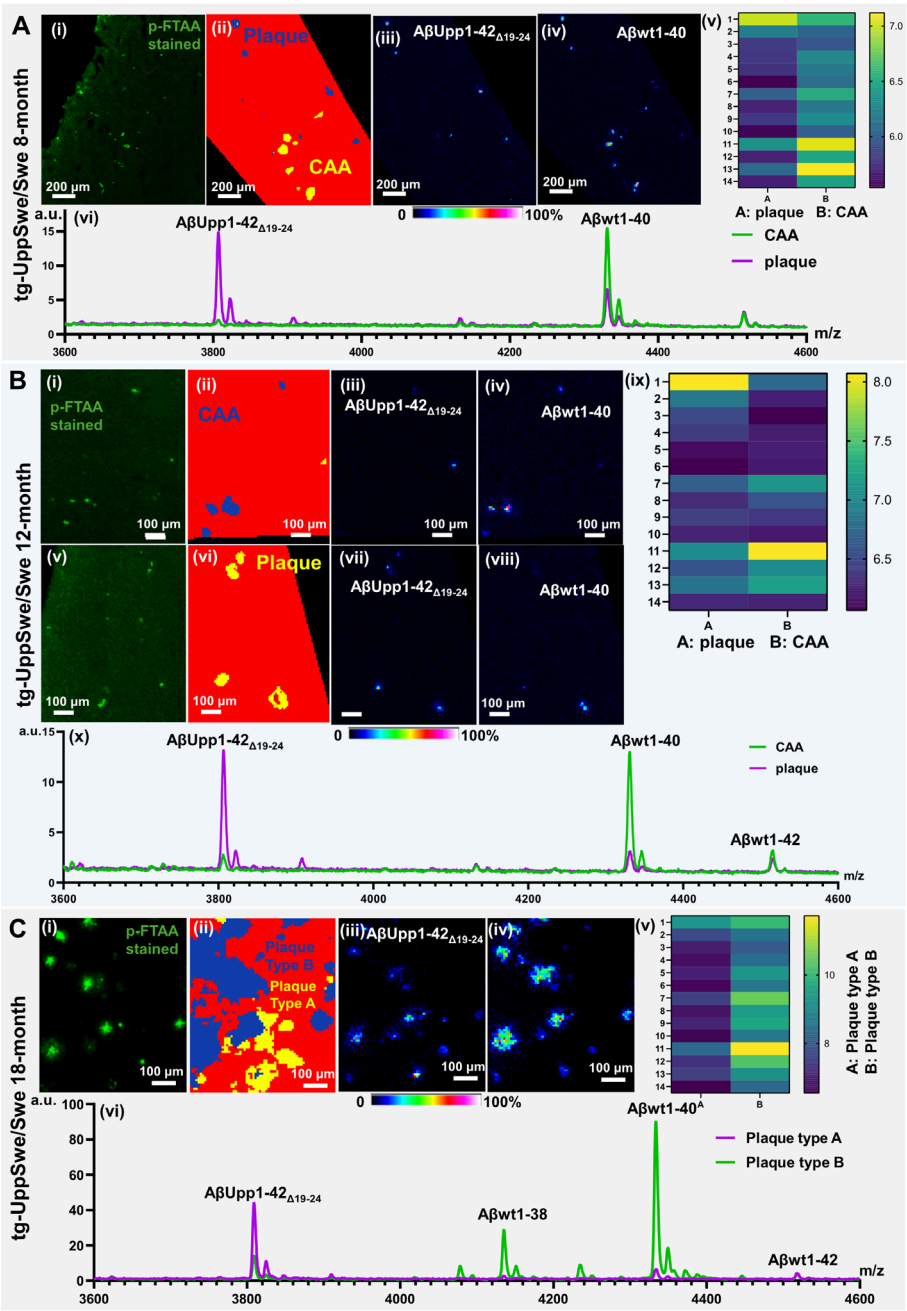

Figure 18. MALDI-MSI results reveals amyloid peptide evolution patterns in tg-UppSwe/Swe mice from 8 to 18 months. (A) Plaque and CAA were identified in LCO (i) and HCA-based segmentation map (ii). MALDI-MSI images (iii and iv), heatmap of amyloid peptides (v) and representative spectra of plaque and CAA (vi) in 8-

month-old mice. (B) Plaque and CAA were identified in LCO (i and v) and HCA-based segmentation map (ii and vi). MALDI-MSI images (iii to iv and vii to viii), heatmap of amyloid peptides (ix) and representative spectra of plaque and CAA (x) in 12-month-old mice. (C) Two types of plaques were identified in LCO (i) and HCA-based segmentation map (ii). MALDI-MSI images (iii and iv), heatmap of amyloid peptides (v) and representative spectra of two types of plaque (vi) in 18-month-old mice. In the heatmap, the amyloid peptides are arranged as follows: 1: Aβupp1-42$_{\Delta 19\text{-}24}$; 2: Aβupp1-42ox$_{\Delta 19\text{-}24}$; 3: Aβupp1-43$_{\Delta 19\text{-}24}$; 4: Aβwt4-40; 5: Aβwt1-37; 6: Aβwt1-37ox; 7: Aβwt1-38; 8: Aβwt1-38ox; 9: Aβwt1-39; 10: Aβwt1-39ox; 11: Aβwt1-40; 12: Aβwt1-40ox; 13: Aβwt1-42; 14: Aβwt1-42ox. (Image from Paper IV)

The recently identified *Uppsala APP* mutation leads to the production of AβUpp$_{\Delta 19\text{-}24}$ in the human brain. To investigate the associated AD pathology, the established tg-UppSwe mouse model was utilized. However, this model lacks Aβwt, differing from the amyloid profile observed in AD patients with the *Uppsala APP* mutation. Based on the hypothesis that the co-existence of AβUpp$_{\Delta 19\text{-}24}$ and Aβwt influences aggregation dynamics and parenchymal plaque deposition, this study utilized a combination of *in vitro* and *in vivo* experiments, along with a new bitransgenic mouse model.

Our findings confirmed the impact of AβUpp$_{\Delta 19\text{-}24}$ on amyloid aggregation in the presence of Aβwt. Specifically, MALDI-MSI analysis of three transgenic mouse models revealed the evolution of amyloid peptides from 8 to 18 months of age, providing robust support for our hypothesis. This discovery enhances our understanding of how the *Uppsala APP* mutation contributes to AD pathology.

4.5 PAPER V

Correlative chemical imaging identifies amyloid peptide signatures of neuritic plaques and dystrophy in human sporadic Alzheimer's disease

The diversity of Aβ aggregates, linked to specific Aβ peptide species, is thought to drive various pathological changes in AD. Numerous types of amyloid deposits have been identified, each with distinct clinical correlations[91]. These deposits are typically categorized into dense-cored plaques, coarse grain plaques, diffuse plaques, and cotton wool plaques. Dense-cored plaques are a more prevalent form of Aβ pathology in AD patients, while diffuse plaques are more commonly observed in CU-AP individuals. Despite the identification of these plaque types, the specific components of these diverse amyloid aggregates remain poorly understood.

Building on our studies of plaque pathology in AD mouse models, we aimed to expand our techniques, using multimodal chemical imaging (including fluorescence imaging and MALDI-MSI), to characterize senile and neuritic plaques in human AD brains. Neuritic plaques (NPs), a subset of plaques positive for tau, are characterized by neurites that can be visualized using IHC with an anti-paired helical filament (PHF)-1 antibody, which marks tau species. These plaques are often associated with dystrophic neurites (DN)—aberrant axons scattered throughout the grey matter in AD brains. Understanding the specific Aβ species within NPs could be crucial for elucidating the relationship between Aβ pathology and neurodegenerative processes.

In this study, we used correlative imaging with MALDI-MSI and IHC to characterize Aβ species in NPs. Mirrored brain sections from sAD cases were used, with one set stained with PHF-1 and anti-RTN3 antibodies alongside q- and h-FTAA fluorophores. While q- and h-FTAA identified amyloid morphologies, PHF-1 marked neuritic plaques, and RTN3 labeled dystrophic neurites. Using these stains, we distinguished plaques as either PHF-1 positive or PHF-1 negative.

MALDI-MSI analysis of peptides was then conducted on the corresponding mirrored sections, with immunostained sections serving as navigation tools to extract MALDI spectra from identical plaques, allowing us to examine peptide signatures from the same plaques (Figure 19a).

Our analysis identified two plaque subtypes: LCO+PHF+ (neuritic plaques) and LCO+PHF- (non-neuritic plaques). LCO+PHF+ plaques were associated with RTN3+ dystrophic neurites, whereas LCO+PHF- plaques were RTN3 negative. This allowed us to categorize the plaques into neuritic (LCO+PHF+) and non-neuritic (LCO+PHF-) types (Figure 19b).

Using MALDI-MSI data, we compared Aβ signatures between NPs and non-NPs. Notably, Aβ1-42(ox) and Aβ2-42 showed significantly higher abundance in NPs compared to non-NPs. Additionally, we examined the correlation between the intensity of the neuritic marker's immunofluorescence (IF) and the levels of different Aβ species within each plaque. Our findings revealed a significant correlation between Aβ1-42(ox) levels and RTN3, suggesting a link between oxidized Aβ1-42 and neuritic pathology (Figure 19c). These findings further underscore the inherently neurotoxic nature of neuritic plaques. Notably, Aβ2-42 has been identified as a more robust indicator of neurodegeneration compared to Aβ1-40/Aβ1-42 in diagnostic contexts[235]. Collectively, our results suggest that elevated levels of Aβ2-42 may be closely linked to neurodegeneration-associated amyloid plaque pathology.

These findings highlight the utility of correlative chemical imaging to explore Aβ signatures and provide insights into amyloid plaque pathology at a detailed biochemical level in AD patients.

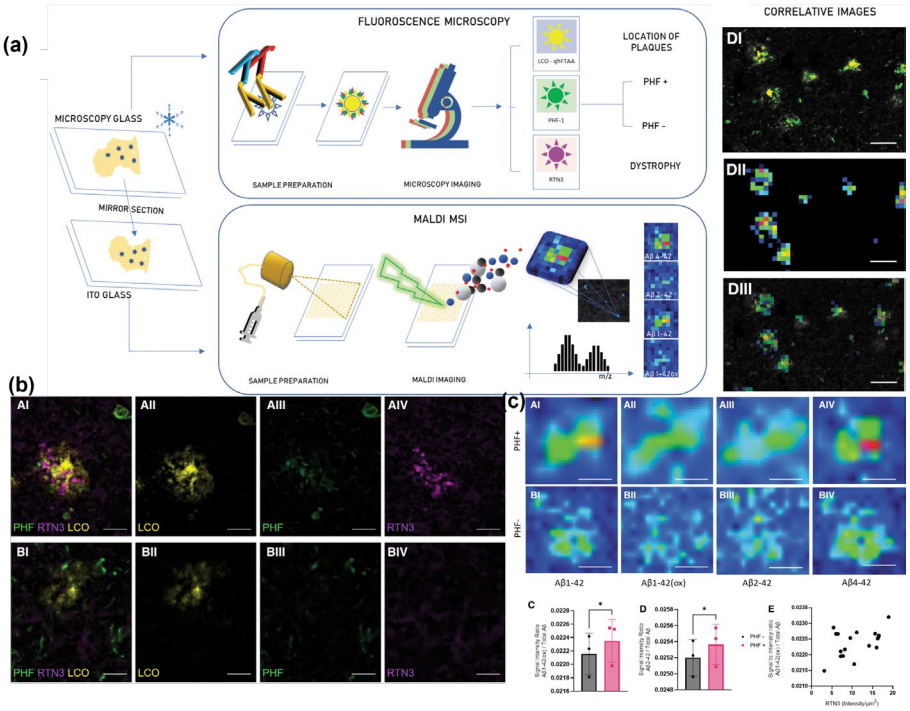

Figure 19. (a) Workflow of correlative chemical imaging of amyloid plaques in human brain tissues. (b) Overlay of light microscopy image reveals two types of plaque: PHF+ and PHF- plaques. (c) MALDI-MSI images of two types of plaque and box plots indicate signal intensity of different Aβ from PHF+ and PHF- plaques. The correlation analysis reveals that Aβ1-42(ox) intensity from PHF+ plaques correlates with the intensity of RTN3. Scale bar: 50 μm (Image adapted from Paper V)

4.6 PAPER VI

Chemical imaging delineates Aβ plaque polymorphism across the Alzheimer's disease spectrum

AD plaque pathology precedes other pathological events and cognitive symptoms, exhibiting a wide polymorphic variety that includes plaques at various stages of amyloid fibrillization, from diffuse to fibrillar, mature forms[236]. The relationship between these polymorphic Aβ plaques and AD pathogenesis, clinical symptoms, and disease progression remains unclear. Understanding this connection is especially important given the development of new amyloid-targeting therapies.

In paper V, we focused on the distinctions between neuritic and non-neuritic plaques in sAD brain tissue. We then expanded our study to characterize additional forms of Aβ aggregation in AD brains using advanced multimodal chemical imaging combined with machine learning. LCO staining was applied to AD brain tissue sections, followed by MALDI-MSI peptide analysis.

This correlative imaging approach allowed us to identify distinct plaque populations across different clinical cases. The LCO/MSI method revealed distinct clusters of plaques. Diffuse plaques (DP), cored plaques (CP) and coarse grain plaques (CG) were found in sAD cases. In fAD cases, we identified primarily two plaque clusters, including CP and CG, with an additional cotton wool plaque (CWP) type observed in one fAD patient (Figure 20). To minimize bias in plaque classification, we utilized a deep learning (DL) model for automatic plaque identification.

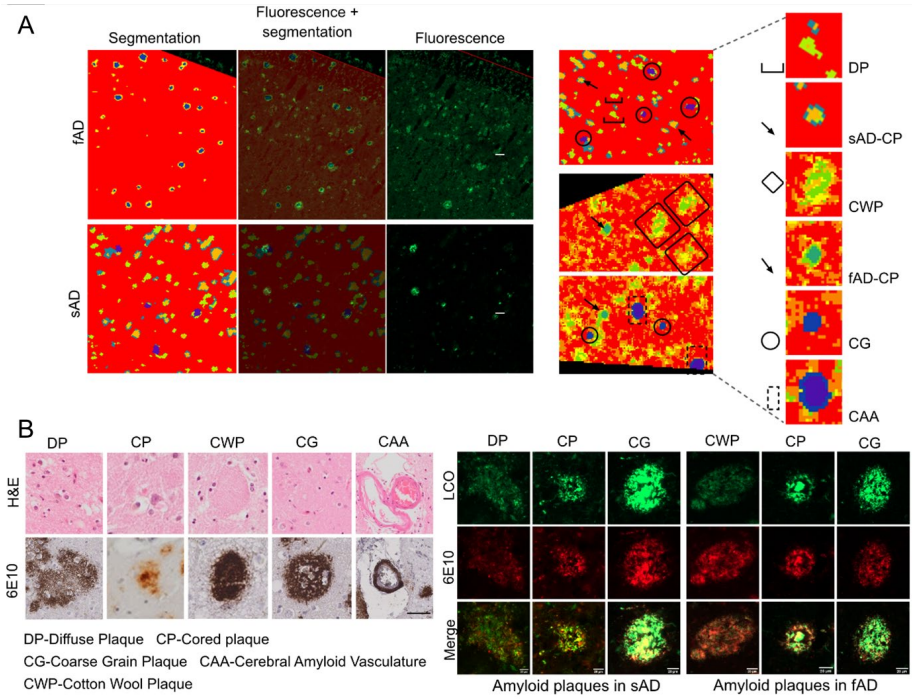

Figure 20. (A) LCO images and segmentation map reveals different plaque types in sAD and fAD. (B) Visualization of different types of plaques via LCO/antiAβ (6E10) co staining. Scale bar: 20μm. Visualizations of diffuse plaque, cored plaque, cotton wool plaque, coarse grain plaque and amyloid vasculature through H&E and antiAβ (6E10) staining. Scale bar: 40μm. (Image from paper VI)

Following DL-based classification, we analyzed peptide signatures associated with different plaque morphologies across AD types. In sAD, OPLS-DA-derived VIP scores identified Aβ1-40, Aβ1-42, and N-terminally truncated, pyroglutamated forms of Aβx-42 (such as Aβ3pE-42 and Aβ11pE-42), as key peptides distinguishing diffuse from cored plaques. Univariate analysis of individual plaque data further demonstrated that Aβ1-40 deposition is linked to plaque maturation and fibrillization in sAD, with increased accumulation of Aβ1-42 and its pyroglutamated forms Aβ3pE-42 and Aβ11pE-42 indicating advanced plaque development.

Interestingly, the multivariate HCA analysis identified a distinctive subtype of fibrillar plaques with a unique morphology, closely resembling what has been previously described as CG plaques[88]. OPLS-DA and univariate statistical analysis showed that coarse grain plaques in both sAD and fAD exhibit elevated levels of Aβx-40 species, including Aβ4-40, Aβ3pE-40, and Aβ1-40. In contrast, Aβx-42 species, such as Aβ11pE-42, Aβ5-42, Aβ3pE-42, and Aβ1-

42, were found at higher levels in cored plaques compared to coarse grain plaques in both sAD and fAD (Figure 21).

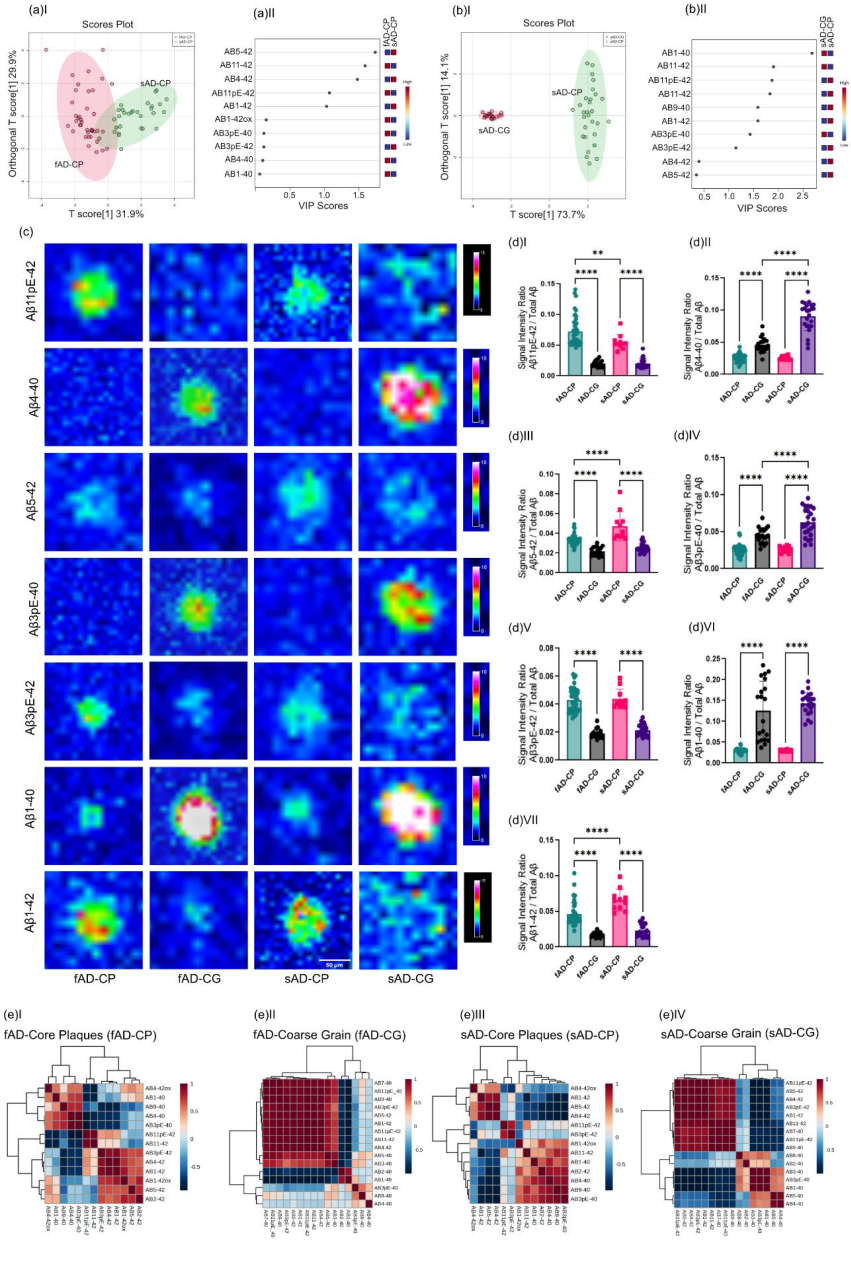

Figure 21. Multivariate and univariate analysis results reveal distinct amyloid peptide signatures across various types of plaques in sAD and fAD cases. (a I)

OPLS-DA of fAD-CP sAD-CP plaques reveals the partial separation of fAD CP and sAD CP with (OPLS model characteristics: R2X-0.319; R2Y-0.624; Q2-0.609). (aII) VIP scores. (b I) OPLS-DA of sAD-CP and sAD-CG plaques show strong separation (OPLS model characteristics: R2X-0.737; R2Y-0.948; Q2-0.947). (bII) VIP scores. (c) MALDI-MSI images of different amyloidβ (Aβ) peptides in various types of plaques. (d) Corresponding box plots showing univariate comparison of single ion intensities with respective plaque types. (e) Pearson's correlation matrix of Aβ peptides in (eI) fAD-CP, (eII) fAD-CG, (eIII) sAD-CP (eIV) sAD-CG plaques. (Image from paper VI)

The MS signatures for coarse grain plaques were predominantly composed of Aβ1-40 species. Previous studies, including our own, have shown that vascular deposits in CAA also exhibit an Aβ1-40-dominant profile[237, 238]. To further investigate, we compared the Aβ patterns between CAA and CG plaques in MALDI-MSI results via OPLS-DA. The results revealed that CG plaques had lower levels of Aβ1-40 and Aβ3pE-40 compared to CAA. Conversely, Aβx-42 species, such as Aβ1-42, Aβ5-42, Aβ3pE-42, and Aβ11pE-42, were more abundant in CG plaques compared to CAA. This result reconfirms the findings of CG plaques reported by Boon in 2020[88]. The greater diameter of these CG plaques can be a result of the dense deposition of Aβx-40, as Aβ1-40, a key component of CG plaques, has a natural tendency to form thick, large fibrils. Additionally, our findings indicate that Aβ3pE-40 is highly enriched in CG plaques. This further supports the fact that the pyroglutamation of Aβx-40 species enhances seeding ability, accelerates aggregation kinetics, and increases neurotoxic effects[239].

In summary, our findings suggest that fibrillar plaques, particularly coarse grain plaques, represent a pathological hallmark associated with both advanced and rapidly progressing AD. The multimodal chemical imaging approach used in this study enabled detailed molecular investigation of amyloid plaque pathology across different AD pathologies. This approach could provide valuable insights that could support future advancements in AD drug development.

5 CONCLUSION AND FUTURE PERSPECTIVES

Understanding amyloidogenic protein pathology has been central in dementia research since amyloid plaques and neurofibrillary tangles were identified as key hallmarks of AD over a century ago. The molecular mechanisms underlying plaque morphology, fibril polymorphism, and lipid-amyloid interactions remain poorly understood. Advanced chemical imaging techniques are thus essential for probing these molecular events to gain deeper insights into diverse plaque pathologies in AD.

Building on previously established multimodal imaging techniques, I expanded to correlative chemical imaging on single tissue sections to provide a more detailed view of molecular events. With this newly established imaging system, lipid and amyloid peptide distributions can be revealed in the mouse models. Together with advanced, chemometric methods we identified biochemical covariation patterns across imaging modalities at single pixel resolution.

The potential of this correlative chemical imaging system was also put to work to understand the link of lipid-amyloid interaction in heterogenous plaque pathology across different plaque types and mouse models of amyloid pathology. Distinct lipid profiles have been reported to be associated with different stages of plaque formation, including seeding, growth, and continuous deposition. Notably, GM1 ganglioside was found to correlate with both plaque seeding and growth. This is important as GM1 has previously been implicated in AD pathology as both a CSF biomarker candidate as well as a key interaction partner in amyloid seeding at the subcellular level[240, 241]. The sequence of ganglioside amyloid co-aggregation and interaction prior or during plaque formation and growth is however difficult to discern using steady state/static imaging tools.

To further explore lipid-amyloid co-aggregation dynamics, advanced stable isotope labeling combined with correlative chemical imaging allowed us to reveal that GM1 is continuously deposited into plaques along with Aβ peptides. Therefore, all these findings support the idea that the role of GM-Aβ interactions are critical to AD pathology.

Leveraging this correlative chemical imaging approach, we also examined Aβ peptide progression in newly developed transgenic mouse models. Combining *in vitro* and *in vivo* experiments with MALDI-MSI analysis of brain tissue, we successfully revealed the amyloid peptide evolution patterns in new mouse models. Additionally, examining different AD cases with correlative chemical imaging systems allowed us to delineate distinct Aβ peptide signatures across plaque types in both sAD and fAD cases. This further highlights the potential of advanced correlative chemical imaging techniques in enhancing our understanding of amyloid plaque heterogeneity and its implications for AD pathology.

However, some limitations remain in these studies. Although we utilized *in situ* MALDI-TOF MS for molecular identification, challenges persist, especially regarding lipid characterization. Additional techniques, such as trapped ion mobility mass spectrometry imaging and *in situ* MS/MS on our transgenic models, have expanded the number of identifiable lipids, but the range is still limited. Given the growing evidence that neutral lipids, such as those in lipid droplets, play a role in the microglia-mediated inflammatory response associated with amyloid pathology, future studies should expand to neutral lipids in microglia. Techniques such as chemical derivatization to enhance cholesterol signals from tissue[242], or the use of silicon nanopost array-assisted laser desorption ionization[243], could improve mass spectrometry imaging of these lipids. Furthermore, techniques like MALDI-2, with higher sensitivity, and AP-MALDI, combined with high-resolution MS (e.g., Orbitrap and FTMS), could also be employed[244-246].

Another critical area for future investigation is the complexity of amyloid plaque pathology in human brains. Although the methods used in this thesis provide valuable information, the sample size was limited, underscoring the need for larger studies to validate these findings and broaden their applicability.

Future studies are essential to expand the scope of our research, and we need to examine a larger number of human samples to thoroughly investigate the molecular events, particularly the interactions between lipids and amyloid peptides in AD pathology.

Analyzing a more diverse set of human samples will not only enhance the robustness of our findings but also provide insights into the variations in lipid-amyloid interactions across individuals and disease stages. This is especially

important given the growing evidence that lipid composition can significantly influence the formation and progression of amyloid plaques.

In addition, improving the spatial resolution of MSI is crucial for targeting specific cell types, such as astrocytes and microglia, which play key roles in the pathogenesis of AD. Higher spatial resolution imaging techniques, such as MALDI-2, significantly enhance the signal of low abundant compounds. This could enable precisely locating amyloid plaques and lipid deposits towards single cells within the brain's complex cellular architecture. By focusing on these specific cell types, we can gain a deeper understanding of how astrocytes and microglia interact with amyloid pathology, including their roles in inflammation, plaque clearance, and the regulation of neurodegenerative processes.

ACKNOWLEDGEMENT

During the process of writing this thesis, I often imagined the moment I would begin drafting my acknowledgments. Now, as I finally write these words, the reality that my four-year doctoral journey is nearing its end has truly sunk in. Looking back on this time, the past four years have flown by. It has been an incredibly valuable period in my life, not only because of the research that I have been working on, but also because of the wonderful people I've met here. I sincerely thank everyone who has supported me during my PhD journey.

First, I want to express my deepest gratitude to my main supervisor, **Jörg Hanrieder**. Four years ago, during the challenging period of the pandemic when many laboratories slowed their operations, you chose to give me the opportunity to join your team despite not having met me in person. I am deeply thankful for this invaluable chance. Your trust and support allowed me to transition from my background in pharmacognosy to a new field of neurodegenerative disease research, with a focus on mass spectrometry imaging techniques. You are not only a passionate and talented researcher but also an excellent mentor and team leader. Your patient guidance enabled me to embark on this journey in neurodegenerative disease research. Your wealth of research experience has helped me navigate critical moments of failure, while your constant encouragement has inspired me to rise above setbacks and face new challenges with confidence. Over these four years, I have learned not only knowledge and technical skills but also the importance of curiosity, persistence, and problem-solving in becoming a good researcher. You are the best mentor and a key guide in my research journey. It has been my honor and joy to be your student, I truly appreciate it!

Next, I wish to thank my co-supervisor, **Henrik Zetterberg**. I still remember how your positive and energetic demeanor during my first online interview eased my nervousness. You are a passionate and dedicated scientist and watching your tireless efforts in the lab has always filled me with admiration for how you manage such a remarkable workload. Thank you for your insightful discussions that have guided and inspired my research, as well as for your encouragement during each of my presentations.

I would also like to express my gratitude to my collaborative supervisors **Emma Sparr** and **Sara Linse**. Your questions and perspectives during discussions, stemming from your expertise in different fields, have given me

valuable opportunities to think about my research from new angles. Thank you for your encouragement and for sharing your rich experiences in research, which have been a great source of inspiration, helping me move forward in my scientific journey.

Thank you, **Gunnar Brinkmalm**, **Ann Brinkmalm Westman**, and **Johan Gobom**—our brilliant MS team in the lab—for your incredible support and expertise. I truly appreciate the insightful conversations we've had about mass spectrometry, which have significantly enhanced my understanding of the field. I'm also grateful for the memorable conference journeys we've shared, which were not only intellectually stimulating but also filled with unforgettable experiences.

Katie Stringer, thank you for your incredible support, starting from reaching out to me on WeChat before I even arrived in Gothenburg, sharing your valuable experiences about life and lab work here. It was a wonderful experience working with you, even though it's unfortunate that our collaboration didn't last longer. I deeply appreciate your help during that time. **Patrick Wehrli**, thank you for being by my side and assisting with all the different tasks right from the start of my journey in the lab. I'm also grateful for introducing me to Pizza Marcus, which led me to discover the best pizza salad in Gothenburg—it's a small joy that made my time here even more enjoyable. **Ambra Dreos**, I still remember when you and Katie gave me a tour of the lab on my first day. When I was unsure about filling out an application form, you kindly helped me complete it. I am truly grateful for your support throughout this incredible journey. It has been a wonderful opportunity to collaborate with you on various projects, expanding my knowledge in new fields. **Srinivas Koutarapu**, it has been my absolute luck and joy to work with you! For nearly two years, we were the only two focusing on imaging work in the lab, and I can't express how much of a relief it was to have you as a collaborator. Working alongside you made the challenges feel lighter. The time we spent together was filled with brilliant project discussions, smooth collaborations, exciting conference trips, and fantastic after-work activities. You brought so much positivity and energy into my PhD life, making it an unforgettable experience. You are truly the best! **Durga Jha**, it's been such a pleasure to have you by my side! From all the happy moments we shared to the smooth collaborations in the lab, to the amazing shows and unforgettable trips we've enjoyed together, and of course, to the fantastic conversations and the best dosa I've ever had—thank you for making my lab work and PhD journey so much more fun and memorable. Thank you so much for everything!

Maciej Dulewicz, our best R expert! Thank you so much for your incredible support, insightful discussions, and inviting me on your Chinese cuisine adventures. I've also greatly appreciated your brilliant "guidance" on pooling—I'll make sure to put it into practice without wasting my "talent" on it:) Your expertise and support have made a significant impact on my work and my PhD journey. I am truly grateful for all the learning and fun we've shared together. **Aleksandra Antic**, it's hard to believe that you've been with the lab for over a year—time really flies! Thank you for the fun time we spent in the lab. Also, I'm not someone who cooks much but thank you for your company and for the wonderful lunchtime we've shared. As we can see, there will be many opportunities for you to use formic acid. I hope you'll be able to open the ampules easily without an opener one day, and I wish you the best of luck on your PhD journey! **Alicja Szadziewska**, I truly appreciate all your efforts and organization in keeping our lab running smoothly, as well as our great collaborative work. And, of course, thank you for all the fantastic hours we've spent together, filled with great food, drinks, and engaging conversations. Your companionship and support have truly been a highlight! **Lydia Fenson**, it has been a pleasure working with you. Thank you for all the joyful moments we've shared together. I wish you the best of luck as you continue your PhD journey, which I'm sure will be filled with endless opportunities and accomplishments. **Sofia Johansson**, thank you so much for all the time we spent together in the lab and all the fun we had during our after-work activities! I am so happy to work with you on a different sample :) Good luck with your ongoing project! **Ajay Pradhan**, it's such a pleasure starting my PhD around the same time as you and working together on the same collaborative project. Thank you for all the support you've given me with courses, projects, and preparation of my thesis. Your help has made this journey much smoother, and I'm grateful to have shared this experience with you. **Sneha Desai** and **Jack Wood**, thank you for all the wonderful memories we created together in London, Gothenburg, and Geilo! From the endless inspiration on projects to the fascinating cultural differences and engaging conversations, I truly cherished the time spent with you. It was a pleasure sharing such enriching experiences and fun moments.

Elena Camporesi, **Juan Lantero Rodriguez**, **Ida Pesämaa**, and **Kübra Tan**, you are the best office buddy! Thank you all for the wonderful time we've shared in the office. The fun conversations and interesting topics we've had have made my PhD journey so much more enjoyable and relaxed! I truly appreciate your company and the positive energy you bring to the workspace!

Andrea Lessa Benedet, **Laia Montoliu-Gaya**, **Johanna Nilsson** and **Bárbara Fernandes Gomes**, thank you for your invaluable help with the lab routine tasks and wonderful time we shared together throughout my PhD journey. **Fernando Gonzalez, Joel Simrén, Sophia Weiner, Burak Arslan, Francisco Meda, Guglielmo Di Molfetta, Ilaria Pola, Przemysław Radosław Kac, Mathias Sauer, Jakub Vávra**, **Luiza Santos Machado** and **Diana Piotrowska**, thank you for all the wonderful moments we shared and the fantastic discussions we had! I wish you all the best with your ongoing projects.

Celia Hök Fröhlander, Rose-Marie Fishman Grell, Anna Pfister, thank you so much for all your incredible help throughout this journey, from managing orders and packages to handling samples and all the small details in between. I truly appreciate your patience and support in keeping everything running smoothly. Your assistance has been invaluable, and I'm deeply grateful for everything you've done to make this experience easier and more enjoyable! **Celia**, I promise that I will share my beef stew recipe with you after my defence😊

Dag Sehlin, María Pagnon de la Vega, Katherine Schwetye, Kaleigh Roberts, Tammaryn Lashley and **Frances Edwards**, thank you for all the samples that you have supported and all the inspirative discussions with you.

Ok, now a small part in Chinese:

俏男老弟，佳禾和嘉姐，在哥德堡的四年感谢有你们的陪伴！我们一起吃过的美食，品过的美酒，那些愉快玩耍畅聊的美好时光，都是我博士生活里的光。分离总在所难免，希望我们聚是一团火，散做满天星！F4 永存！

感谢三十年来支持爱护我的最好的爸爸妈妈和各位家人。在疫情期间做出让我独自出国读博的决定不易，感谢爸爸妈妈的理解和支持。谢谢你们做我坚实的后盾，希望早日也成为你们坚实的后盾。

虽然我从不是个对自己所做的决定轻易后悔的人，但是博士四年，唯一的遗憾是没能在疫情期间回国，没能亲口跟爱我呵护我的长辈说再见。爷爷，三奶奶，和我的姥姥，感谢你们养育、爱护我健康成长。

REFERENCES

1. 2024 Alzheimer's disease facts and figures. *Alzheimers Dement* **2024,** *20* (5), 1-146.
2. Alzheimer, A.; Stelzma, R. A.; Schnitzlein, H. N., et al., An EnglishTranslation of Alzheimer's 1907 Paper, "Uber eine eigenartige Erlranliung der Hirnrinde". *Clinical Anatomy* **1995,** *8*, 429-431.
3. Janssen, J. C. e. a., Early onset familial Alzheimer's disease_Mutation frequency in 31 families. *Neurology* **2003,** *60* (2), 235-239.
4. Nichols, E.; Steinmetz, J. D.; Vollset, S. E., et al., Estimation of the global prevalence of dementia in 2019 and forecasted prevalence in 2050: an analysis for the Global Burden of Disease Study 2019. *The Lancet Public Health* **2022,** *7* (2), e105-e125.
5. Dubois, B.; Hampel, H.; Feldman, H. H., et al., Preclinical Alzheimer's disease: Definition, natural history, and diagnostic criteria. *Alzheimers Dement* **2016,** *12* (3), 292-323.
6. Anderson, N. D., State of the science on mild cognitive impairment (MCI). *CNS Spectr* **2019,** *24* (1), 78-87.
7. Blennow, K.; de Leon, M. J.; Zetterberg, H., Alzheimer's disease. *Lancet* **2006,** *368* (9533), 387-403.
8. Hodges, J. R., Alzheimer's centennial legacy: origins, landmarks and the current status of knowledge concerning cognitive aspects. *Brain* **2006,** *129* (Pt 11), 2811-22.
9. Zetterberg, H.; Bendlin, B. B., Biomarkers for Alzheimer's disease-preparing for a new era of disease-modifying therapies. *Mol Psychiatry* **2021,** *26* (1), 296-308.
10. Tapiola, T.; Alafuzoff, I.; Herukka, S.-K., et al., Cerebrospinal Fluid β-Amyloid 42 and Tau Proteins as Biomarkers of Alzheimer-Type Pathologic Changes in the Brain. *Arch Neurol* **2009,** *66* (3), 382-389.
11. Samgard, K.; Zetterberg, H.; Blennow, K., et al., Cerebrospinal fluid total tau as a marker of Alzheimer's disease intensity. *Int J Geriatr Psychiatry* **2010,** *25* (4), 403-10.
12. Blom, E. S.; Giedraitis, V.; Zetterberg, H., et al., Rapid progression from mild cognitive impairment to Alzheimer's disease in subjects with elevated levels of tau in cerebrospinal fluid and the APOE epsilon4/epsilon4 genotype. *Dement Geriatr Cogn Disord* **2009,** *27* (5), 458-64.
13. Karikari, T. K.; Ashton, N. J.; Brinkmalm, G., et al., Blood phospho-tau in Alzheimer disease: analysis, interpretation, and clinical utility. *Nat Rev Neurol* **2022,** *18* (7), 400-418.
14. Edison, P.; Carter, S. F.; Rinne, J. O., et al., Comparison of MRI based and PET template based approaches in the quantitative analysis of amyloid imaging with PIB-PET. *Neuroimage* **2013,** *70*, 423-33.

15. Ikonomovic, M. D.; Klunk, W. E.; Abrahamson, E. E., et al., Post-mortem correlates of in vivo PiB-PET amyloid imaging in a typical case of Alzheimer's disease. *Brain* **2008,** *131* (Pt 6), 1630-45.
16. Knopman, D. S.; Jack, C. R., Jr.; Wiste, H. J., et al., 18F-fluorodeoxyglucose positron emission tomography, aging, and apolipoprotein E genotype in cognitively normal persons. *Neurobiol Aging* **2014,** *35* (9), 2096-106.
17. Franke, T. N.; Irwin, C.; Bayer, T. A., et al., In vivo Imaging With (18)F-FDG- and (18)F-Florbetaben-PET/MRI Detects Pathological Changes in the Brain of the Commonly Used 5XFAD Mouse Model of Alzheimer's Disease. *Front Med (Lausanne)* **2020,** *7*, 529.
18. Sengoku, R., Aging and Alzheimer's disease pathology. *Neuropathology* **2020,** *40* (1), 22-29.
19. Sinha, S.; Lieberburg, I., Cellular mechanisms of β-amyloid production and secretion. *Proc. Natl. Acad. Sci. USA* **1999,** *96*, 11049–11053.
20. Storey, E.; Cappai, R., The amyloid precursor protein of Alzheimer's disease and the Abeta peptide. *Neuropathol Appl Neurobiol* **1999,** *25* (2), 81-97.
21. Kummer, M. P.; Heneka, M. T., Truncated and modified amyloid-beta species. *Alzheimer's Research & Therapy* **2014,** *6* (28), 1-9.
22. Gomez, W.; Morales, R.; Maracaja-Coutinho, V., et al., Down syndrome and Alzheimer's disease: common molecular traits beyond the amyloid precursor protein. *Aging* **2020,** *12* (1), 1011-1033.
23. O'Brien, R. J.; Wong, P. C., Amyloid precursor protein processing and Alzheimer's disease. *Annu Rev Neurosci* **2011,** *34*, 185-204.
24. König, G.; Mönning, U.; Czech, C., et al., Identification and differential expression of a novel alternative splice isoform of the beta A4 amyloid precursor protein (APP) mRNA in leukocytes and brain microglial cells. *Journal of Biological Chemistry* **1992,** *267* (15), 10804-10809.
25. Menendez-Gonzalez, M.; Perez-Pinera, P.; Martinez-Rivera, M., et al., APP processing and the APP-KPI domain involvement in the amyloid cascade. *Neurodegener Dis* **2005,** *2* (6), 277-83.
26. Ben Khalifa, N.; Tyteca, D.; Marinangeli, C., et al., Structural features of the KPI domain control APP dimerization, trafficking, and processing. *FASEB J* **2012,** *26* (2), 855-67.
27. Kwak, Y.-D.; Brannen, C. L.; Qu, T., et al., Amyloid Precursor Protein Regulates Differentiation of Human Neural Stem Cells. *Stem Cells and Development* **2006,** *15*, 381–389.
28. Coronel, R.; Lachgar, M.; Bernabeu-Zornoza, A., et al., Neuronal and Glial Differentiation of Human Neural Stem Cells Is Regulated by Amyloid Precursor Protein (APP) Levels. *Mol Neurobiol* **2019,** *56* (2), 1248-1261.

29. Wang, B.; Li, H.; Mutlu, S. A., et al., The Amyloid Precursor Protein Is a Conserved Receptor for Slit to Mediate Axon Guidance. *eNeuro* **2017,** *4* (3).
30. Sosa, L. J.; Bergman, J.; Estrada-Bernal, A., et al., Amyloid precursor protein is an autonomous growth cone adhesion molecule engaged in contact guidance. *PLoS One* **2013,** *8* (5), e64521.
31. Jung, C. K.; Herms, J., Role of APP for dendritic spine formation and stability. *Exp Brain Res* **2012,** *217* (3-4), 463-70.
32. Lee, K. J.; Moussa, C. E.; Lee, Y., et al., Beta amyloid-independent role of amyloid precursor protein in generation and maintenance of dendritic spines. *Neuroscience* **2010,** *169* (1), 344-56.
33. Zou, C.; Crux, S.; Marinesco, S., et al., Amyloid precursor protein maintains constitutive and adaptive plasticity of dendritic spines in adult brain by regulating D-serine homeostasis. *EMBO J* **2016,** *35* (20), 2213-2222.
34. Wilkins, H. M.; Swerdlow, R. H., Amyloid precursor protein processing and bioenergetics. *Brain Res Bull* **2017,** *133*, 71-79.
35. Castro, M. A.; Hadziselimovic, A.; Sanders, C. R., The vexing complexity of the amyloidogenic pathway. *Protein Sci* **2019,** *28* (7), 1177-1193.
36. Zhang, S.; Wang, Z.; Cai, F., et al., BACE1 Cleavage Site Selection Critical for Amyloidogenesis and Alzheimer's Pathogenesis. *J Neurosci* **2017,** *37* (29), 6915-6925.
37. Song, W.; Zhang, J., The role of APP and BACE1 trafficking in APP processing and amyloid-β generation. *Alzheimer's Research & Therapy* **2013,** *5* (46), 1-8.
38. Zhou, Z. D.; Chan, C. H.; Ma, Q. H., et al., The roles of amyloid precursor protein (APP) in neurogenesis: Implications to pathogenesis and therapy of Alzheimer disease. *Cell Adh Migr* **2011,** *5* (4), 280-92.
39. Lichtenthaler, S. F., Alpha-secretase in Alzheimer's disease: molecular identity, regulation and therapeutic potential. *J Neurochem* **2011,** *116* (1), 10-21.
40. Vingtdeux, V.; Marambaud, P., Identification and biology of alpha-secretase. *J Neurochem* **2012,** *120 Suppl 1*, 34-45.
41. Tan, J. Z. A.; Gleeson, P. A., The trans-Golgi network is a major site for alpha-secretase processing of amyloid precursor protein in primary neurons. *J Biol Chem* **2019,** *294* (5), 1618-1631.
42. Kwak, Y. D.; Dantuma, E.; Merchant, S., et al., Amyloid-beta precursor protein induces glial differentiation of neural progenitor cells by activation of the IL-6/gp130 signaling pathway. *Neurotox Res* **2010,** *18* (3-4), 328-38.
43. Cole, S. L.; Vassar, R., The Alzheimer's disease beta-secretase enzyme, BACE1. *Mol Neurodegener* **2007,** *2*, 22.

44. Tan, J. Z. A.; Fourriere, L.; Wang, J., et al., Distinct anterograde trafficking pathways of BACE1 and amyloid precursor protein from the TGN and the regulation of amyloid-beta production. *Mol Biol Cell* **2020,** *31* (1), 27-44.
45. Ahmed, R. R.; Holler, C. J.; Webb, R. L., et al., BACE1 and BACE2 enzymatic activities in Alzheimer's disease. *J Neurochem* **2010,** *112* (4), 1045-53.
46. Yan, R.; Munzner, J. B.; Shuck, M. E., et al., BACE2 functions as an alternative alpha-secretase in cells. *J Biol Chem* **2001,** *276* (36), 34019-27.
47. Lu, P.; Bai, X. C.; Ma, D., et al., Three-dimensional structure of human gamma-secretase. *Nature* **2014,** *512* (7513), 166-170.
48. Bai, X. C.; Yan, C.; Yang, G., et al., An atomic structure of human gamma-secretase. *Nature* **2015,** *525* (7568), 212-217.
49. Fernandez, M. A.; Biette, K. M.; Dolios, G., et al., Transmembrane Substrate Determinants for gamma-Secretase Processing of APP CTFbeta. *Biochemistry* **2016,** *55* (40), 5675-5688.
50. Wolfe, M. S., Processive proteolysis by gamma-secretase and the mechanism of Alzheimer's disease. *Biol Chem* **2012,** *393* (9), 899-905.
51. Qi-Takahara, Y.; Morishima-Kawashima, M.; Tanimura, Y., et al., Longer forms of amyloid beta protein: implications for the mechanism of intramembrane cleavage by gamma-secretase. *J Neurosci* **2005,** *25* (2), 436-45.
52. Kakuda, N.; Yamaguchi, H.; Akazawa, K., et al., γ-Secretase Activity Is Associated with Braak Senile Plaque Stages. *The American Journal of Pathology* **2020,** *190* (6), 1323-1331.
53. Chalifour, R. J.; McLaughlin, R. W.; Lavoie, L., et al., Stereoselective interactions of peptide inhibitors with the beta-amyloid peptide. *J Biol Chem* **2003,** *278* (37), 34874-81.
54. Liu, R.; McAllister, C.; Lyubchenko, Y., et al., Residues 17-20 and 30-35 of beta-amyloid play critical roles in aggregation. *J Neurosci Res* **2004,** *75* (2), 162-171.
55. Thal, D. R.; Walter, J.; Saido, T. C., et al., Neuropathology and biochemistry of Abeta and its aggregates in Alzheimer's disease. *Acta Neuropathol* **2015,** *129* (2), 167-82.
56. Chen, Y. R.; Glabe, C. G., Distinct early folding and aggregation properties of Alzheimer amyloid-beta peptides Abeta40 and Abeta42: stable trimer or tetramer formation by Abeta42. *J Biol Chem* **2006,** *281* (34), 24414-22.
57. Agrawal, N.; Skelton, A. A., Structure and Function of Alzheimer's Amyloid betaeta Proteins from Monomer to Fibrils: A Mini Review. *Protein J* **2019,** *38* (4), 425-434.
58. Ono, K.; Watanabe-Nakayama, T., Aggregation and structure of amyloid beta-protein. *Neurochem Int* **2021,** *151*, 105208.

59. Linse, S., Mechanism of amyloid protein aggregation and the role of inhibitors. *Pure and Applied Chemistry* **2019,** *91* (2), 211-229.
60. Gurry, T.; Stultz, C. M., Mechanism of amyloid-beta fibril elongation. *Biochemistry* **2014,** *53* (44), 6981-91.
61. Sinnige, T., Molecular mechanisms of amyloid formation in living systems. *Chem Sci* **2022,** *13* (24), 7080-7097.
62. Hardy, J. A.; Higgins, G. A., Alzheimer's Disease: The Amyloid Cascade Hypothesis. *Science* **1992,** *256*, 184-185.
63. Oide, T.; Kinoshita, T.; Arima, K., Regression stage senile plaques in the natural course of Alzheimer's disease. *Neuropathol Appl Neurobiol* **2006,** *32* (5), 539-56.
64. Blennow, K.; Bogdanovic, N.; Alafuzoff, I., et al., Synaptic pathology in Alzheimer's disease: relation to severity of dementia, but not to senile plaques, neurofibrillary tangles, or the ApoE4 allele. *J Neural Transm* **1996,** *103*, 603-618.
65. Dickson, D. W., The Pathogenesis of Senile Plaques. *Journal of Neuropathology & Experimental Neurology* **1997,** *56* (4), 321-339.
66. Svenningsson, A. L.; Stomrud, E.; Insel, P. S., et al., Beta-amyloid pathology and hippocampal atrophy are independently associated with memory function in cognitively healthy elderly. *Sci Rep* **2019,** *9* (1), 11180.
67. Dennis W. Dickson, H. A. C., Linda A. Mattiace, David M. Masur, Alan D. Blau, Peter Davies, Shu-Hui Yen, Miriam K. Aronson,, Identification of normal and pathological aging in prospectively studied nondemented elderly humans. *Neurobiology of Aging* **1992,** *13* (1), 179-189.
68. Larson, M. E.; Lesne, S. E., Soluble Abeta oligomer production and toxicity. *J Neurochem* **2012,** *120 Suppl 1* (Suppl 1), 125-139.
69. Ferreira, S. T.; Lourenco, M. V.; Oliveira, M. M., et al., Soluble amyloid-beta oligomers as synaptotoxins leading to cognitive impairment in Alzheimer's disease. *Front Cell Neurosci* **2015,** *9*, 191.
70. Sakono, M.; Zako, T.; Ueda, H., et al., Formation of highly toxic soluble amyloid beta oligomers by the molecular chaperone prefoldin. *FEBS J* **2008,** *275* (23), 5982-93.
71. Cras, P.; Kawai, M.; Lowery, D., et al., Senile plaque neurites in Alzheimer disease accumulate amyloid precursor protein. *Proceedings of the National Academy of Sciences* **1991,** *88* (17), 7552-7556.
72. Mufson, E. J.; Ikonomovic, M. D.; Counts, S. E., et al., Molecular and cellular pathophysiology of preclinical Alzheimer's disease. *Behav Brain Res* **2016,** *311*, 54-69.
73. Gold, M., Phase II clinical trials of anti-amyloid beta antibodies: When is enough, enough? *Alzheimers Dement (N Y)* **2017,** *3* (3), 402-409.
74. Liu, E.; Schmidt, M. E.; Margolin, R., et al., Amyloid-β 11C-PiB-PET imaging results from 2 randomized bapineuzumab phase 3 AD trials. *Neurology* **2015,** *85* (8), 692-700.

75. Mullane, K.; Williams, M., Alzheimer's therapeutics: continued clinical failures question the validity of the amyloid hypothesis-but what lies beyond? *Biochem Pharmacol* **2013,** *85* (3), 289-305.
76. Howie, A. J.; Brewer, D. B., Optical properties of amyloid stained by Congo red: history and mechanisms. *Micron* **2009,** *40* (3), 285-301.
77. Wisniewski, H. M.; Wen, G. Y.; Kim, K. S., Comparison of four staining methods on the detection of neuritic plaques. *Acta Neuropathol* **1989,** *78*, 22-27.
78. Urbanc, B.; Cruz, L.; Le, R., et al., Neurotoxic effects of thioflavin S-positive amyloid deposits in transgenic mice and Alzheimer's disease. *Proceedings of the National Academy of Sciences* **2002,** *99* (22), 13990-13995.
79. Anne K Vehmas, C. H. K., Walter F Stewart, Juan C Troncoso, Immune reactive cells in senile plaques and cognitive decline in Alzheimer's disease. *Neurobiology of Aging* **2003,** *24* (2), 321-331.
80. **Dickson, D. W. e. a.**, Identification of Normal and Pathological Aging in Prospectively Studied Nondemented Elderly Humans. *Neurobiol Aging* **1992,** *13*, 179-189.
81. Michno, W.; Nystrom, S.; Wehrli, P., et al., Pyroglutamation of amyloid-betax-42 (Abetax-42) followed by Abeta1-40 deposition underlies plaque polymorphism in progressing Alzheimer's disease pathology. *J Biol Chem* **2019,** *294* (17), 6719-6732.
82. Mori, H.; Takio, K.; Ogawara, M., et al., Mass spectrometry of purified amyloid beta protein in Alzheimer's disease. *Journal of Biological Chemistry* **1992,** *267* (24), 17082-17086.
83. Iwatsubo, T.; Odaka, A.; Suzuki, N., et al., Visualization of Aβ42 (43) and Aβ40 in senile plaques with end-specific Aβ monoclonals: evidence that an initially deposited species is Aβ42 (43). *Neuron* **1994,** *13* (1), 45-53.
84. Näslund, J.; Schierhorn, A.; Hellman, U., et al., Relative abundance of Alzheimer A beta amyloid peptide variants in Alzheimer disease and normal aging. *Proceedings of the National Academy of Sciences* **1994,** *91* (18), 8378-8382.
85. Houlden, H.; Baker, M.; McGowan, E., et al., Variant Alzheimer's disease with spastic paraparesis and cotton wool plaques is caused by PS-1 mutations that lead to exceptionally high amyloid-? concentrations. *Annals of Neurology* **2000,** *48* (5), 806-808.
86. Crook, R.; Verkkoniemi, A.; Perez-Tur, J., et al., A variant of Alzheimer's disease with spastic paraparesis and unusual plaques due to deletion of exon 9 of presenilin 1. *Nature Medicine* **1998,** *4* (4), 452-455.
87. Le, T. V.; Crook, R.; Hardy, J., et al., Cotton Wool Plaques in Non-Familial Late-Onset Alzheimer Disease. *Journal of Neuropathology & Experimental Neurology* **2001,** *60* (11), 1051-1061.

88. Boon, B. D. C.; Bulk, M.; Jonker, A. J., et al., The coarse-grained plaque: a divergent Abeta plaque-type in early-onset Alzheimer's disease. *Acta Neuropathol* **2020,** *140* (6), 811-830.
89. Thal, D. R.; Rüb, U.; Orantes, M., et al., Phases of Aβ-deposition in the human brain and its relevance for the development of AD. *Neurology* **2002,** *58* (12), 1791-1800.
90. Hampel, H.; Hardy, J.; Blennow, K., et al., The Amyloid-β Pathway in Alzheimer's Disease. *Mol. Psychiatry* **2021,** *26* (10), 5481-5503.
91. Walker, L. C., Abeta Plaques. *Free Neuropathol* **2020,** *1*.
92. Guerreiro, R.; Bras, J., The age factor in Alzheimer's disease. *Genome Med* **2015,** *7*, 106.
93. Michaelson, D. M., APOE epsilon4: the most prevalent yet understudied risk factor for Alzheimer's disease. *Alzheimers Dement* **2014,** *10* (6), 861-8.
94. Roses, M. D., Allen D., Apolipoprotein E alleles as risk factors in Alzheimer's disease. *Annual Review of Medicine* **1996,** *47* (Volume 47, 1996), 387-400.
95. Dubal, D. B.; Rogine, C., Apolipoprotein E epsilon4 and Risk Factors for Alzheimer Disease-Let's Talk About Sex. *JAMA Neurol* **2017,** *74* (10), 1167-1168.
96. Buckley, R. F.; Mormino, E. C.; Rabin, J. S., et al., Sex Differences in the Association of Global Amyloid and Regional Tau Deposition Measured by Positron Emission Tomography in Clinically Normal Older Adults. *JAMA Neurol* **2019,** *76* (5), 542-551.
97. Digma, L. A.; Madsen, J. R.; Rissman, R. A., et al., Women can bear a bigger burden: ante- and post-mortem evidence for reserve in the face of tau. *Brain Commun* **2020,** *2* (1), fcaa025.
98. Zhang, X. X.; Tian, Y.; Wang, Z. T., et al., The Epidemiology of Alzheimer's Disease Modifiable Risk Factors and Prevention. *J Prev Alzheimers Dis* **2021,** *8* (3), 313-321.
99. Bi, C.; Bi, S.; Li, B., Processing of Mutant beta-Amyloid Precursor Protein and the Clinicopathological Features of Familial Alzheimer's Disease. *Aging Dis* **2019,** *10* (2), 383-403.
100. Masters, C. L.; Bateman, R.; Blennow, K., et al., Alzheimer's disease. *Nat Rev Dis Primers* **2015,** *1*, 15056.
101. Gessel, M. M.; Bernstein, S.; Kemper, M., et al., Familial Alzheimer's disease mutations differentially alter amyloid beta-protein oligomerization. *ACS Chem Neurosci* **2012,** *3* (11), 909-18.
102. Kelleher, R. J., 3rd; Shen, J., Presenilin-1 mutations and Alzheimer's disease. *Proc Natl Acad Sci U S A* **2017,** *114* (4), 629-631.
103. Tyan, S.-H.; Shih, A. Y.-J.; Walsh, J. J., et al., Amyloid precursor protein (APP) regulates synaptic structure and function. *Molecular and Cellular Neuroscience* **2012,** *51* (1), 43-52.

104. Klevanski, M.; Herrmann, U.; Weyer, S. W., et al., The APP Intracellular Domain Is Required for Normal Synaptic Morphology, Synaptic Plasticity, and Hippocampus-Dependent Behavior. *The Journal of Neuroscience* **2015,** *35* (49), 16018-16033.
105. Mullan, M.; Crawford, F.; Axelman, K., et al., A pathogenic mutation for probable Alzheimer's disease in the APP gene at the N–terminus of β–amyloid. *Nature Genetics* **1992,** *1* (5), 345-347.
106. Kumar, S.; Walter, J., Phosphorylation of amyloid beta (Aβ) peptides - a trigger for formation of toxic aggregates in Alzheimer's disease. *Aging (Albany NY)* **2011,** *3* (8), 803-12.
107. Ju, Y.; Asahi, T.; Sawamura, N., Arctic mutant Abeta40 aggregates on alpha7 nicotinic acetylcholine receptors and inhibits their functions. *J Neurochem* **2014,** *131* (5), 667-74.
108. Pagnon de la Vega, M.; Giedraitis, V.; Michno, W., et al., The Uppsala APP deletion causes early onset autosomal dominant Alzheimer's disease by altering APP processing and increasing amyloid β fibril formation. *Science Translational Medicine* **2021,** *13* (606), eabc6184.
109. Bertram, L.; Tanzi, R. E., Genomic mechanisms in Alzheimer's disease. *Brain Pathol* **2020,** *30* (5), 966-977.
110. Corder, E. H.; Lannfelt, L.; Bogdanovic, N., et al., The role of APOE polymorphisms in late-onset dementias. *Cellular and Molecular Life Sciences CMLS* **1998,** *54* (9), 928-934.
111. Liu, C.-C.; Kanekiyo, T.; Xu, H., et al., Apolipoprotein E and Alzheimer disease: risk, mechanisms and therapy. *Nature Reviews Neurology* **2013,** *9* (2), 106-118.
112. Husain, M. A.; Laurent, B.; Plourde, M., APOE and Alzheimer's Disease: From Lipid Transport to Physiopathology and Therapeutics. *Front Neurosci* **2021,** *15*, 630502.
113. Farmer, B. C.; Kluemper, J.; Johnson, L. A., Apolipoprotein E4 Alters Astrocyte Fatty Acid Metabolism and Lipid Droplet Formation. *Cells* **2019,** *8* (2).
114. Rodriguez, G. A.; Tai, L. M.; LaDu, M. J., et al., Human APOE4 increases microglia reactivity at Aβ plaques in a mouse model of Aβ deposition. *Journal of Neuroinflammation* **2014,** *11* (1), 111.
115. Liu, C. C.; Wang, N.; Chen, Y., et al., Cell-autonomous effects of APOE4 in restricting microglial response in brain homeostasis and Alzheimer's disease. *Nat Immunol* **2023,** *24* (11), 1854-1866.
116. Sun, G. Z.; He, Y. C.; Ma, X. K., et al., Hippocampal synaptic and neural network deficits in young mice carrying the human APOE4 gene. *CNS Neurosci Ther* **2017,** *23* (9), 748-758.
117. Chen, Y.; Durakoglugil, M. S.; Xian, X., et al., ApoE4 reduces glutamate receptor function and synaptic plasticity by selectively impairing ApoE receptor recycling. *Proc Natl Acad Sci U S A* **2010,** *107* (26), 12011-6.

118. Colonna, M.; Wang, Y., TREM2 variants: new keys to decipher Alzheimer disease pathogenesis. *Nat Rev Neurosci* **2016,** *17* (4), 201-7.
119. Vasquez, J. B.; Fardo, D. W.; Estus, S., ABCA7 expression is associated with Alzheimer's disease polymorphism and disease status. *Neurosci Lett* **2013,** *556*, 58-62.
120. Hickman, S. E.; El Khoury, J., TREM2 and the neuroimmunology of Alzheimer's disease. *Biochem Pharmacol* **2014,** *88* (4), 495-8.
121. Ulrich, J. D.; Holtzman, D. M., TREM2 Function in Alzheimer's Disease and Neurodegeneration. *ACS Chem Neurosci* **2016,** *7* (4), 420-7.
122. Song, W.; Hooli, B.; Mullin, K., et al., Alzheimer's disease-associated TREM2 variants exhibit either decreased or increased ligand-dependent activation. *Alzheimers Dement* **2017,** *13* (4), 381-387.
123. Jin, S. C.; Benitez, B. A.; Karch, C. M., et al., Coding variants in TREM2 increase risk for Alzheimer's disease. *Hum Mol Genet* **2014,** *23* (21), 5838-46.
124. Lamartinière, Y.; Boucau, M.-C.; Dehouck, L., et al., ABCA7 Downregulation Modifies Cellular Cholesterol Homeostasis and Decreases Amyloid-β Peptide Efflux in an in vitro Model of the Blood-Brain Barrier. *Journal of Alzheimer's Disease* **2018,** *64*, 1195-1211.
125. Sakae, N.; Liu, C. C.; Shinohara, M., et al., ABCA7 Deficiency Accelerates Amyloid-beta Generation and Alzheimer's Neuronal Pathology. *J Neurosci* **2016,** *36* (13), 3848-59.
126. Foley, P., Lipids in Alzheimer's disease: A century-old story. *Biochim Biophys Acta* **2010,** *1801* (8), 750-3.
127. Mirdha, L., Aggregation Behavior of Amyloid Beta Peptide Depends Upon the Membrane Lipid Composition. *The Journal of Membrane Biology* **2024,** *257* (3), 151-164.
128. Getz, G. S.; Reardon, C. A., Apoprotein E and Reverse Cholesterol Transport. *Int. J. Mol. Sci.* **2018,** *19* (11), 3479.
129. Yu, C.-J.; Wang, M.; Li, R.-Y., et al., TREM2 and Microglia Contribute to the Synaptic Plasticity: from Physiology to Pathology. *Mol. Neurobiol.* **2023,** *60* (2), 512-523.
130. Cuyvers, E.; De Roeck, A.; Van den Bossche, T., et al., Mutations in ABCA7 in a Belgian cohort of Alzheimer's disease patients: a targeted resequencing study. *The Lancet Neurology* **2015,** *14* (8), 814-822.
131. C, L.; M, S., Cholesterol Homeostasis Imbalance and Brain Functioning: Neurological Disorders and Behavioral Consequences. *Journal of Neurology and Neurological Disorders* **2014,** *1* (1).
132. Pfrieger, F. W., Cholesterol homeostasis and function in neurons of the central nervous system. *Cell Mol Life Sci* **2003,** *60* (6), 1158-71.
133. Silvius, J. R., Role of cholesterol in lipid raft formation: lessons from lipid model systems. *Biochim Biophys Acta* **2003,** *1610* (2), 174-83.

134. Megha; London, E., Ceramide selectively displaces cholesterol from ordered lipid domains (rafts): implications for lipid raft structure and function. *J Biol Chem* **2004,** *279* (11), 9997-10004.
135. Kabouridis, P. S.; Janzen, J.; Magee, A. L., et al., Cholesterol depletion disrupts lipid rafts and modulates the activity of multiple signaling pathways in T lymphocytes. *Eur J Immunol* **2000,** *30* (3), 954-63.
136. Saher, G.; Brugger, B.; Lappe-Siefke, C., et al., High cholesterol level is essential for myelin membrane growth. *Nat Neurosci* **2005,** *8* (4), 468-75.
137. Mathews, E. S.; Appel, B., Cholesterol Biosynthesis Supports Myelin Gene Expression and Axon Ensheathment through Modulation of P13K/Akt/mTor Signaling. *J Neurosci* **2016,** *36* (29), 7628-39.
138. Blanchard, J. W.; Akay, L. A.; Davila-Velderrain, J., et al., APOE4 impairs myelination via cholesterol dysregulation in oligodendrocytes. *Nature* **2022,** *611* (7937), 769-779.
139. Chen, L.; Zhao, Z. W.; Zeng, P. H., et al., Molecular mechanisms for ABCA1-mediated cholesterol efflux. *Cell Cycle* **2022,** *21* (11), 1121-1139.
140. Wang, X.; Li, H.; Sheng, Y., et al., The function of sphingolipids in different pathogenesis of Alzheimer's disease: A comprehensive review. *Biomed Pharmacother* **2024,** *171*, 116071.
141. Olsen, A. S. B.; Faergeman, N. J., Sphingolipids: membrane microdomains in brain development, function and neurological diseases. *Open Biol* **2017,** *7* (5).
142. Svennerholm, L.; Boström, K.; Jungbjer, B., et al., Membrane Lipids of Adult Human Brain: Lipid Composition of Frontal and Temporal Lobe in Subjects of Age 20 to 100 Years. *Journal of Neurochemistry* **1994,** *63* (5), 1802-1811.
143. Pernber, Z.; Blennow, K.; Bogdanovic, N., et al., Altered distribution of the gangliosides GM1 and GM2 in Alzheimer's disease. *Dement Geriatr Cogn Disord* **2012,** *33* (2-3), 174-88.
144. Matsuzaki, K., How do membranes initiate Alzheimer's Disease? Formation of toxic amyloid fibrils by the amyloid beta-protein on ganglioside clusters. *Acc Chem Res* **2014,** *47* (8), 2397-404.
145. Okada, T.; Ikeda, K.; Wakabayashi, M., et al., Formation of toxic Abeta(1-40) fibrils on GM1 ganglioside-containing membranes mimicking lipid rafts: polymorphisms in Abeta(1-40) fibrils. *J Mol Biol* **2008,** *382* (4), 1066-74.
146. Lin, C. F.; Chen, C. L.; Chiang, C. W., et al., GSK-3beta acts downstream of PP2A and the PI 3-kinase-Akt pathway, and upstream of caspase-2 in ceramide-induced mitochondrial apoptosis. *J Cell Sci* **2007,** *120* (Pt 16), 2935-43.
147. Tafesse, F. G.; Vacaru, A. M.; Bosma, E. F., et al., Sphingomyelin synthase-related protein SMSr is a suppressor of ceramide-induced mitochondrial apoptosis. *J Cell Sci* **2014,** *127* (Pt 2), 445-54.

148. Wang, Y.; Cella, M.; Mallinson, K., et al., TREM2 lipid sensing sustains the microglial response in an Alzheimer's disease model. *Cell* **2015,** *160* (6), 1061-71.
149. Cannon, J. P.; O'Driscoll, M.; Litman, G. W., Specific lipid recognition is a general feature of CD300 and TREM molecules. *Immunogenetics* **2012,** *64* (1), 39-47.
150. Shirotani, K.; Hori, Y.; Yoshizaki, R., et al., Aminophospholipids are signal-transducing TREM2 ligands on apoptotic cells. *Sci Rep* **2019,** *9* (1), 7508.
151. Fourgeaud, L.; Traves, P. G.; Tufail, Y., et al., TAM receptors regulate multiple features of microglial physiology. *Nature* **2016,** *532* (7598), 240-244.
152. Grassi, S.; Prioni, S.; Cabitta, L., et al., The Role of 3-O-Sulfogalactosylceramide, Sulfatide, in the Lateral Organization of Myelin Membrane. *Neurochem Res* **2016,** *41* (1-2), 130-43.
153. Eckhardt, M., The role and metabolism of sulfatide in the nervous system. *Mol Neurobiol* **2008,** *37* (2-3), 93-103.
154. Ishibashi, T.; Dupree, J. L.; Ikenaka, K., et al., A Myelin Galactolipid, Sulfatide, Is Essential for Maintenance of Ion Channels on Myelinated Axon But Not Essential for Initial Cluster Formation. *The Journal of Neuroscience* **2002,** *22* (15), 6507-6514.
155. McGonigal, R.; Barrie, J. A.; Yao, D., et al., Glial Sulfatides and Neuronal Complex Gangliosides Are Functionally Interdependent in Maintaining Myelinating Axon Integrity. *J Neurosci* **2019,** *39* (1), 63-77.
156. Shroff, S. M.; Pomicter, A. D.; Chow, W. N., et al., Adult CST-null mice maintain an increased number of oligodendrocytes. *J Neurosci Res* **2009,** *87* (15), 3403-14.
157. Hirahara, Y.; Bansal, R.; Honke, K., et al., Sulfatide is a negative regulator of oligodendrocyte differentiation: development in sulfatide-null mice. *Glia* **2004,** *45* (3), 269-77.
158. Palavicini, J. P.; Wang, C.; Chen, L., et al., Novel molecular insights into the critical role of sulfatide in myelin maintenance/function. *J Neurochem* **2016,** *139* (1), 40-54.
159. Marcus, J.; Honigbaum, S.; Shroff, S., et al., Sulfatide is essential for the maintenance of CNS myelin and axon structure. *Glia* **2006,** *53* (4), 372-81.
160. Han, X., Potential mechanisms contributing to sulfatide depletion at the earliest clinically recognizable stage of Alzheimer's disease: a tale of shotgun lipidomics. *J Neurochem* **2007,** *103 Suppl 1* (Suppl 1), 171-9.
161. Kaya, I.; Nilsson, A.; Luptakova, D., et al., Spatial lipidomics reveals brain region-specific changes of sulfatides in an experimental MPTP Parkinson's disease primate model. *NPJ Parkinsons Dis* **2023,** *9* (1), 118.

162. Novakova, L.; Singh, A. K.; Axelsson, M., et al., Sulfatide isoform pattern in cerebrospinal fluid discriminates progressive MS from relapsing-remitting MS. *J Neurochem* **2018,** *146* (3), 322-332.
163. Han, X.; Fagan, A. M.; Cheng, H., et al., Cerebrospinal fluid sulfatide is decreased in subjects with incipient dementia. *Ann Neurol* **2003,** *54* (1), 115-9.
164. Han, X.; D, M. H.; McKeel, D. W., Jr., et al., Substantial sulfatide deficiency and ceramide elevation in very early Alzheimer's disease: potential role in disease pathogenesis. *J Neurochem* **2002,** *82* (4), 809-18.
165. Cheng, H.; Wang, M.; Li, J. L., et al., Specific changes of sulfatide levels in individuals with pre-clinical Alzheimer's disease: an early event in disease pathogenesis. *J Neurochem* **2013,** *127* (6), 733-8.
166. Han, X.; Cheng, H.; Fryer, J. D., et al., Novel role for apolipoprotein E in the central nervous system. Modulation of sulfatide content. *J Biol Chem* **2003,** *278* (10), 8043-51.
167. Qiu, S.; Palavicini, J. P.; Han, X., Myelin lipid deficiency: a new key driver of Alzheimer's disease. *Neural Regen Res* **2023,** *18* (1), 121-122.
168. Qiu, S.; Palavicini, J. P.; Wang, J., et al., Adult-onset CNS myelin sulfatide deficiency is sufficient to cause Alzheimer's disease-like neuroinflammation and cognitive impairment. *Mol Neurodegener* **2021,** *16* (1), 64.
169. Michno, W.; Wehrli, P. M.; Koutarapu, S., et al., Structural amyloid plaque polymorphism is associated with distinct lipid accumulations revealed by trapped ion mobility mass spectrometry imaging. *J Neurochem* **2022,** *160* (4), 482-498.
170. Michno, W.; Kaya, I.; Nystrom, S., et al., Multimodal Chemical Imaging of Amyloid Plaque Polymorphism Reveals Abeta Aggregation Dependent Anionic Lipid Accumulations and Metabolism. *Anal Chem* **2018,** *90* (13), 8130-8138.
171. Yu, W.; Ying, J.; Wang, X., et al., The Involvement of Lactosylceramide in Central Nervous System Inflammation Related to Neurodegenerative Disease. *Front Aging Neurosci* **2021,** *13*, 691230.
172. Chatterjee, S.; Balram, A.; Li, W., Convergence: Lactosylceramide-Centric Signaling Pathways Induce Inflammation, Oxidative Stress, and Other Phenotypic Outcomes. *Int J Mol Sci* **2021,** *22* (4).
173. Chatterjee, S.; Pandey, A., The Yin and Yang of lactosylceramide metabolism: implications in cell function. *Biochim Biophys Acta* **2008,** *1780* (3), 370-82.
174. Pannu, R.; Won, J. S.; Khan, M., et al., A novel role of lactosylceramide in the regulation of lipopolysaccharide/interferon-gamma-mediated inducible nitric oxide synthase gene expression: implications for neuroinflammatory diseases. *J Neurosci* **2004,** *24* (26), 5942-54.

175. Oizumi, H.; Sugimura, Y.; Totsune, T., et al., Plasma sphingolipid abnormalities in neurodegenerative diseases. *PLoS One* **2022,** *17* (12), e0279315.
176. Won, J.-S.; Singh, A. K.; Singh, I., Lactosylceramide: a lipid second messenger in neuroinflammatory disease. *J. Neurochem.* **2007,** *103* (s1), 180-191.
177. Iuliano, M.; Seeley, C.; Sapp, E., et al., Disposition of Proteins and Lipids in Synaptic Membrane Compartments Is Altered in Q175/Q7 Huntington's Disease Mouse Striatum. *Front Synaptic Neurosci* **2021,** *13*, 618391.
178. Yamashita, A.; Oka, S.; Tanikawa, T., et al., The actions and metabolism of lysophosphatidylinositol, an endogenous agonist for GPR55. *Prostaglandins Other Lipid Mediat* **2013,** *107*, 103-16.
179. Chen, L.; Dar, N. J.; Na, R., et al., Enhanced defense against ferroptosis ameliorates cognitive impairment and reduces neurodegeneration in 5xFAD mice. *Free Radic Biol Med* **2022,** *180*, 1-12.
180. Sheikh, A. M.; Nagai, A., Lysophosphatidylcholine modulates fibril formation of amyloid beta peptide. *The FEBS Journal* **2011,** *278* (4), 634-642.
181. Sheikh, A. M.; Michikawa, M.; Kim, S. U., et al., Lysophosphatidylcholine increases the neurotoxicity of Alzheimer's amyloid beta1-42 peptide: role of oligomer formation. *Neuroscience* **2015,** *292*, 159-69.
182. Muramatsu, R.; Kuroda, M.; Matoba, K., et al., Prostacyclin prevents pericyte loss and demyelination induced by lysophosphatidylcholine in the central nervous system. *J Biol Chem* **2015,** *290* (18), 11515-25.
183. Farmer, B. C.; Walsh, A. E.; Kluemper, J. C., et al., Lipid Droplets in Neurodegenerative Disorders. *Front Neurosci* **2020,** *14*, 742.
184. Barbosa, A. D.; Savage, D. B.; Siniossoglou, S., Lipid droplet–organelle interactions: emerging roles in lipid metabolism. *Curr. Opin. Cell Biol.* **2015,** *35*, 91-97.
185. Ralhan, I.; Chang, C. L.; Lippincott-Schwartz, J., et al., Lipid droplets in the nervous system. *J Cell Biol* **2021,** *220* (7).
186. Boucher, D. M.; Vijithakumar, V.; Ouimet, M., Lipid Droplets as Regulators of Metabolism and Immunity. *Immunometabolism* **2021,** *3* (3).
187. Marschallinger, J.; Iram, T.; Zardeneta, M., et al., Lipid-droplet-accumulating microglia represent a dysfunctional and proinflammatory state in the aging brain. *Nat Neurosci* **2020,** *23* (2), 194-208.
188. Sienski, G.; Narayan, P.; Bonner, J. M., et al., APOE4 disrupts intracellular lipid homeostasis in human iPSC-derived glia. *Sci. Transl. Med.* **2021,** *13* (583), eaaz4564.
189. Games, D.; Adams, D.; Alessandrini, R., et al., Alzheimer-type neuropathology in transgenic mice overexpressing V717F β-amyloid precursor protein. *Nature* **1995,** *373* (6514), 523-527.

190. Hsiao, K.; Chapman, P.; Nilsen, S., et al., Correlative Memory Deficits, Aβ Elevation, and Amyloid Plaques in Transgenic Mice. *Science* **1996,** *274* (5284), 99-103.
191. Sturchler-Pierrat, C.; Abramowski, D.; Duke, M., et al., Two amyloid precursor protein transgenic mouse models with Alzheimer disease-like pathology. *Proceedings of the National Academy of Sciences* **1997,** *94* (24), 13287-13292.
192. Oddo, S.; Caccamo, A.; Shepherd, J. D., et al., Triple-transgenic model of Alzheimer's disease with plaques and tangles: intracellular Abeta and synaptic dysfunction. *Neuron* **2003,** *39* (3), 409-21.
193. Mucke, L.; Masliah, E.; Yu, G.-Q., et al., High-Level Neuronal Expression of Aβ_{1–42} in Wild-Type Human Amyloid Protein Precursor Transgenic Mice: Synaptotoxicity without Plaque Formation. *The Journal of Neuroscience* **2000,** *20* (11), 4050-4058.
194. Holcomb, L.; Gordon, M. N.; McGowan, E., et al., Accelerated Alzheimer-type phenotype in transgenic mice carrying both mutant amyloid precursor protein and presenilin 1 transgenes. *Nat. Med.* **1998,** *4* (1), 97-100.
195. Oakley, H.; Cole, S. L.; Logan, S., et al., Intraneuronal β-Amyloid Aggregates, Neurodegeneration, and Neuron Loss in Transgenic Mice with Five Familial Alzheimer's Disease Mutations: Potential Factors in Amyloid Plaque Formation. *The Journal of Neuroscience* **2006,** *26* (40), 10129-10140.
196. Joanna L Jankowsky, H. H. S., Tamara Ratovitski, Nancy A Jenkins, Neal G Copeland, David R Borchelt,, Co-expression of multiple transgenes in mouse CNS: a comparison of strategies. *Biomolecular Engineering* **2001,** *17* (6), 157-165.
197. Philipson, O.; Hammarstrom, P.; Nilsson, K. P., et al., A highly insoluble state of Abeta similar to that of Alzheimer's disease brain is found in Arctic APP transgenic mice. *Neurobiol Aging* **2009,** *30* (9), 1393-405.
198. Saito, T.; Matsuba, Y.; Mihira, N., et al., Single App knock-in mouse models of Alzheimer's disease. *Nat. Neurosci.* **2014,** *17* (5), 661-663.
199. Sakakibara, Y.; Sekiya, M.; Saito, T., et al., Amyloid-β plaque formation and reactive gliosis are required for induction of cognitive deficits in App knock-in mouse models of Alzheimer's disease. *BMC Neurosci.* **2019,** *20* (1), 13.
200. Karas, M.; Krüger, R., Ion Formation in MALDI: The Cluster Ionization Mechanism. *Chem. Rev.* **2003,** *103* (2), 427-440.
201. Karas, M.; Bachmann, D.; Hillenkamp, F., Influence of the wavelength in high-irradiance ultraviolet laser desorption mass spectrometry of organic molecules. *Anal. Chem.* **1985,** *57* (14), 2935-2939.
202. Tanaka, K.; Waki, H.; Ido, Y., et al., Protein and polymer analyses up to m/z 100 000 by laser ionization time-of-flight mass spectrometry. *Rapid Commun. Mass Spectrom.* **1988,** *2* (8), 151-153.

203. Spengler, B.; Hubert, M.; Kaufmann, R. In *Ion imaging and confocal microscopy with a new scanning UV-laser microprobe*, PROCEEDINGS OF THE ASMS CONFERENCE ON MASS SPECTROMETRY AND ALLIED TOPICS, AMERICAN SOCIETY FOR MASS SPECTROMETRY (ASMS): 1994; pp 1041-1041.
204. Caprioli, R. M.; Farmer, T. B.; Gile, J., Molecular imaging of biological samples: localization of peptides and proteins using MALDI-TOF MS. *Anal. Chem.* **1997,** *69* (23), 4751-4760.
205. Goodwin, R. J., Sample preparation for mass spectrometry imaging: small mistakes can lead to big consequences. *J. Proteomics* **2012,** *75* (16), 4893-4911.
206. Zhou, Q.; Fülöp, A.; Hopf, C., Recent developments of novel matrices and on-tissue chemical derivatization reagents for MALDI-MSI. *Analytical and Bioanalytical Chemistry* **2021,** *413* (10), 2599-2617.
207. Liu, H.; Pan, Y.; Xiong, C., et al., Matrix-assisted laser desorption/ionization mass spectrometry imaging (MALDI MSI) for in situ analysis of endogenous small molecules in biological samples. *TrAC Trends in Analytical Chemistry* **2022,** *157*, 116809.
208. van Kampen, J. J.; Luider, T. M.; Ruttink, P. J., et al., Metal ion attachment to the matrix meso ‐ tetrakis (pentafluorophenyl) porphyrin, related matrices and analytes: an experimental and theoretical study. *Journal of mass spectrometry* **2009,** *44* (11), 1556-1564.
209. Norris, J. L.; Caprioli, R. M., Analysis of Tissue Specimens by Matrix-Assisted Laser Desorption/Ionization Imaging Mass Spectrometry in Biological and Clinical Research. *Chemical Reviews* **2013,** *113* (4), 2309-2342.
210. Jiang, S., *Investigation of Neuropeptidomics and Proteomics by Multifaceted Approaches Coupled to Mass Spectrometry*. The University of Wisconsin-Madison: 2016.
211. Liu, D.; Liu, X.; Huang, S., et al., Simultaneous Mapping of Amino Neurotransmitters and Nucleoside Neuromodulators on Brain Tissue Sections by On-Tissue Chemoselective Derivatization and MALDI-MSI. *Analytical Chemistry* **2023,** *95* (45), 16549-16557.
212. Shariatgorji, M.; Nilsson, A.; Fridjonsdottir, E., et al., Comprehensive mapping of neurotransmitter networks by MALDI–MS imaging. *Nature Methods* **2019,** *16* (10), 1021-1028.
213. de Godoy, L. M. F.; Olsen, J. V.; de Souza, G. A., et al., Status of complete proteome analysis by mass spectrometry: SILAC labeled yeast as a model system. *Genome Biology* **2006,** *7* (6), R50.
214. Gevaert, K.; Impens, F.; Ghesquière, B., et al., Stable isotopic labeling in proteomics. *PROTEOMICS* **2008,** *8* (23-24), 4873-4885.

215. Paterson, R. W.; Gabelle, A.; Lucey, B. P., et al., SILK studies - capturing the turnover of proteins linked to neurodegenerative diseases. *Nat Rev Neurol* **2019,** *15* (7), 419-427.
216. Wojciech Michno1, Katie M. Stringer1,2, Thomas Enzlein3, Melissa K. Passarelli4,5, Stephane Escrig4, Karina Vitanova2, Jack Wood2, Kaj Blennow1,6, Henrik Zetterberg1,6,7,8, Anders Meibom4,9, Carsten Hopf3, Frances A. Edwards2, Jörg Hanrieder1,7*, Following spatial Aβ aggregation dynamics in evolving Alzheimer's disease pathology by imaging stable isotope labeling kinetics. *Sci Adv* **2021**.
217. Nilsson, K. P. R.; Herland, A.; Hammarström, P., et al., Conjugated Polyelectrolytes: Conformation-Sensitive Optical Probes for Detection of Amyloid Fibril Formation. *Biochemistry* **2005,** *44* (10), 3718-3724.
218. Åslund, A.; Sigurdson, C. J.; Klingstedt, T., et al., Novel Pentameric Thiophene Derivatives for in Vitro and in Vivo Optical Imaging of a Plethora of Protein Aggregates in Cerebral Amyloidoses. *ACS Chemical Biology* **2009,** *4* (8), 673-684.
219. Nilsson, K. P. R.; Åslund, A.; Berg, I., et al., Imaging Distinct Conformational States of Amyloid-β Fibrils in Alzheimer's Disease Using Novel Luminescent Probes. *ACS Chemical Biology* **2007,** *2* (8), 553-560.
220. Cavallucci, V.; D'Amelio, M.; Cecconi, F., Aβ Toxicity in Alzheimer's Disease. *Mol. Neurobiol.* **2012,** *45* (2), 366-378.
221. Vitek, G. E.; Decourt, B.; Sabbagh, M. N., Lecanemab (BAN2401): an anti–beta-amyloid monoclonal antibody for the treatment of Alzheimer disease. *Expert Opinion on Investigational Drugs* **2023,** *32* (2), 89-94.
222. Kaya, I.; Brinet, D.; Michno, W., et al., Delineating Amyloid Plaque Associated Neuronal Sphingolipids in Transgenic Alzheimer's Disease Mice (tgArcSwe) Using MALDI Imaging Mass Spectrometry. *ACS Chem Neurosci* **2017,** *8* (2), 347-355.
223. Verbeeck, N.; Spraggins, J. M.; Murphy, M. J. M., et al., Connecting imaging mass spectrometry and magnetic resonance imaging-based anatomical atlases for automated anatomical interpretation and differential analysis. *Biochimica et Biophysica Acta (BBA) - Proteins and Proteomics* **2017,** *1865* (7), 967-977.
224. Kaya, I.; Brinet, D.; Michno, W., et al., Novel Trimodal MALDI Imaging Mass Spectrometry (IMS3) at 10 μm Reveals Spatial Lipid and Peptide Correlates Implicated in Aβ Plaque Pathology in Alzheimer's Disease. *ACS Chem. Neurosci.* **2017,** *8* (12), 2778-2790.
225. Michno, W.; Wehrli, P.; Meier, S. R., et al., Chemical imaging of evolving amyloid plaque pathology and associated Abeta peptide aggregation in a transgenic mouse model of Alzheimer's disease. *J Neurochem* **2020,** *152* (5), 602-616.
226. Michno, W.; Wehrli, P. M.; Zetterberg, H., et al., GM1 locates to mature amyloid structures implicating a prominent role for glycolipid-protein

interactions in Alzheimer pathology. *Biochim Biophys Acta Proteins Proteom* **2019,** *1867* (5), 458-467.
227. Wehrli, P. M.; Ge, J.; Michno, W., et al., Correlative Chemical Imaging and Spatial Chemometrics Delineate Alzheimer Plaque Heterogeneity at High Spatial Resolution. *JACS Au* **2023,** *3* (3), 762-774.
228. Kakio, A.; Nishimoto, S.-i.; Yanagisawa, K., et al., Cholesterol-dependent Formation of GM1 Ganglioside-bound Amyloid β-Protein, an Endogenous Seed for Alzheimer Amyloid *J. Biol. Chem.* **2001,** *276* (27), 24985-24990.
229. Haney, M. S.; Palovics, R.; Munson, C. N., et al., APOE4/4 is linked to damaging lipid droplets in Alzheimer's microglia. *bioRxiv* **2023**.
230. Marschallinger, J.; Iram, T.; Zardeneta, M., et al., Lipid-droplet-accumulating microglia represent a dysfunctional and proinflammatory state in the aging brain. *Nat. Neurosci.* **2020,** *23* (2), 194-208.
231. Ge, J.; Koutarapu, S.; Jha, D., et al., Tetramodal Chemical Imaging Delineates the Lipid-Amyloid Peptide Interplay at Single Plaques in Transgenic Alzheimer's Disease Models. *Anal Chem* **2023,** *95* (10), 4692-4702.
232. Zhang, D. Y.; Wang, J.; Fleeman, R. M., et al., Monosialotetrahexosylganglioside Promotes Early Aβ42 Oligomer Formation and Maintenance. *ACS Chem. Neurosci.* **2022,** *13* (13), 1979-1991.
233. Tachi, Y.; Okamoto, Y.; Okumura, H., Conformational Change of Amyloid-beta 40 in Association with Binding to GM1-Glycan Cluster. *Sci. Rep.* **2019,** *9* (1), 6853.
234. Chakravorty, A.; McCalpin, S. D.; Sahoo, B. R., et al., Free Gangliosides Can Alter Amyloid-beta Aggregation. *J. Phys. Chem. Lett.* **2022**, 9303-9308.
235. Bibl, M.; Gallus, M.; Welge, V., et al., Cerebrospinal fluid amyloid-β 2-42 is decreased in Alzheimer's, but not in frontotemporal dementia. *Journal of Neural Transmission* **2012,** *119* (7), 805-813.
236. Castellani, R. J.; Perry, G., The complexities of the pathology–pathogenesis relationship in Alzheimer disease. *Biochem. Pharmacol.* **2014,** *88* (4), 671-676.
237. Gkanatsiou, E.; Portelius, E.; Toomey, C. E., et al., A distinct brain beta amyloid signature in cerebral amyloid angiopathy compared to Alzheimer's disease. *Neuroscience Letters* **2019,** *701*, 125-131.
238. Michno, W.; Koutarapu, S.; Camacho, R., et al., Chemical traits of cerebral amyloid angiopathy in familial British-, Danish-, and non-Alzheimer's dementias. *J Neurochem* **2022,** *163* (3), 233-246.
239. Bayer, T. A., Pyroglutamate Aβ cascade as drug target in Alzheimer's disease. *Molecular Psychiatry* **2022,** *27* (4), 1880-1885.
240. Guo, Z., Ganglioside GM1 and the Central Nervous System. *Int. J. Mol. Sci.* **2023,** *24* (11), 9558.

241. Liu, L.; Zhang, K.; Tan, L., et al., Alterations in Cholesterol and Ganglioside GM1 Content of Lipid Rafts in Platelets From Patients With Alzheimer Disease. *Alzheimer Dis. Assoc. Disord.* **2015,** *29* (1).
242. Angelini, R.; Yutuc, E.; Wyatt, M. F., et al., Visualizing Cholesterol in the Brain by On-Tissue Derivatization and Quantitative Mass Spectrometry Imaging. *Anal Chem* **2021,** *93* (11), 4932-4943.
243. Fincher, J. A.; Korte, A. R.; Dyer, J. E., et al., Mass spectrometry imaging of triglycerides in biological tissues by laser desorption ionization from silicon nanopost arrays. *J. Mass Spectrom.* **2020,** *55* (4), e4443.
244. Michael, J. A.; Mutuku, S. M.; Ucur, B., et al., Mass Spectrometry Imaging of Lipids Using MALDI Coupled with Plasma-Based Post-Ionization on a Trapped Ion Mobility Mass Spectrometer. *Analytical Chemistry* **2022,** *94* (50), 17494-17503.
245. Bowman, A. P.; Bogie, J. F. J.; Hendriks, J. J. A., et al., Evaluation of lipid coverage and high spatial resolution MALDI-imaging capabilities of oversampling combined with laser post-ionisation. *Analytical and Bioanalytical Chemistry* **2020,** *412* (10), 2277-2289.
246. Schaepe, K.; Bhandari, D. R.; Werner, J., et al., Imaging of Lipids in Native Human Bone Sections Using TOF–Secondary Ion Mass Spectrometry, Atmospheric Pressure Scanning Microprobe Matrix-Assisted Laser Desorption/Ionization Orbitrap Mass Spectrometry, and Orbitrap–Secondary Ion Mass Spectrometry. *Analytical Chemistry* **2018,** *90* (15), 8856-8864.